What the Heck – An Investigation into Palladium Leaching and their Kinetics

By

Oliver James Newton

Imperial College London

Department of Chemistry

2022

A thesis submitted in partial fulfilment of the requirements

for the degree of Doctor of Philosophy

Declaration of Originality

I hereby declare that all work presented in this thesis is my own work, apart from where specific reference has been made. All research was performed in the Department of Chemistry, Imperial College London; all other sources used have been completely referenced where appropriate. This work has not been submitted previously for the reward of a degree course at this or any other university.

Oliver James Newton

2022

The copyright of this thesis rests with the author. Unless otherwise indicated, its contents are licensed under a Creative Commons Attribution-Non Commercial 4.0 International Licence (CC BY-NC). Under this licence, you may copy and redistribute the material in any medium or format. You may also create and distribute modified versions of the work. This is on the condition that: you credit the author and do not use it, or any derivative works, for a commercial purpose. When reusing or sharing this work, ensure you make the licence terms clear to others by naming the licence and linking to the licence text. Where a work has been adapted, you should indicate that the work has been changed and describe those changes. Please seek permission from the copyright holder for uses of this work that are not included in this licence or permitted under UK Copyright Law.

Acknowledgements

First of all, I would like to thank my supervisors, Mimi Hii and Kalus Hellgardt for the opportunity to study at Imperial College London. The encouragement and support to explore new ideas has truly helped me progress as a researcher, whilst creating an enjoyable and challenging environment for the KKH group as a whole.

I would like to thank my industry supervisor Jeffery Richardson for his industrial insight into the project and Eli Lilly for my PhD sponsorship as part of the Pharmacat consortium.

I am very grateful to all of the KKH group members past and present for making my PhD all the more enjoyable. A special mention to Ben Deadman and everyone involved at the ROAR lab for their technical assistance and expert advice.

To my partner Poppy, thank you for your patience, support and understanding through the years; your belief in me never faulters.

Finally thank you to my family for your unconditional support. To my parents, you gave me the best possible start and as I have aged, your generosity and care have remained as strong as ever. Thank you.

Abstract

This PhD thesis investigates aspects of the Mizoroki-Heck reaction which can be broadly divided into two parts: (1) employing a flow reactor to distinguish between surface and solution catalysed reactions of heterogenous catalysts whilst assessing their leaching behaviour under various reaction conditions; (2) investigating the catalytic behaviour of ligandless palladium at ultra-low catalyst loadings through reaction kinetics and kinetic modelling.

A flow reactor was constructed in two operational configurations: configuration 1 was used to study the surface and solution contributions of heterogenous catalysts which revealed that the majority of conversion is actually attributed to turnover in the homogenous phase; configuration 2 probed the influence of individual reactants on the leaching process showing that both the aryl halide and base have the largest impact on leaching.

To date, little is known about the mechanism and speciation of $Pd(OAc)_2$ at ultra-low catalyst loadings. Kinetic profiling of the Heck reaction catalysed by "homeopathic" loadings of $Pd(OAc)_2$ have been studied to gain an insight into the nature of the catalyst and its speciation. Orders in reagents and catalyst were extracted from relevant reaction profiles by utilising variable time normalisation analysis and reaction progress kinetic analysis. The reactions were monitored *in situ* by IR accompanied with offline HPLC quantification. Comparison of the results for reactions under varying reaction conditions are made to probe their impact on the homeopathic palladium catalysed Heck reaction.

The study reveals two distinctive kinetic regimes: between [Pd] of 0.003-0.01 mol% (30-100 ppm), catalyst deactivation was found to be minimal, and the observed rates showed a 1.7 order of dependence on [Pd]. In contrast, when [Pd] > 0.02 mol% (200 ppm), catalyst deactivation becomes competitive, whereupon the order of dependence on [Pd] decreased to 0.9. A simplified microkinetics model revealed the presence of at least two kinetically competent catalysts, represented by a monomeric (Pd_1) and dimeric (Pd_2) species in a 1:3 ratio. Surprisingly, Pd_2 was found to be nearly 90 times more active than Pd_1. This work provides direct kinetic evidence that a higher-order Pd species can be more active than a monomeric species, and the key role played by catalyst deactivation at higher catalyst loadings.

Abbreviations

δ	Chemical shift (down field from TMS)
“	Inch
Ø	Diameter
°C	Degrees Celsius
ΔH	Enthalpy change
$\Delta H^{‡}$	Enthalpy of activation
µg	Microgram
µL	Microliter
Å	Ångström(s)
A	Pre-exponential factor
AAS	Atomic absorption spectroscopy
API	Active pharmaceutical ingredient
Ar	Aryl group
BM	Berkeley Madonna
Bu	Butyl
C-C	Carbon-carbon bond
cm	Centimetre
C-N	Carbon-nitrogen bond
C-O	Carbon-oxygen bond
d	Doublet
dba	dibenzylideneacetone
dd	Doublet of doublets

DMA	Dimethylacetamide
DMF	Dimethylformamide
E_a	Activation energy
eq.	Equivalent (relative to limiting reagent)
ESI	Electrospray ionisation
Et_3N	Triethylamine
Fc	Ferrocene group
FT	Fourier transform
g	Gram
GC	Gas chromatography
GLC	Gas liquid chromatography
h	Hour(s)
HA	Hydroxyapatite
HPLC	High performance liquid chromatography
Hz	Hertz
ICP	Inductively coupled plasma
i-Pr	Isopropyl
IR	Infrared
J	Coupling constant
K	Equilibrium constant
k	Rate constant
kcal	Kilocalorie
kJ	Kilojoules

Lit	Literature reference
M	Moles per litre
m	Multiplet
Me	Methyl
MeAc	Methyl acrylate
MeCN	Acetonitrile
mg	Milligram
min	Minute(s)
mL	Millilitre(s)
mm	Millimetre
mmol	Millimole(s)
mol	Mole
mol%	Molar amount as a percentage of the limiting regent
MS	Mass spectrometry
NIR	Near infrared
nm	Nanometre
NMP	N-Methyl-2-pyrrolidone
NMR	Nuclear magnetic resonance
NP	Nanoparticle
OA	Oxidative addition
OAc	Acetate (Ethanoate)
OES	Optical emission spectroscopy
p	Pentet

PBR	Packed bed reactor
PET	Polyethylene terephthalate
PFR	Plug flow reactor
Ph	Phenyl
ppm	Part per million
q	Quartet
QX	Quaternary ammonium salt
R	Organic fragment, ideal gas constant
RDS	Rate determining step
RMS	Root mean squared
RPKA	Reaction progress kinetic analysis
s	Second(s), singlet
SBA-15	Santa Barbra Amophous-15
SEM	Scanning emission microscopy
T	Absolute temperature
t	Triplet
t, tert	Tertiary
TBAB	Tetrabutylammonium bromide
TEM	Transmission electron microscopy
TFA	Trifluoracetic acid
TOF	Turnover frequency, Time of flight
TOGA	Tetraoctylammonium glycolate
Tol	Toluene

TON	Turnover number
TPP	Triphenylphosphine
UV	Ultraviolet
Vis	Visible (referring to the frequency of light)
VTNA	Variable time normalisation analysis
wt%	Weight percent
X	Generic halogen atom
[x]	Square brackets indicate the concentration of x
XAS	X-ray absorption spectroscopy
XPS	X-ray photoelectron spectroscopy
XRD	X-ray diffraction

List of Schemes

Scheme 1.1: Simplified catalytic cycle for the Mizoroki-Heck reaction.

Scheme 1.2: The development of the Heck reaction from 1969 – 1984.

Scheme 1.3: Application of DavePhos for the tandem reaction involving an intramolecular Heck coupling [40].

Scheme 1.4: First example of a palladacycle used in the Heck reaction developed by Herrmann and Beller [41].

Scheme 1.5: The Heck reaction of 4-bromoanisole and styrene catalysed by Pd with the phosphite ligand – tris(2,4-di-*t*-butylphenyl) phosphite [47].

Scheme 1.6: The Heck reaction of 2-iodobenzoic acid with propanoic acid under 'homeopathic dose' of Pd [49].

Scheme 1.7: De Vries' proposed catalytic cycle for the ligandless Heck reaction, adapted from reference [50].

Scheme 1.8: Proposed mechanism of aggregation and deactivation for Pd species under ligandless conditions, adapted from reference [51].

Scheme 1.9: The Heck reaction between bromobenzene and *n*-butyl acrylate at 135 °C in NMP [51].

Scheme 1.10: Simplified catalyst cycle involving nanoparticle behaving as an off-cycle reservoir. Recreated from the literature [56].

Scheme 1.11: Simplified catalyst cycle involving nanoparticles proposed by Beletskaya et al. recreated from the literature [56].

Scheme 1.12: Reaction of bromobenzene and styrene catalysed by $PdCl_2(C_6H_5CN)_2$ in NMP [57].

Scheme 1.13: reaction of bromobenzene and ethyl acrylate catalysed by $Pd(OAc)_2$ under Jeffery conditions in DMA [57].

Scheme 1.14: The Heck reaction studied by Van Leeuwen between iodobenzene and styrene catalysed by a palladacycle catalyst [59].

Scheme 1.15: Proposed catalytic cycle for the Heck reaction involving a dimeric off cycle species recreated from ref [59].

Scheme 1.16: The Heck reaction between bromobenzaldehyde and butyl acrylate catalysed by a palladacycle [60].

Scheme 2.1: Reaction of iodobenzene with methyl acrylate with conventional supported palladium catalysts Pd/SiO_2 and Pd/C in the presence of NMP and Et_3N.

Scheme 2.2: Heck coupling between bromoarenes and styrene conducted in DMA, toluene or NMP.

Scheme 2.3: One pot synthesis of 4-(p-methoxyphenyl) butan-2-one using either Pd on MgO, HA, γ-Al_2O_3 and TiO_2.

Scheme 2.4: The Heck reaction between haloarenes and methyl acrylate.

Scheme 2.5: Heck reaction between iodo/bromoacetophenone and butyl acrylate in DMF catalysed by Pd-SH-SBA-15.

Scheme 2.6: Heck reaction between halo arenes and styrene in catalysed by Pd/NaY in NMP.

Scheme 2.7: The Heck reaction between iodobenzene and butyl acrylate in the presence of NaOAc which is insoluble in DMF.

Scheme 2.8: Schematic of the flow set up for the Heck reaction between 4-iodobenzonitrile and butyl acrylate consisting of a pump, catalyst cartridge in a heating block and back pressure regulator [123].

Scheme 2.9: Diagram of the reactor designed by Plucinski and co-workers for the sequential Heck and hydrogenation reactions for the synthesis of 1,2-diphenylethane [126].

Scheme 2.10: The Heck reaction conducted for *in situ* XAS experiments.

Scheme 2.11: The Heck reaction between iodobenzene and methyl acrylate catalysed by the polyurea encapsulated Pd catalyst PdEnCat®30 in DMF.

Scheme 2.12: Schematic of the tandem flow reactor used in the study conducted by Hii, Hellgardt and co-workers [86].

Scheme 2.13: Scheme of the flow reactor designed by Bellefon et. al. for the assessment of leaching in the Suzuki-Miyaura reaction [135].

Scheme 2.14: Suzuki-Miyaura reaction catalysed by Siliacat Pd between phenylboronic acid and 4-iodoacetophenone in the presence of sodium methanolate in ethanol.

Scheme 2.15: The model Heck reaction applied throughout this study between iodobenzene and methyl acrylate.

Scheme 3.1: Schematic of configuration 1 of the tandem flow reactor.

Scheme 3.2: Schematic of configuration 2 of the tandem flow reactor.

Scheme 4.1: The Heck reaction between iodobenzene, methyl acrylate and triethylamine (base) in the presence of a heterogeneous Pd catalyst.

Scheme 4.2: Ligation and reduction of palladium acetate by DMF.

Scheme 4.3: The Heck reaction between iodobenzene and methyl acrylate catalysed by PdEnCat®30 in the presence of triethylamine in DMF.

Scheme 5.1: The Heck reaction between bromobenzene and *n*-butyl acrylate at 135 °C in NMP.

Scheme 5.2: Kinetic model and associated differential equations incorporating two catalytically active species and two (independent) deactivation rates.

Scheme 5.3: Proposed catalytic cycles involving Pd_1 and Pd_2 in a 'ligandless' system.

List of Figures

Figure 1.1: Examples of bulky biaryl dialkylphosphine ligands compatible with Buchwald's pre-catalysts.

Figure 1.2: Pd(II) palladacycle utilised by Herrmann for the Heck reaction [33, 41, 42].

Figure 1.3: $Pd(OAc)_2$ loading vs yield (%) highlighting the optimum substrate to catalyst ratio for the reaction of bromobenzene and *n*-butyl acrylate [51].

Figure 1.4: Formation of Pd nanoparticles from soluble Pd species [55].

Figure 1.5: Plot of yield (y) vs time (t) for the reaction of bromobenzene and styrene [57].

Figure 1.6: Plot of yield (y) vs time (t) for the reaction of bromobenzene and ethyl acrylate catalysed by $Pd(OAc)_2$ [57].

Figure 1.7: Co-ordination of a dipalladium (I) complex incorporated with a ferrocene group (Fc) from reference [58].

Figure 1.8: Monomer and dimer interconversion of the phosphoramidite Pd precursor recreated from reference [62].

Figure 1.9: Reaction profile obtained using the phosphoramidite Pd precursor as a catalyst for the reaction of iodobenzene with *n*-butyl acrylate in NMP [62].

Figure 2.1: Chemical functionalisation of SiliaMetS-Thiol (left) and Smopex-103 (right).

Figure 2.2: atom by atom detachment and cluster displacement leaching processes reproduced from reference [86].

Figure 2.3: local leaching, leaching of soluble monometallic species, leaching of metal clusters and crushing/destruction of metal nanoparticles. The figure is reproduced from reference [55].

Figure 2.4: XRD of 10 wt.% Pd/C catalyst before and after the Heck reaction between iodobenzene and methyl acrylate at 160 °C in NMP. Reproduced from reference [92].

Figure 2.5: Investigation of activity and Pd leaching as a function of time for the Heck reaction between bromobenzene and styrene. The figure is reproduced from reference [94].

Figure 2.6: Palladium conversions in the Heck reaction as proposed by Schmidt et. al. (ArX – aryl halide, Nu-LG nucleophilic coupling partner) The figure is reproduced from reference [96].

Figure 2.7: immobilisation methods to secure the catalyst onto solid supports.

Figure 2.8: Graph of diminishing conversion with each recycle experiment. Recreated from reference [112].

Figure 2.9: structure of SH-SBA-15 and how it poisons labile Pd.

Figure 2.10: Two compartment membrane reactor employed by Rothenberg's group to prove the participation of soluble Pd species in a C-C coupling reactions [121].

Figure 2.11: Suggested mechanism for the migration of Pd from side **A** to side **B**. Top - nanoparticle fragmentation followed by small cluster transfer; middle – Pd^0 atom leaching and transfer under non-oxidising conditions; bottom – formation and transfer of Pd^{II} species under oxidising conditions. Image recreated from reference [97].

Figure 2.12: A comparison of the possible mechanisms of leaching in a batch reactor compared with a flow reactor.

Figure 2.13: Structures of the heterogeneous catalysts which were investigated by Kappe and co-workers (a) polymer-bound Pd Tetrakis, (b) FiberCat 1001, (c) Encat® TPP30 and (d) SiliaCat DPP-Pd [124].

Figure 2.14: Structures of the Pd@MOF complexes used for the catalysis of the Heck reaction for *in situ* XAS experiments [128].

Figure 2.15: Custom reactor for the operando analysis of various Pd species in the Heck reaction [128].

Figure 3.1: Photograph of the packed catalyst cartridge.

Figure 3.2: A labelled image of the tandem flow reactor set up in configuration 1.

Figure 3.3: A labelled image of the tandem flow reactor set up in configuration 2.

Figure 3.4: Breakthrough curve for the flow reactor eluting from S1 at 0.5 mL/min.

Figure 3.5: Breakthrough curve for the flow reactor eluting from S2 at 0.5 mL/min.

Figure 3.6: Experimental set up in the EasyMax reactor for the kinetic studies.

Figure 4.1: Reaction profile of the Heck reaction for the formation of methyl cinnamate in toluene. S1 (red dots) corresponding to the conversion (%) after the PBR and S2 (blue dots) corresponding to the conversion (%) after the PFR.

Figure 4.2: Reaction profile of the Heck reaction for the formation of methyl cinnamate in dioxane. S1 (red dots) corresponding to the conversion (%) after the PBR and S2 (blue dots) corresponding to the conversion (%) after the PFR.

Figure 4.3: Reaction profile of the Heck reaction for the formation of methyl cinnamate in DMF. S1 (red dots) corresponding to the conversion (%) after the PBR and S2 (blue dots) corresponding to the conversion (%) after the PFR.

Figure 4.4: Reaction profiles for the Heck arylation of iodobenzene with methyl acrylate performed in the solvents DMF (green dots), dioxane (red squares) and toluene (blue triangles).

Figure 4.5: Images of the Heck arylation of iodobenzene with methyl acrylate performed in the solvents toluene (left), dioxane (centre) and DMF (right) after 90 minutes.

Figure 4.6: Superimposed reaction profiles of the Heck reaction in scheme 3 conducted at various PBR temperatures in the tandem flow reactor using configuration 1. Conversion from S1 sample (**A**) conversion from S2 samples (**B**).

Figure 4.7: (left) structure of FiberCat 1001 covalently bonded to polypropylene and (right) structure of PdEnCat®30 where $Pd(OAc)_2$ is encapsulated in a polyurea matrix.

Figure 4.8: Heck reaction catalysed by Pd/Al_2O_3 with the PBR at 90 °C (**A**) or 30 °C (**B**) and the PFR at 110 °C.

Figure 4.9: Heck reaction catalysed by Pd/Al_2O_3 with the PBR at 90 °C and PFR at 90/100/110/110 °C.

Figure 4.10: Reaction profiles from S2 for the Heck reaction catalysed by FibreCat 1001 with the PBR at 90 °C and PFR at 90/100/110/110 °C (**A**) and with the PBR at 30 °C and PFR at 90/100/110/110 °C (**B**).

Figure 4.11: Heck reaction catalysed by FibreCat 1001 with the PBR at 30/70/90/110 °C and PFR at 110 °C.

Figure 4.12: Conversion at S2 from the Heck reaction catalysed by PdEnCat®30 before and after washing with DMF with the PBR and PFR set at 110 °C.

Figure 4.13: Conversion at S2 from the Heck reaction catalysed by $PdAl_2O_3$ before and after washing with DMF with the PBR set at 90 °C and PFR set at 110 °C.

Figure 4.14: Conversion at S2 from the Heck reaction catalysed by PdEnCat®30 washed intermittently with DMF in 20 min reaction cycles when the PBR and PFR are set at 110 °C (**A**) or 30 °C and 110 °C respectively (**B**).

Figure 4.15: Reaction profile from DMF (**A**) and a mixture of DMF and methyl acrylate (**B**) passing through the PBR at 30 °C which was then elevated 90 °C after 90 mins.

Figure 4.16: Reaction profile from a mixture of DMF and iodobenzene passing through the PBR at 30 °C which was then elevated to 90 °C after 90 mins.

Figure 4.17: Reaction profile from a mixture of DMF and triethylamine passing through the PBR at 30 °C which was then elevated to 90 °C after 90 mins.

Figure 4.18: Reaction profile from a mixture of DMF and iodobenzene passing through the PBR containing FiberCat 1001 at 30 °C which was then elevated to 90 °C after 90 mins.

Figure 4.19: Reaction profile from a mixture of DMF and triethylamine passing through the PBR containing FiberCat 1001 at 30 °C which was then elevated to 90 °C after 90 mins.

Figure 4.20: Reaction profile from a mixture of DMF and iodobenzene passing through the PBR containing Pd/Al_2O_3 at 90 °C for 90 mins.

Figure 5.1: Reaction profiles of $Pd(dba)_2$ vs $Pd(OAc)_2$. Iodobenzene (1 eq.), methyl acrylate (1.5 eq.) and triethylamine (1.5 eq.), 110 °C, 1 mL of catalyst stock solution (100 ppm, corresponding to 0.01 mol%). Graph constructed from *in situ* IR data quantified with offline HPLC samples.

Figure 5.2: Reaction profiles of the Heck reaction catalysed by $Pd(OAc)_2$ (100 ppm, corresponding to 0.01 mol% Pd loading). Reaction conditions: Iodobenzene (1 eq.), methyl

acrylate (1.5 eq.) and triethylamine (1.5 eq.), reactions performed at 80 °C (monitored by quantitative HPLC).

Figure 5.3: Visual identification of Pd nanoparticles in DMF over a 24 hour period at room temperature.

Figure 5.4: UV-Vis spectra of 100 ppm (**A**) and 1000 ppm (**B**) stock solutions monitored over a 48 hour period at room temperature in DMF.

Figure 5.5: Absorbance at 450 nm vs time graphs for 100 ppm (left) 1000 ppm (right) stock solutions over a 48 hour period at room temperature in DMF.

Figure 5.6: Consecutive dosing experiments to determine deactivation. **A**: 100 ppm $Pd(OAc)_2$ (no catalyst deactivation), **B**: 1000 ppm $Pd(OAc)_2$ (catalyst deactivation).

Figure 5.7: Initial rates of the Heck arylation reaction using 100 ppm of $Pd(OAc)_2$ between 80-110 °C.

Figure 5.8: Arrhenius plot of the Heck arylation reaction catalysed by $Pd(OAc)_2$ and associated activation energy.

Figure 5.9: Eyring plot of the Heck arylation reaction catalysed by $Pd(OAc)_2$ and associated enthalpy of activation.

Figure 5.10: Dependence of TON's on catalyst loading from 30-1000 ppm of [Pd].

Figure 5.11: Dependence of TOF's on catalyst loading from 30-1000 ppm of [Pd], assuming a monomeric catalytically active Pd species for model reaction.

Figure 5.12: Pre-equilibration of the reaction mixture before the addition of 50 ppm of the Pd stock solution.

Figure 5.13: Visual plots showing the consumption of the limiting reagent (methyl acrylate) for the 'control', 'same excess' and 'different excess' RPKA experiments which show no catalyst deactivation and zero order dependency of global reaction rate on [PhI].

Figure 5.14: Concentration vs time profiles showing the consumption of iodobenzene for 'control', 'same excess' and 'different excess' of methyl acrylate (MeAc). Time shift applied to the same excess profile to achieve overlay indicating a zero-order dependency in MeAc.

Figure 5.15: Concentration vs time profiles showing the consumption of iodobenzene for 'control', 'same excess' and 'different excess' of triethylamine (Et_3N). Time shift applied to the same excess profile to assess overlay which indicates a zero-order dependency in Et_3N.

Figure 5.16: First 60 minutes of each reaction profile for the Heck reaction with catalyst loadings from 30 to 1000 ppm.

Figure 5.17: [Pd] vs initial rate constructed from the data obtained in the first 5 minutes of the reaction. ([Pd] = 30, 50, 100, 200, 400, 600, 800, 1000 ppm)

Figure 5.18: Catalyst order determined by VTNA for 'high' (**A**, 200-1000 ppm) and 'low' (**B**, 30-200 ppm) catalyst loading groups.

Figure 5.19: VTNA reaction profiles fitted to first order Pd, assuming presence of 33 ppm of catalyst poison.

Figure 5.20: Conversion vs Time profile for the Heck reaction between iodobenzene and methyl acrylate at 110 °C using 5 ppm (0.0005 mol%) of $Pd(OAc)_2$.

Figure 5.21: Expansion of the fit of the model to experimental data (full fitting was performed between 0-400 min). Dots represent the experimental data; solid lines represent the simulated data from the model.

Figure 5.22: Possible catalyst activation pathway at low concentrations superimposed on the reaction profile obtained with 5 ppm [Pd] loading.

List of Tables

Table 1.1: Ligands and conditions for the Heck reaction of aryl chlorides.

Table 2.1: Comparison between the main advantages/disadvantages of homogeneous and heterogeneous catalysis.

Table 2.2: Quantity of Pd leaching from Pd/C under various mobile phase compositions [123].

Table 3.1: List of chemicals used in this project.

Table 3.2: Sample code for the final kinetic model.

Table 4.1: Proposed conclusions depending on product concentration at each sample outlet [86].

Table 4.2: Comparison of solvent properties [139].

Table 4.3: Comparison of the type and method of support for the catalysts screened.

Table 5.1: Calculated TON and averaged TOF values at 95% conversion (Figures 5.10 and 5.11).

Table 5.2: Concentrations of each reactant used for the control, same excess and different excess experiments.

Table 5.3: Concentrations of reactants and reagents used for 'control', 'same excess' and 'different excess' of methyl acrylate (MeAc).

Table 5.4: Concentrations of reactants and reagents used for 'control', 'same excess' and 'different excess' of triethylamine (Et_3N).

Table 5.5: A description of set up of the kinetic model.

Table 5.6: Kinetic rate constants and RMS values extracted from fitting the kinetic model (Scheme 5.2) to the experimental data.

Table 6.1: visual representation of previous models with their associated assumptions and outcomes.

Contents

Declaration of Originality..... 1

Acknowledgements..... 2

Abstract..... 3

Abbreviations..... 4

List of Schemes..... 9

List of Figures..... 12

List of Tables..... 18

Contents..... 19

Chapter 1. Introduction

1.1 Introduction to C-C Bond Formations..... 22

1.2 Phosphine Ligands..... 26

1.3 Ligandless Systems..... 29

1.4 'Cocktail' Type Catalyst Systems..... 33

1.5 Conclusion..... 43

Chapter 2. Heterogeneous Catalysed Heck Reactions

2.1 Homogeneous vs Heterogeneous Catalysis..... 44

2.2 Metal Scavengers..... 45

2.3 Conventional Leaching Tests..... 46

2.4 Mechanisms of Leaching..... 48

2.5 Development of Heterogeneous Catalysts..... 53

2.6 Reactors for Assessing Leaching..... 59

2.7 Conclusion..... 69

2.8 Aims..... 69

Chapter 3. Experimental Protocol and Methodology

3.1 Introduction..... 71

3.2 Chemicals..... 71

3.3 Methods 72

3.3.1 General..... 72

3.3.2 Nuclear Magnetic resonance (NMR) 72

3.3.3 High Pressure Liquid Chromatography (HPLC) 72

3.3.4 Infra-red Spectroscopy (IR) **73**

3.3.5 *In situ* Infra-red spectroscopy (ReactIR) **73**

3.3.6 UV-Vis formation of Pd NP's **73**

3.3.7 Mass Spectrometry (MS) **73**

3.3.8 Inductively coupled plasma (ICP) **73**

3.3.9 Catalyst packing **74**

3.4 Configuration 1 of the Tandem Flow Reactor **74**

3.5 Standard Experimental Procedure for Configuration 1 ..... **76**

3.6 Configuration 2 of the Tandem Flow Reactor **77**

3.7 Standard Experimental Procedure for Configuration 2 ..... **78**

3.8 Flow Reactor Profile - Breakthrough Curve **79**

3.9 EasyMax 102 Advanced Thermostat System **81**

3.10 Standard Procedure for the Kinetic Analysis of the Pd Catalysed Heck Reaction **82**

3.11 Kinetic Reactions (catalyst dosing) **83**

3.12 IR Calibration Data **83**

3.13 Data Processing for *in situ* IR Quantification **84**

3.14 RPKA and VTNA Data Processing **85**

3.15 Kinetic Modelling **85**

Chapter 4. Catalysis in Flow – Leaching

4.1 Introduction **87**

4.2 Results and Discussion **88**

4.2.1 Leaching Studies – Configuration 1 ..... **89**

4.2.2 Solvent Screen **90**

4.2.3 Toluene **91**

4.2.4 1,4-Dioxane **92**

4.2.5 Dimethylformamide (DMF) **93**

4.2.6 Batch Comparison **94**

4.2.7 Effect of Temperature on Catalyst Leaching **96**

4.2.8 Catalyst Screen **97**

4.2.9 Performance of Pd/Al_2O_3 in Configuration 1 ..... **98**

4.2.10 Performance of FiberCat 1001 in Configuration 1 ..... **100**

4.2.11 Performance of Pd/C in Configuration 1 ..... **101**

4.2.12 Catalyst Regeneration **102**

4.2.13 Reactant screen **105**

4.2.14 Reactant effects on the leaching of Pd from PdEnCat®30 ..... **105**

4.2.15 Reactant effects on the leaching of Pd from FiberCat 1001 ..... **108**

4.2.16 Reactant effects on the leaching of Pd from Pd/Al_2O_3 ..... **111**

4.3 Conclusions **111**

Chapter 5. Kinetic analysis of ligandless palladium species using 'homeopathic' quantities

5.1 Introduction **113**

5.2 Results and Discussion **115**

5.2.1 Experimental Precautions **115**

5.2.2 Catalyst Screen - Choice of 'Ligandless' Palladium Precursors **115**

5.2.3 Solvent Screen **117**

5.2.4 UV-Vis Analysis of the Stability of Pd in DMF **118**

5.2.5 Catalyst Stability **120**

5.2.6 Temperature Dependence (Arrhenius Plot) **121**

5.2.7 Dependence of TON and TOF on Catalyst Loading **124**

5.2.8 Kinetic Analysis – Order in Reactants **127**

5.2.9 Order in Iodobenzene **128**

5.2.10 Order in Methyl Acrylate & Triethylamine **129**

5.2.11 Kinetic Analysis - Initial Rates Method **131**

5.2.12 Kinetic Analysis - Virtual Time Normalisation Analysis (VTNA) **133**

5.2.13 Kinetic Modelling **136**

5.3 Conclusions **143**

6. Appendix **145**

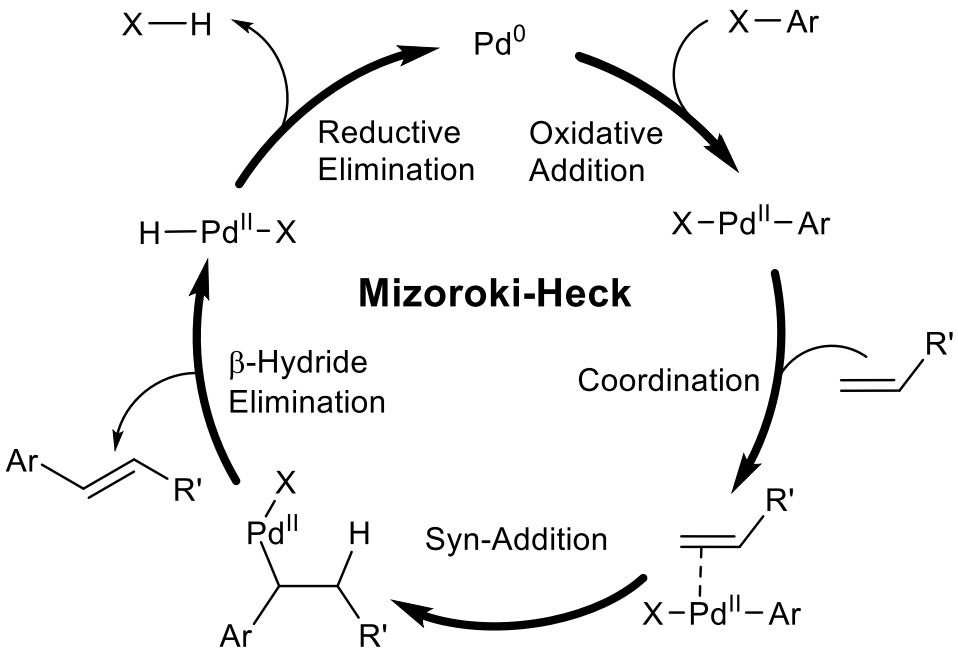
7. References **147**

Chapter 1. Introduction

1.1 Introduction to C-C Bond Formations

The assembly of carbon chains allows the formation of more complex molecules which are a prerequisite for all life on earth. Carbon-carbon bond forming reactions are therefore of the upmost importance for chemists in order to synthesise molecules, from natural products to pharmaceuticals.

Prolific research into transition metal chemistry has since led to the discovery of numerous palladium catalysed carbon-carbon coupling reactions [1, 2, 3]. It took until the 21st century for the potential of these palladium cross coupling reactions to be truly appreciated resulting in the Mizoroki-Heck [4,5], Negishi [6,7] and Suzuki [8,9] cross coupling reactions being awarded the 2010 Noble Prize in Chemistry [10]. Despite the variety of Pd cross coupling reactions, they tend to follow a general catalytic cycle (Scheme 1.1).



Scheme 1.1: Simplified catalytic cycle for the Mizoroki-Heck reaction.

The catalytic cycle starts with an oxidative addition (OA) step where the Pd inserts into the aryl halide bond. After the OA step, an olefin coordinates to the Pd species and forms a π-complex through syn-addition. β-hydride elimination follows which delivers the new C-C bond between the olefin and the aryl group. Base assisted reduction of Pd^{II} to Pd^{0} regenerates the active species and allows the catalytic cycle to turnover.

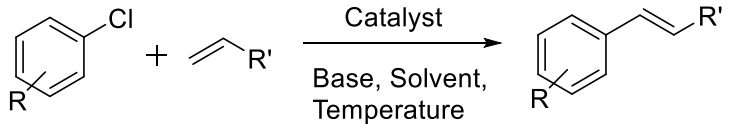
An alternative ionic pathway for the Heck reaction can occur if an anionic halide ligand dissociates from the OA palladium species. This affects the regioselectivity of the product due to the stabilisation of the carbocation [11]. The pathway is promoted when pseudo halides are used such as triflates and acetates as they are weakly associated to the Pd and therefore dissociate more easily. Other additive can promote the cationic pathway such as hydrogen bond donors (HBD) which can hydrogen bond to the halide which drives the rate of dissociation [12].

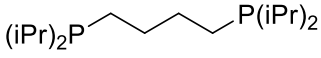
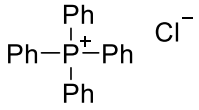
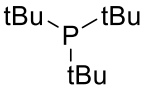
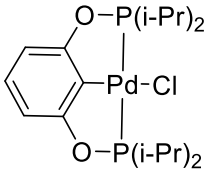
There are many conflicting hypotheses on what the rate determining step (RDS) is in the Heck reaction with oxidative addition [13, 14], olefin insertion [15, 16] and β-hydride elimination [17, 18] all being proposed in the literature. The assumption which all of these hypotheses make is that the mechanism of the Heck reaction has a single route reflecting Heck's original ideas on the catalytic cycle [5]. However, there is evidence that catalyst activation and deactivation processes can have a significant influence [19].

In the mechanism of the Heck reaction the nature of the aryl halide reactant can influence the rate determining step (RDS). This is because the rate of oxidative addition depends on the aryl halide, with the following trend generally being observed from fastest to slowest I>Br>Cl [1, 20]. As a result, oxidative addition with aryl chlorides and unactivated aryl bromides is often proposed to be the RDS [21, 22]. The use of aryl chloride substrates as a reactant is an attractive prospect as they are more widely available, provide a better E-factor and cheaper than using the corresponding iodides or bromides.

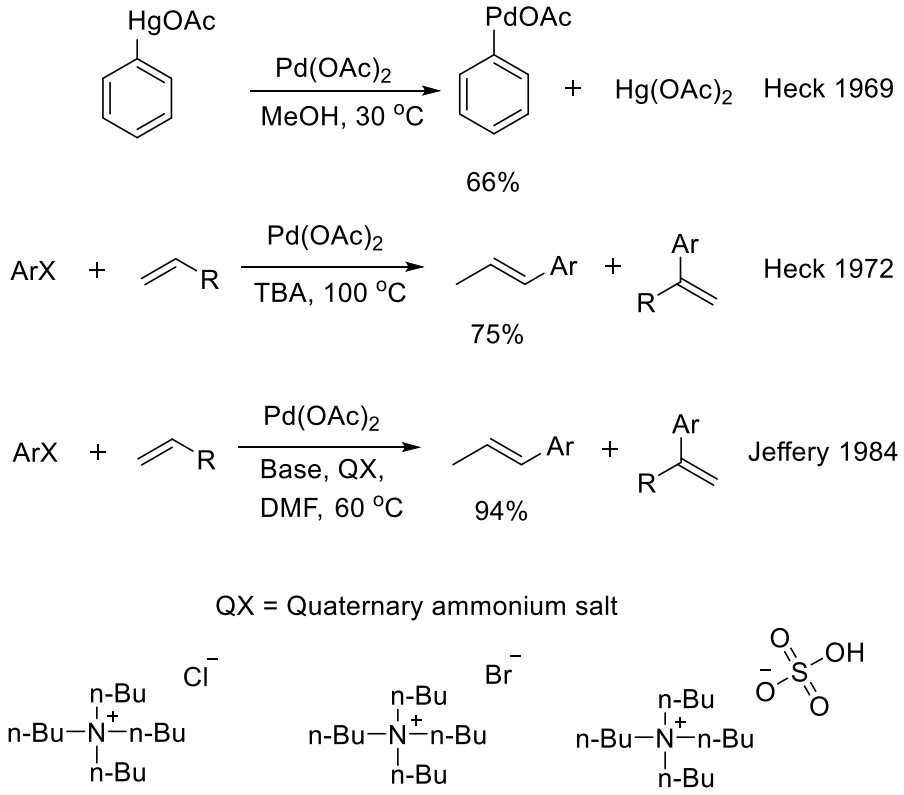
The original reports by Mizoroki and Heck employed Pd(II) pre-catalysts such as $Pd(OAc)_2$ and $PdCl_2$ in a homogeneous reaction mixture without any added ligands [4, 5]. Since then, these Pd salts are frequently used in combination with ligands due to their instability and inability to activate aryl chloride bonds (Table 1.1). The purpose of these ligands is to increase the catalytic activity and stability by preventing deactivation. The main categories of ligands for Pd catalysis will be discussed in more detail in the following section.

Table 1.1: Ligands and conditions for the Heck reaction of aryl chlorides.



Entry	R	R'	Catalyst	Conditions	Yield
1[23]	H, CH_3, CHO, 4-NO_2	Ph	$Pd(OAc)_2$ 	NaOAc, DMF, 150 °C	50-90%
2[24]	H, 4-CHO	Ph	$[PdCl_2(MeCN)_2]$ 	NaOAc, NMP, 150 °C	79-96%
3[25]	H, 2-Me, OMe, 4-COMe	Ph, CO_2Me	$[Pd_2(dba)_3]$ 	Cs_2CO_3, Dioxane, 100-120 °C	70-84%
4[26]	H, 2-Me, OMe, COMe, 4-CHO	Ph		CsOAc, Dioxane, 120 °C	81-99%

The development of the Heck reaction began with the use of toxic organomercury, tin and lead compounds (Scheme 1.2: Heck 1969) [27]. Improvements on the fundamental studies led to the first conditions for the use of ligands in conjunction with a Pd catalyst, whereby sterically hindered amines were added in combination with the palladium salt (Scheme 1.2: Heck 1972) [5]. Jeffery later utilised tetraalkylammonium salts with an inorganic base and simple palladium salts to improve the catalytic activity (Scheme 1.2: Jeffery 1984) [28]. This combination of reactants is now known generally as “Jeffery conditions” and are effective in the catalysis of aryl iodides and bromides [29].



Scheme 1.2: The development of the Heck reaction from 1969 – 1984.

Jeffery's conditions have certainly advanced the procedure for 'ligandless' reactions by using tetraalkylammonium salts, especially for the Heck reactions with aryl iodides. The major advantage of using tetraalkylammonium salts in 'ligandless' Heck reactions is to stabilise the palladium and slow down the aggregation process, i.e. act as a ligand.

Following on from Jeffery's conditions the literature exploded with a plethora of reports on new ligands (for homogeneous catalysis), each claiming to be more efficient or selective than the last, adding a new layer of complexity to the original Heck reaction. The coordination of a ligand to Pd changes the physical and chemical properties of the catalyst, and it is therefore the choice of ligand which can influence the solubility, the steric and shielding properties, the reactivity, the lifetime and turnover-numbers (TON) of the active catalyst species. The ligands found to be effective for Heck reactions included phosphines [30], carbenes [31], ammonium salts [29] and palladacycles [32].

1.2 Phosphine Ligands

While phosphines are not necessary for the Heck reaction of aryl iodides, they are often employed when aryl bromides are used as a precursor. Electron-donating phosphine ligands can coordinate to Pd species to facilitate the oxidative addition of the aryl bromide to Pd. Furthermore, the steric hindrance associated with bulky phosphines play an important role in stabilising the palladium species and preventing deactivation [33]. This is exemplified by the series of Buchwald's pre-catalysts which are used in combination with bulky phosphine ligands (Figure 1.1) [33-35].

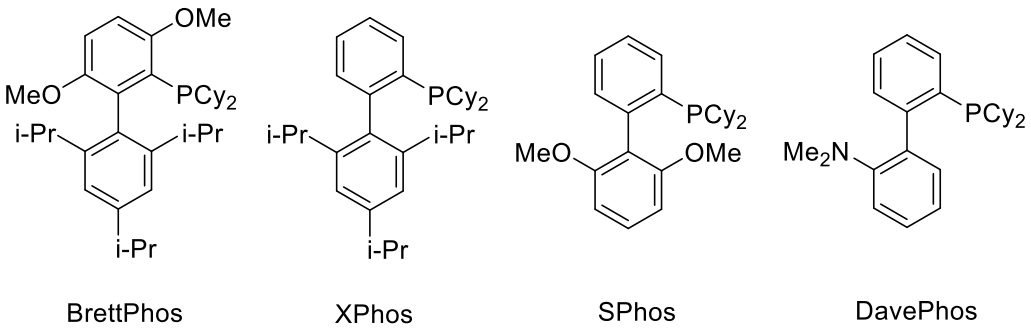
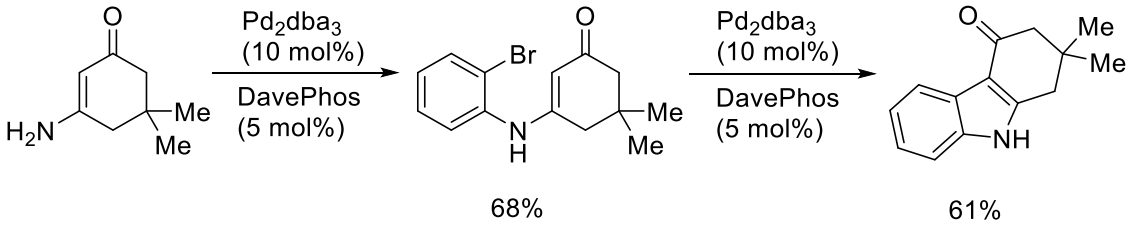


Figure 1.1: Examples of bulky biaryl dialkylphosphine ligands compatible with Buchwald's pre-catalysts.

These biaryl dialkylphosphines were reported in 1999 by Buchwald et. al., who showed that they are excellent supporting ligands for Pd species in the formation of C-C [36], C-N [37] and C-O [38] bonds with aryl chlorides and bromides. The characteristic biaryl phosphine decorated with cyclohexyl groups on the phosphorus enhances the steric and electron donating properties of the phosphine ligand, which improves the stability and activity of the palladium catalyst. The formation of monoligated Pd species with biaryl phosphines is thought to be responsible for the enhanced reactivity of the Pd centre with the activity of the Pd species depending on the ligand to Pd ratio [20]. In comparison to triphenylphosphine, the more electron rich phosphine ligand increases the electron density on the Pd centre, which accelerates the formation of the active Pd species and the oxidative addition step [39].

Edmondson and co-workers at Merk applied Buchwald's ligand DavePhos in a tandem synthesis via an intramolecular Heck reaction to form an indole (Scheme 1.3) [40]. This reaction did not proceed using other phosphine ligands, such as triphenyl phosphine or BINAP, highlighting the effectiveness of biaryl phosphines. However, the further addition of

Pd and ligand were required for the second step, suggesting that the catalyst deactivates during the first amination reaction.



Scheme 1.3: Application of DavePhos for the tandem reaction involving an intramolecular Heck coupling [40].

The increased stability of palladium salts when combined with coordinating ligands such as these sterically demanding phosphines helps suppress the precipitation of Pd which results in deactivation whilst also improving catalyst efficiency. An example of this has been demonstrated with the application of a cyclometalated dimeric Pd (II) complex (Figure 1.2) in the Heck reaction between bromobenzaldehyde and butyl acrylate (Scheme 1.4) [32, 41]. This catalyst successfully affected the reaction achieving a TON of 200,000.

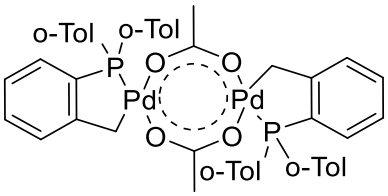
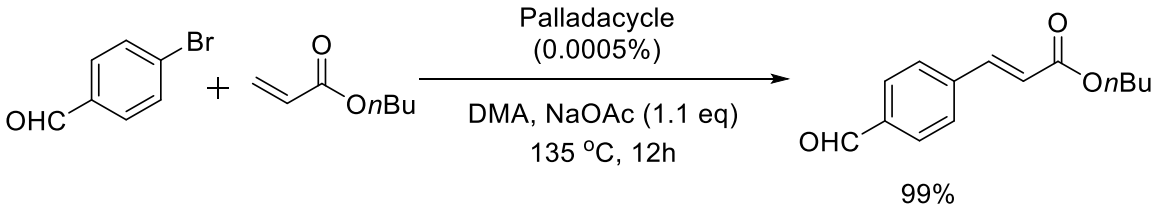


Figure 1.2: Pd(II) palladacycle utilised by Herrmann for the Heck reaction [32, 41, 42].

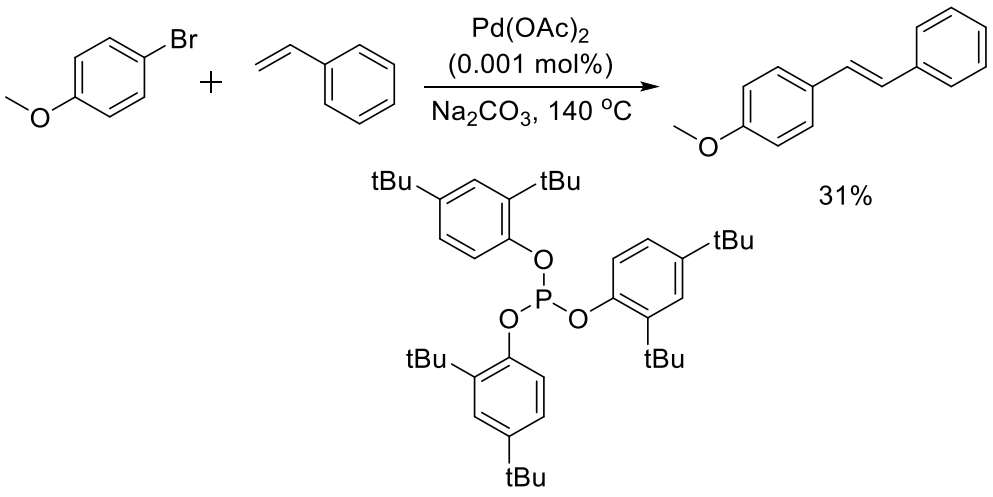


Scheme 1.4: First example of a palladacycle used in the Heck reaction developed by Herrmann and Beller [41].

Not only do phosphines stabilise the palladium catalyst but they also play an important role in the activation of palladium in the Heck reaction, which has been the focal point of a series

of studies conducted by Amatore et al. [43-46]. The reduction of $Pd(OAc)_2$ to a zerovalent palladium complex is an essential step in the catalytic cycle [43]. However, there had been some speculation as to which reagent was responsible for reducing the palladium from Pd^{II} to Pd^0 [44]. Using ^{31}P NMR spectroscopy and cyclic voltammetry, Amatore et al presented evidence that triphenylphosphine was responsible for the intramolecular reduction. It was later found that halide and acetate ions from the palladium precursors $PdCl_2$ and $Pd(OAc)_2$ can also independently influence the rate of oxidative addition of the catalytic palladium species [45, 46]. This highlighted that not only does the ligand for the palladium catalyst dictate the efficiency, but the palladium precursor and its associated anions also play an important role in catalyst activity.

Phosphite ligands for palladium have also been described to catalyse activated aryl bromides with catalyst concentrations as low as 0.001 mol% (10 ppm) with TON's reaching 31,000 (Scheme 1.5) [47]. The optimised conditions for the Heck reaction with phosphite ligands require an excess of ligand to palladium ratio - from 10:1 to 100:1 - depending on the substrate. Heck coupling with aryl chloride substrates can also be effected using phosphite ligands; however, harsher conditions (160 °C) and lower yields (15%) were achieved. Although phosphites are cheaper than phosphine ligands, their catalytic activity were not benchmarked against other ligands in this communication. Indeed, despite myriad of ligands which have been reported for the Heck reaction [48], the lack of benchmark reactions (against PPh_3 or ligandless conditions) impedes an objective comparison between the catalytic activities.



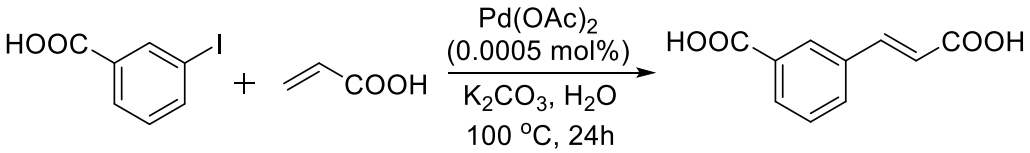
Scheme 1.5: The Heck reaction of 4-bromoanisole and styrene catalysed by Pd with the phosphite ligand – tris(2,4-di-*t*-butylphenyl) phosphite [47].

Additionally, while phosphine ligands clearly have their merits for the Heck reaction, they also have certain drawbacks, such as: being costly, toxic and air-sensitive. These aspects restrict their applications on process and industrial scales, as their toxicity and economic burdens often overshadow the use of palladium itself.

1.3 Ligandless Systems

In Heck's original work, simple palladium pre-catalysts such as $Pd(OAc)_2$ were frequently used on their own, without the addition of any ligands. Indeed, high TON's in the order of 10^5-10^6 can be achieved, particularly for reactions involving aryl iodides and aryl bromides, with electron-deficient alkenes, such as acrylates [21]. A key focus of this thesis is to understand the speciation and kinetics of Pd species during the Heck reaction in the absence of any ligands.

In 2000, Beletskaya and Cheprakov published a seminal review of the Heck reaction where the phrase 'homeopathic doses' was first coined to define reactions which occur in the presence of extremely low quantities of catalysts [49]. This was demonstrated by using 0.0005 mol% (5 ppm) of $Pd(OAc)_2$ in an aqueous media with 2-iodobenzoic acid and methyl acrylate, which proceeded to full conversion, equating to a TON of 200,000 (Scheme 1.6).

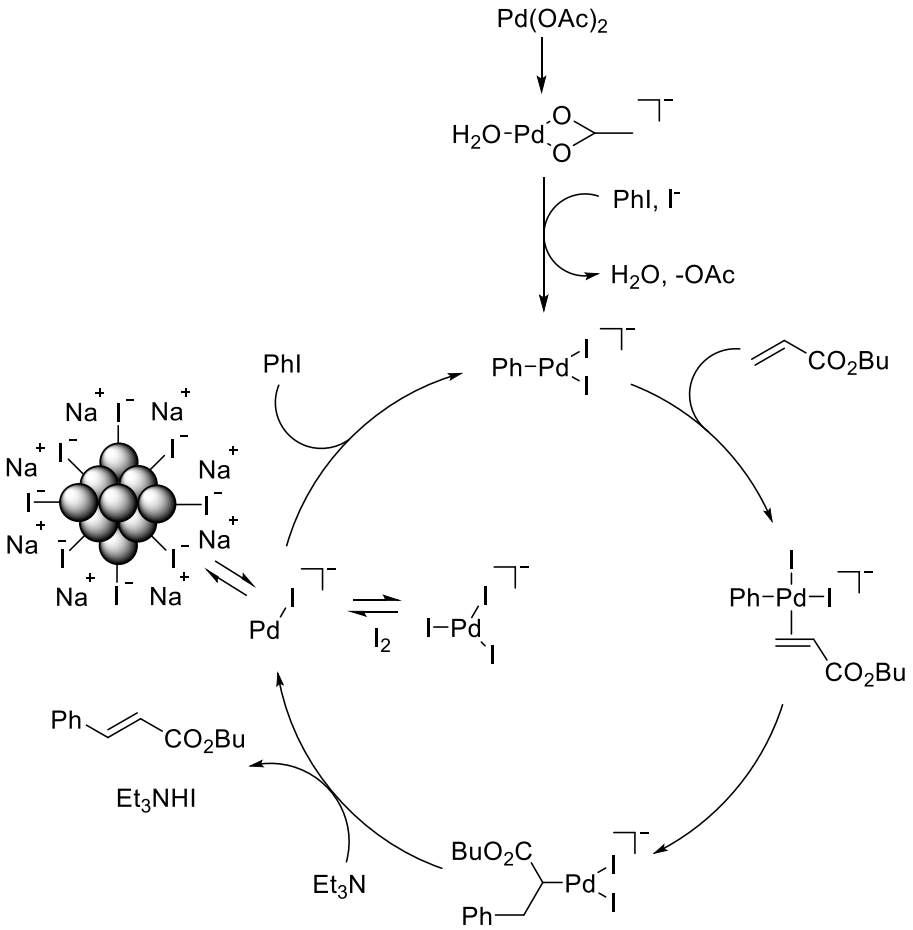


Scheme 1.6: The Heck reaction of 2-iodobenzoic acid with propanoic acid under 'homeopathic dose' of Pd [49].

De Vries and co-workers investigated the speciation and recyclability of a ligand-free Heck reaction between iodobenzene and *n*-butyl acrylate catalysed by $Pd(OAc)_2$ in the presence of sodium halide additives [50]. They observed the formation of Pd black in all reactions, whether full conversion was achieved or not, when using a catalyst loading of 0.2 mol%. However, with the addition of iodine or bromine the catalyst was re-activated and gave full conversion for three successive runs. Additionally, in their studies MS (ESI-) was used to identify the formation of Pd anionic complexes during the catalysed reaction. During the

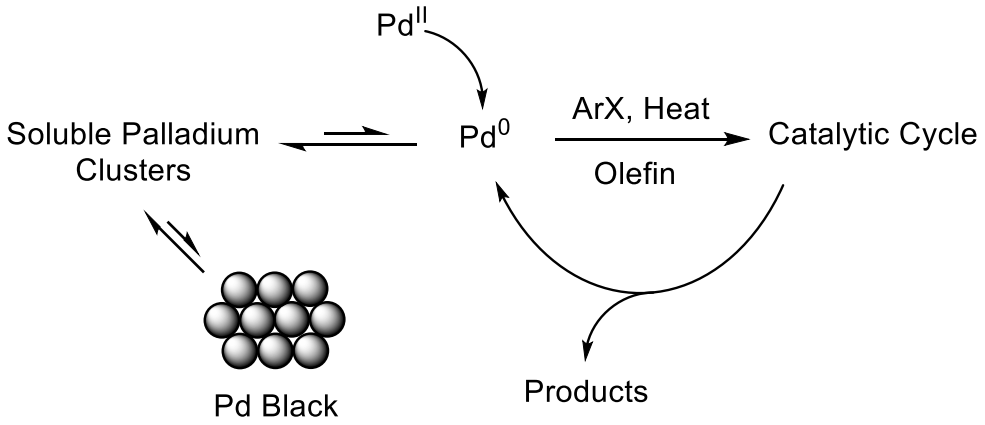
initial phase of the reaction the Pd^0 species $[(H_2O)PdOAc]^-$ was observed whilst the Pd^{II} species $[ArPdI_2]^-$ and $[PdI_3]^-$ were observed at higher conversions (>5%).

Based on these observations, de Vries and co-workers proposed a catalytic cycle (Scheme 1.7), the $[(H_2O)PdOAc]^-$ species is proposed as the catalytically active species that undergoes oxidative addition step. Following the series of migratory insertion and β-hydride elimination to afford the product, the $[PdI]^-$ species can: (1) form off-cycle nanoparticles which leads to the precipitation of Pd black, (2) form off-cycle $[PdI_3]^-$ or (3) undergo oxidative addition with another molecule of iodobenzene, to restart another catalytic turnover. As the rate of oxidative addition is favoured for aryl iodides, the catalytic cycle proceeds thus reducing the off-cycle events such as (1) and (2). However, once the substrates have been consumed, the off-cycle events predominate and aggregation of Pd is observed in the form of palladium black. Initial conditions such as starting the reaction with a high substrate to catalyst ratio can cause these detrimental off-cycle aggregation events to occur more readily.



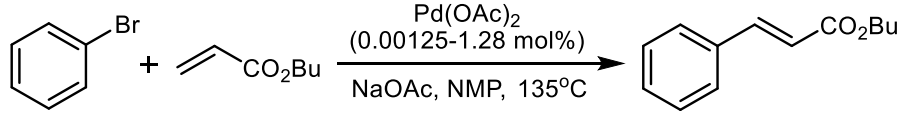
Scheme 1.7: De Vries' proposed catalytic cycle for the ligandless Heck reaction, adapted from reference [50].

Conversely, aryl bromides present a different case to aryl iodides as the rate of oxidative addition is slower, this leads to the palladium accumulating in the form of Pd^0. Now the off-cycle aggregation event becomes a competing process with the catalytic cycle (Scheme 1.8). Once the aggregated Pd surpass a certain size they will form inactive Pd black, stopping the reaction prematurely [51].



Scheme 1.8: Proposed mechanism of aggregation and deactivation for Pd species under ligandless conditions, adapted from reference [51].

It was found by de Vries et al. that the reaction of bromobenzene with butyl acrylate proceeds at its optimum with catalyst loadings of $Pd(OAc)_2$ between 0.1 and 0.01 mol% (Scheme 1.9) [51]. $Pd(OAc)_2$ loadings outside of this range gave lower yields. This supports the theory that by lowering the substrate to catalyst ratio the rate of aggregation is suppressed for aryl bromides [51, 52]. De Vries and co-workers found that below the catalyst loading of 0.01 mol% the aggregation of Pd can be effectively eliminated, due to the infrequency of collisions between palladium particles. However, higher temperatures and longer reaction times are required for the reaction to reach maximum TON due to the low catalyst loading. On the other hand, above the catalyst loading of 0.1 mol%, aggregation of the active palladium species is observed via the formation of palladium black. This is the reason for the early termination of the catalytic process at higher catalyst loadings.



Scheme 1.9: The Heck reaction between bromobenzene and *n*-butyl acrylate at 135 °C in NMP [51].

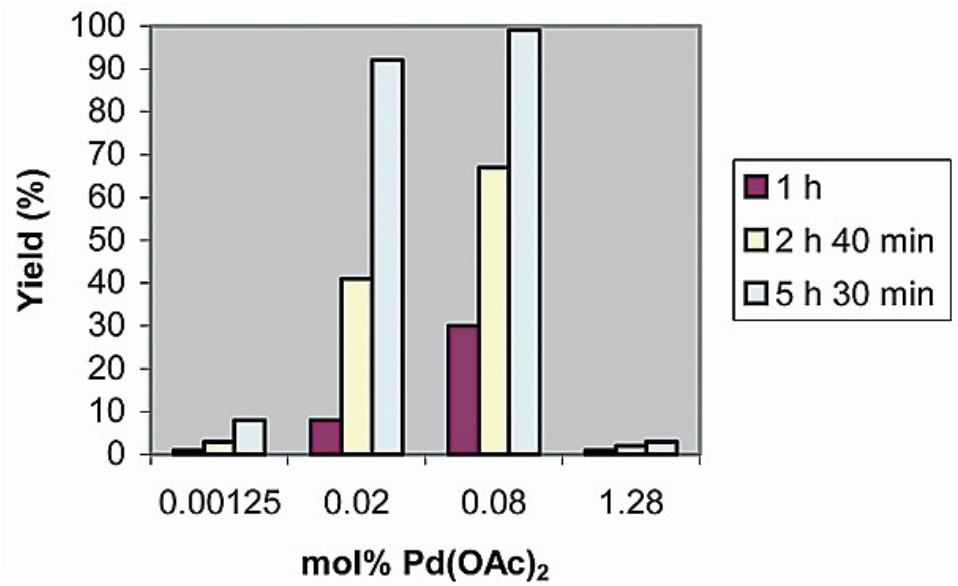


Figure 1.3: $Pd(OAc)_2$ loading vs yield (%) highlighting the optimum substrate to catalyst ratio for the reaction of bromobenzene and *n*-butyl acrylate [51].

The yields for the reaction conducted at four different catalyst loadings was presented by de Vries and co-workers at three different time points: 1 h, 2 h 40 min and 5 h 30 min (Figure 1.3). [51] As the TON's were not reported in the paper, they were estimated from Figure 1.3 to be 4750 for 0.02 mol% and 1250 for 0.08 mol% $Pd(OAc)_2$ loading (assuming 95% and 100% conversions after 5 h 30 min respectively). The TOF and activity of the catalyst were also not reported but were calculated from the estimated TON's to be 14.4 min^{-1} and 3.8 min^{-1} for 0.02 mol% and 0.08 mol% after 5 h 30 min respectively. This aligns with the take home message from the paper being 'the lower the [Pd] the higher the TOF's'. The statement 'the lower the [Pd] the higher the TOF's' also holds true when deviating below the concentration of 0.02 mol% as the TON for 0.00125 mol% is estimated to be 6400 from Figure 1.3, converting to a TOF of 19.4 min^{-1} which is impressive but too slow to be practical as only 8% yield was achieved in 5.5 h at 135 °C. The results were dubbed as a homeopathic effect by de Vries for aryl bromides [53]. Using ES-MS a $PdBr_3^-$ species was detected, as this is a monomeric species it can be inferred that it will be more stable at lower catalyst concentrations which will account for the homeopathic effect [51].

Indeed, de Vries was not the only one to report the reaction of aryl bromides with olefins using 'ligandless' conditions with the pre-catalyst $Pd(OAc)_2$. The reaction between bromobenzene and styrene was shown to convert with high TON's reaching 38,500 with

careful consideration of the base [54]. The highest activity was achieved when K_3PO_4 was used as the base producing 95% conversion after 44h in DMA at 140 °C with only 0.00247 mol% (25 ppm) of $Pd(OAc)_2$ needed. There was no detectable conversion when Et_3N was used as the base under the same conditions but with 0.1 mol% (1000 ppm) of $Pd(OAc)_2$, further highlighting improved reaction rates when the catalyst loading is lowered.

1.4 'Cocktail' Type Catalyst Systems

The formation of palladium black is a well-known pathway for catalyst deactivation in both ligand-enabled and ligandless systems. Understanding this phenomenon is important to develop highly active Pd catalysts and more efficient catalyst systems by preventing deactivation. In 2017 Ananikov and Eremin reviewed the aggregation of metal species in homogeneous systems and proposed various process for the growth of nanoparticles [55]. These proposed processes are 1) orientated attachment 2) atom by atom attachment and 3) hybrid growth (Figure 1.4). The formation of metal clusters by oriented attachment leads to clusters of specific morphology with a narrow particle size distribution. With atom-by-atom growth, a wider particle size distribution is obtained with irregular morphologies, whilst hybrid growth is a combination of both oriented attachment and atom-by-atom growth.

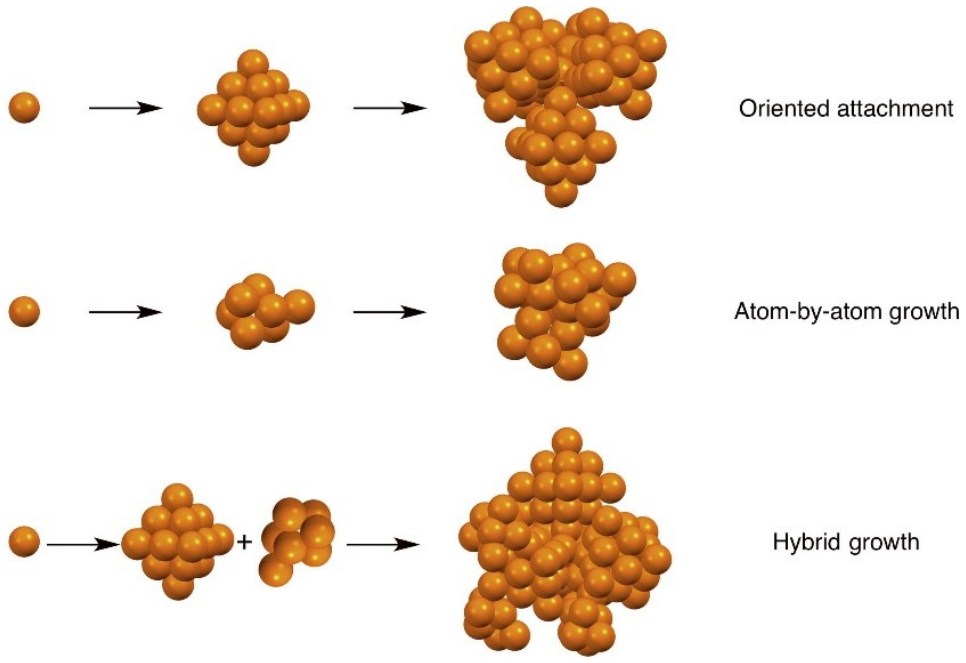
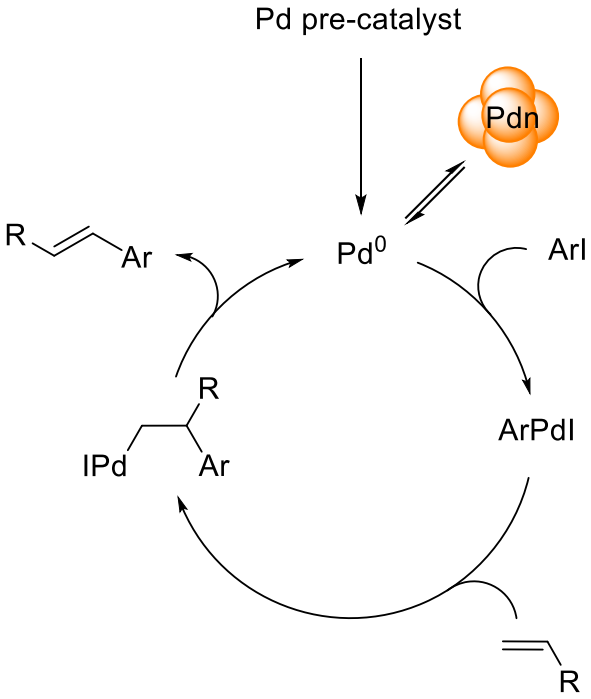


Figure 1.4: Formation of Pd nanoparticles from soluble Pd species [55].

The transformation of the catalyst throughout the reaction can lead to a diverse range of palladium complexes, clusters and nanoparticles which can be defined as:

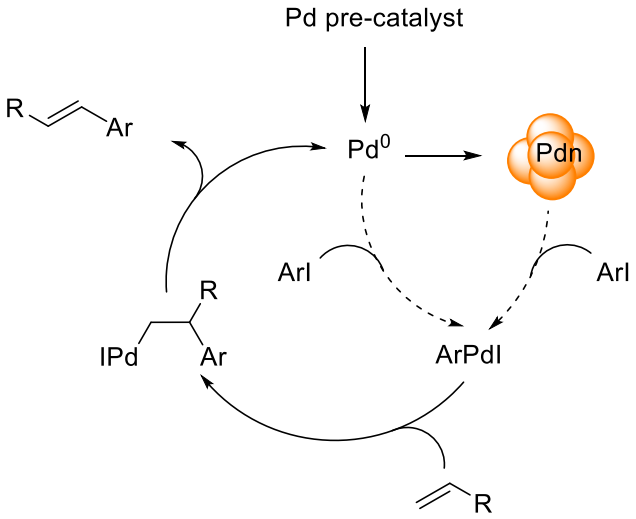
- Palladium complexes – Pd particles co-ordinated to other soluble species (e.g. ligands, reactants or solvent).
- Palladium clusters – Clusters of defined particle sizes, structure and chemical composition.
- Palladium nanoparticles – Particles of less precise sizes and characterisation which are larger than one nanoparticle in size.

The consequences of such a diverse catalyst system raised the question of what the active species may be. Ananikov and Eremin described catalytic systems consisting of a homogeneous and heterogeneous nature as a catalyst 'cocktail' where the catalyst resides in various forms [55]. Although not all of the species are proposed to be catalytically active in the 'cocktail', each species still plays a major role in the reaction. Beletskaya et al have reported a phosphine free Heck reaction where nanoparticles act as reservoirs for the catalytically active species [55]. The conclusion that nanoparticles are involved in the catalytic cycle was drawn from a positive mercury poisoning test. It was then proposed that the nanoparticle reservoirs form, when the rate of Pd^0 released from the pre-catalyst is faster than the net rate of the reaction. The nanoparticles are then able to release some of the active palladium back into the catalytic cycle by a dissolution process. As the nanoparticles can form soluble Pd species, the deactivation process is delayed, as an equilibrium is reached preventing the nanoparticles from precipitating out of solution. Instead, the aggregation process is halted at the nanoparticle stage as they are stabilised by anions liberated from the reaction (Scheme 1.10).



Scheme 1.10: Simplified catalyst cycle involving nanoparticle behaving as an off-cycle reservoir. Recreated from the literature [56].

Beletskaya et al. could not rule out the possibility that there can also be a system where there are several types of active species, which make comparative contributions to the product formation (Scheme 1.11). In this scenario, the Pd nanoparticles participate in the reaction cycle through the oxidative addition step. It is thought that mononuclear species are cleaved from the nanoparticle rather than the process occurring on the surface of the nanoparticle. In each of the two proposed scenarios, the involvement of nanoparticles is due to the instability of Pd^0 species. At higher concentrations of catalyst, the agglomeration of Pd^0 is driven by the thermodynamic preference for a more stable system. However, at low catalyst concentrations, the mononuclear pathway is expected to dominate, as the concentration of Pd^0 species is too low to allow nucleation and the formation of nanoparticles.

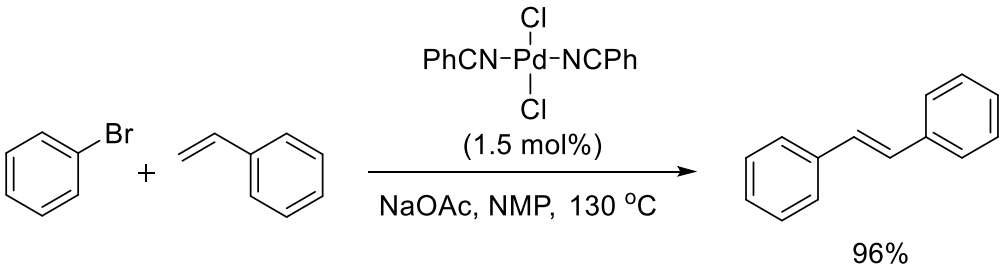


Scheme 1.11: Simplified catalyst cycle involving nanoparticles proposed by Beletskaya et al. recreated from the literature [56].

Detecting the formation of clusters and nanoparticles is routine but determining their catalytic contribution is less trivial. Kinetic experiments and various other techniques such as modelling can be applied to distinguish between these possible scenarios.

Reetz and Westermann undertook a mechanistic study to find out the role of nanoparticles in a phosphine-free Heck reaction [57]. The reaction between styrene and bromobenzene catalysed by $PdCl_2(C_6H_5CN)_2$ (1.5 mol%) was conducted in NMP (Scheme 1.12). Aliquots of the reaction were taken periodically and analysed with both gas chromatography (GC) and transmission electron microscopy (TEM) to correlate the reaction profile with the formation and size of the nanoparticles formed. A sigmoid reaction profile was obtained from reaction aliquots analysed by GC (Figure 1.5). The samples were directly deposited on carbon film coated TEM grids by dip-coating, with no workup step, so that the TEM images can offer the presence of Pd NP "*in situ*". TEM analysis of these samples revealed the presence of Pd NP's with an average particle size distribution of 1.6 nm throughout the reaction. The reaction profile has an induction period (40 mins) and only after this period were nanoparticles detected in the extracted samples. Based on this evidence, the authors suggest that the reaction is initiated once the nanoparticles have been formed and are therefore catalytically active. However, relating this to the earlier study by Beletskaya, the most likely catalyst pathway would be where the nanoparticles are directly involved in the catalysis, as shown in Scheme 1.11. Considering that the reaction with $PdCl_2(C_6H_5CN)_2$) is not conducted with a

particularly low catalyst loading (1.5 mol%), the formation of nanoparticles is to be expected under ligand-free conditions. Instead, the sigmoid curvature of the graph in Figure 1.5 could be explained by a slow dissociation of Pd^0 from the pre-catalyst rather than formation of active nanoparticles.



Scheme 1.12: Reaction of bromobenzene and styrene catalysed by $PdCl_2(C_6H_5CN)_2$ in NMP [57].

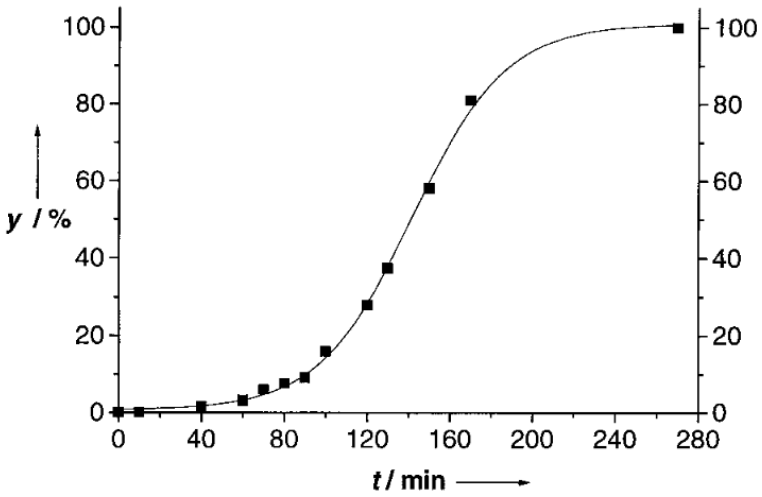
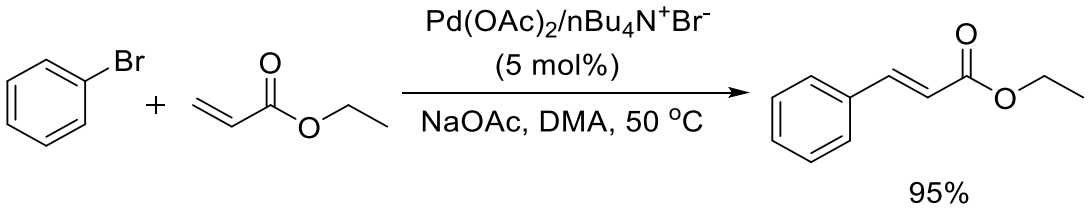


Figure 1.5: Plot of yield (y) vs time (t) for the reaction of bromobenzene and styrene [57].

A separate study was also conducted by Reetz and Westermann by using palladium acetate (5 mol%) as the catalyst for the reaction between iodobenzene and ethyl acrylate under Jeffery's conditions (NaOAc, $n Bu_4N^+Br^-$) in DMA (Scheme 1.13) [57]. In this case, the reaction is initiated with a much shorter induction period (Figure 1.6). Yet, the average particle size detected by TEM was still found to be ca. 1.6 nm in every reaction aliquot extracted. This evidence led the authors to suggest that particles of this size are active and stable in the phosphine free Heck reaction. Despite this key discovery correlating the nanoparticle size to the reaction profile, the kinetics of the nanoparticle formation is still undetermined.



Scheme 1.13: Reaction of bromobenzene and ethyl acrylate catalysed by $Pd(OAc)_2$ under Jeffery conditions in DMA [57].

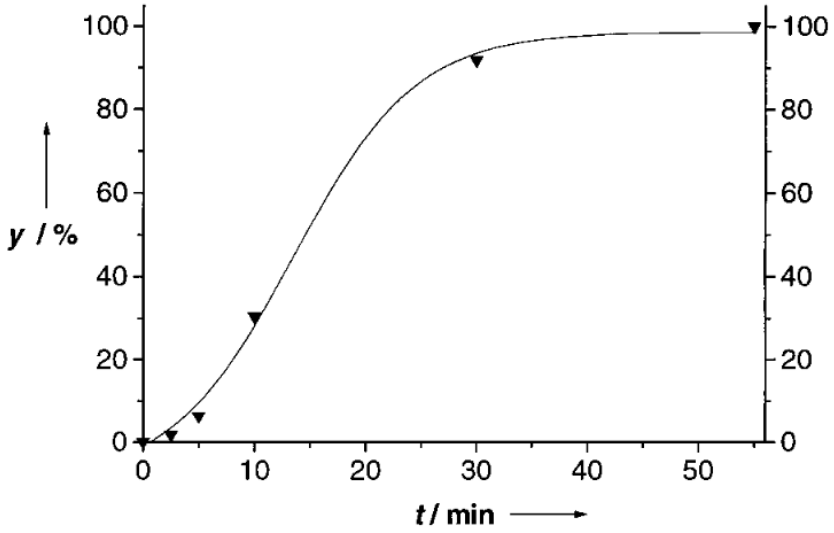


Figure 1.6: Plot of yield (y) vs time (t) for the reaction of bromobenzene and ethyl acrylate catalysed by $Pd(OAc)_2$ [57].

Work by Bera et al. synthesised a bimetallic palladium complex bridged by two amide-linked naphthyridine ferrocene ligands, which was utilised as a catalyst for the Heck reaction (Figure 1.7) [58]. The high TOF's observed for the coupling between electron deficient aryl bromides with styrene subsequently led the authors to proposed that catalysis occurs on the bimetallic platform, even though this was not supported by any kinetic studies.

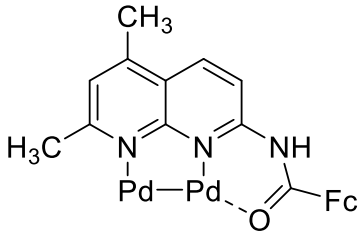
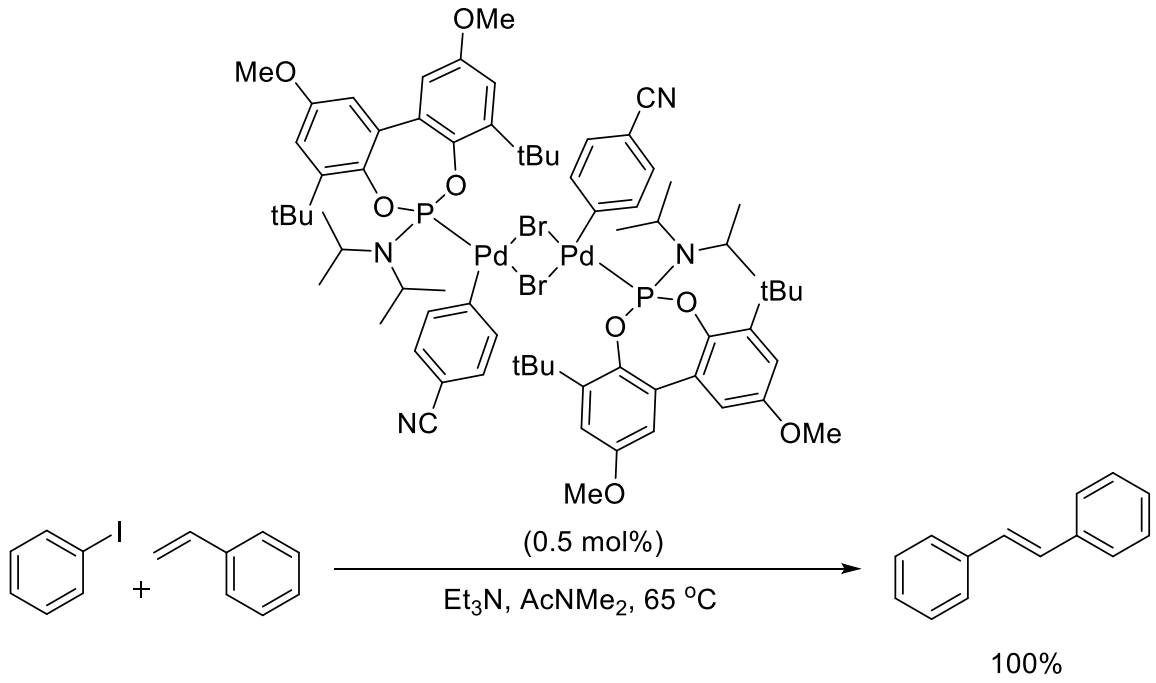
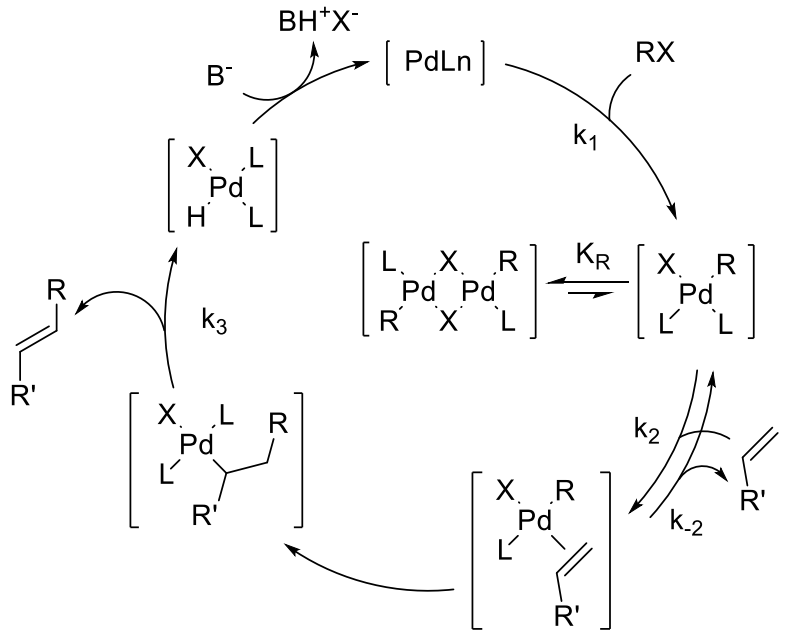


Figure 1.7: Co-ordination of a dipalladium (I) complex incorporated with a ferrocene group (Fc) from reference [58].

The involvement of an *in situ* generated dimeric catalyst was also proposed by van Leeuwen and co-workers, based on the observation of a nonlinear dependence of the reaction rate on Pd concentration [59]. A palladacycle catalyst (0.5 mol%) was employed for the reaction between iodobenzene and styrene in acetonitrile (Scheme 1.14). Using the initial rates method, the reaction rate was found to have half order dependence on the catalyst, which was attributed to the formation of an off-cycle dimeric species. Iodobenzene and triethylamine were found to have a zero-order dependence in the reaction and styrene has a first order in the initial reaction turnovers. Based on the kinetic data, a catalyst cycle was proposed for this system (Scheme 1.15).



Scheme 1.14: The Heck reaction studied by Van Leeuwen between iodobenzene and styrene catalysed by a palladacycle catalyst [59].

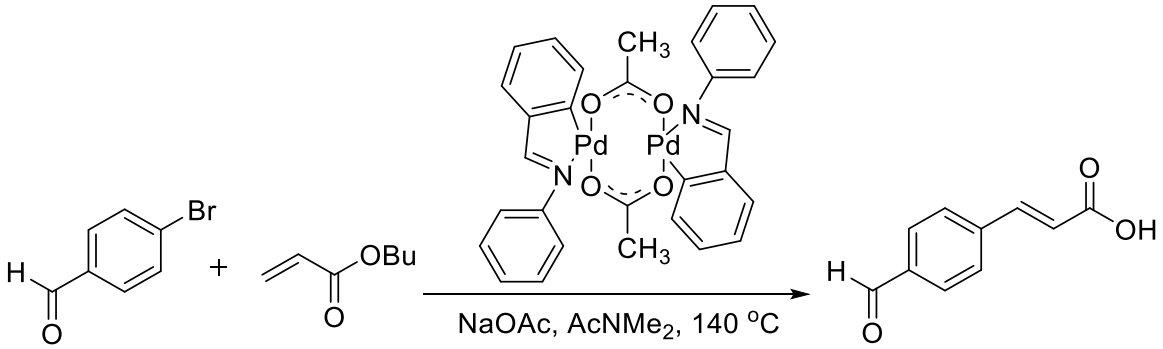


Scheme 1.15: Proposed catalytic cycle for the Heck reaction involving a dimeric off cycle species recreated from ref [59].

As the reaction rate is independent of iodobenzene concentration, the oxidative addition step (k_1) is deemed not to be the RDS in this case. However, the reaction is first order with styrene which means that either the alkene complexation (k_2) or migratory insertion step is the rate limiting step. As a result, the catalyst resting state will be the step prior to the alkene complexation which is the oxidative adduct. Whilst in this resting state it is proposed, based on the half order dependence on catalyst concentration, that the Pd forms an off-cycle dimer. However, as the initial rates method was used to determine the reaction orders, the rest of the reaction profile was disregarded, which could have implications as to what the actual catalyst resting state is.

Blackmond and co-workers have also investigated the kinetics of a dimeric palladacycle catalyst in the Heck reaction between *p*-bromobenzaldehyde and butyl acrylate (Scheme 1.16) [60]. In this work, the entire course of the reaction was monitored using *in situ* calorimetry which was further correlated with samples analysed by GC. By performing the reaction at different catalyst loadings (0.08, 0.04 and 0.02 mol%), it was found that the reaction did not follow first order kinetics; the order in Pd was between half and first order. Steady state treatment of the elementary steps in Scheme 1.15 was used to form a reaction rate expression. Despite the use of an aryl bromide, the rate limiting step was proposed to be

either the complexation or insertion of the olefin. The data obtained from the reactions was used for kinetic modelling, which revealed that the majority of Pd resides outside of the catalytic cycle as a dimer species, which interconverts to an active monomeric Pd species. It was also shown that catalyst TON increased with lower catalyst loadings which is indicative of a system which proceeds via a monomeric species and supports the homeopathic effect reported by de Vries [51, 52].



Scheme 1.16: The Heck reaction between bromobenzaldehyde and butyl acrylate catalysed by a palladacycle [60].

Burés independently applied variable time normalisation analysis (VTNA) to uncover the order in catalyst for the reaction presented by Blackmond and co-workers in Scheme 1.16 [61]. The method works by normalising the total catalyst concentration with time and rising it to a power which represents the order with respect to catalyst. Due to the equilibrium between the monomer and the dimer, the total Pd concentration is not linear to the active monomer species and therefore catalysts order depends on the catalyst's concentration. It was found that at lower concentrations the catalysts order tends to 1 whilst at concentrations between 0.5-1 mol% the order tends to 0.55. This reflects the observations made by Blackmond and co-workers of higher TON with lower catalyst loading. Catalyst orders of close to 0.5 therefore reflect that most of the catalyst resides as an inactive dimer, as proposed earlier by van Leeuwen and co-workers.

Rothenberg et al. used *in situ* FT-NIR spectroscopy and GC to monitor the Heck reaction of iodobenzene with *n*-butyl acrylate in NMP using a catalyst loading of 1 mol% with Pd black being observed [62]. The subsequent reaction profiles were fitted to kinetic models to investigate the speciation of a palladium catalyst co-ordinated with phosphoramidite ligands (Figure 1.8). The resulting reaction profile displayed an induction period which was proposed

to be influenced by the monomer-dimer equilibrium of the catalyst (Figure 1.9). Using the reaction data, a kinetic model was constructed to account for the catalyst's equilibrium. The model was developed with a Pd monomer, a dimer, reactants, product and a deactivation step. This was to ensure that the model is kept simple, and chemically relevant, all deactivation events regardless of the Pd species was confined to one deactivation step. The best fit of the model with the reaction profile was achieved when the dimer is modelled as inactive and acts as a reservoir for an active monomeric species. From these results it was proposed that the induction period is influenced by the monomer-dimer equilibrium of the catalyst. If the reaction were to be run at lower catalyst loadings it would be interesting to see if the deactivation step would still have a role or any contribution in the model.

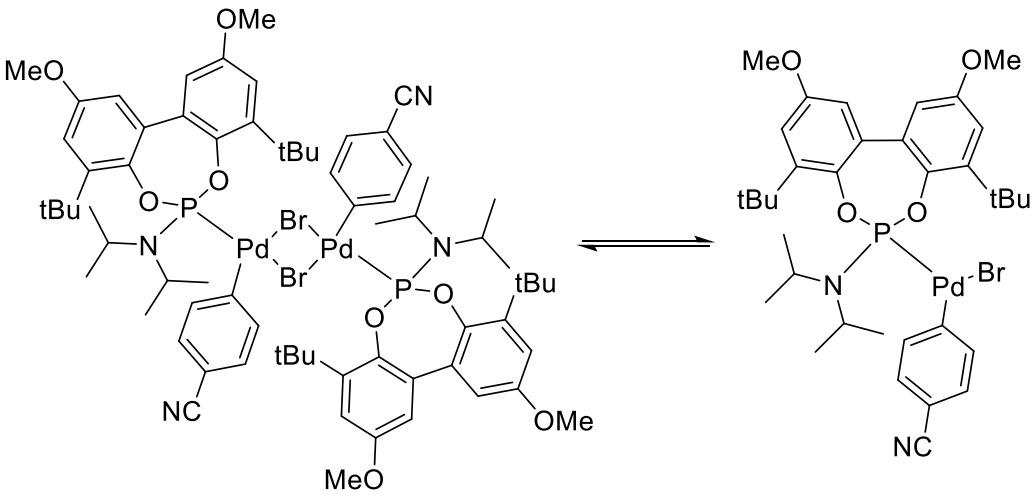


Figure 1.8: Monomer and dimer interconversion of the phosphoramidite Pd precursor recreated from reference [62].

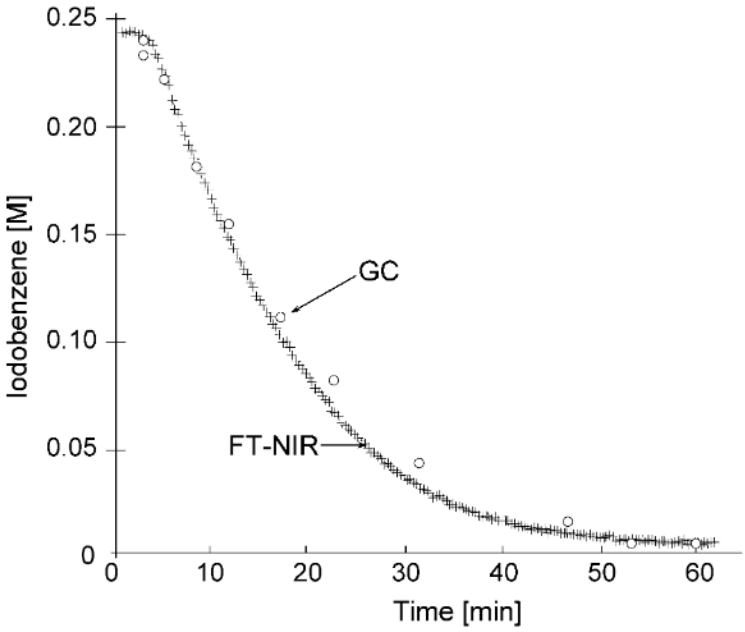


Figure 1.9: Reaction profile obtained using the phosphoramidite Pd precursor as a catalyst for the reaction of iodobenzene with *n*-butyl acrylate in NMP [62].

1.5 Conclusion

A common theme throughout the literature for homeopathic reactions is that they are usually conducted using aryl iodides with acrylates in DMF at high temperatures. Turnover numbers in excess of 100,000 are frequently achieved in these systems with simple Pd salts [21, 49, 54]. Yet the literature is overwhelmed by the popularity and desire to discover and utilise ligands in these Heck reactions.

In comparison, corresponding reactions which employ ligands display turnover numbers in the region of 10,000 [21, 47] which are much lower than their ligandless counterparts. This makes the ligandless Heck reaction a very interesting system to study. A lot of previous studies with phosphine ligands have been conducted but investigations into the origin of the high TON's exhibited in ligandless systems are very sparce and are not well known which is why they have been investigated and addressed in this thesis.

Chapter 2. Heterogeneous Catalysed Heck Reactions

2.1 Homogeneous vs Heterogeneous Catalysis

A comparison of the advantages and disadvantages of homogeneous and heterogeneous catalysis is provided in Table 2.1. A major drawback of homogeneous catalysts is the complexity involved in recycling and re-using them for successive reactions, something which is avoidable with heterogeneous catalysts. The ease of removing a heterogeneous catalyst from a reaction mixture is one of the numerous advantages of heterogeneous catalysis that is widely exploited by the chemical industry [63]. This coupled with high thermal and pressure stability increases the robustness of heterogeneous catalysts which is why they have been conveniently employed in a variety of industrial process from ammonia synthesis to cracking.

Table 2.1: Comparison between the main advantages/disadvantages of homogeneous and heterogeneous catalysis.

	Homogeneous	**Heterogeneous**
Advantages	- High selectivity - High reproducibility - Well-defined active sites	- Easy separation and catalyst recovery - High thermal and pressure stability - Simple recycling
Disadvantages	- Difficult and expensive separation - Low temperature stability - Expensive recycling	- Lower selectivity - Difficult to define active sites - Surface leaching and poisoning
Examples of industrial applications	- Terephthalic acid (Precursor to PET) - Acetic acid	- Harber-Bosch NH_3 synthesis - Fisher-Tropsch process - Cracking

However, a major downfall of heterogeneous catalysts is when the catalyst is lost into the reaction media. This is known as leaching, which eliminates the advantage of simple catalyst separation. Leaching also results in the loss of the active catalyst leading to reduced catalytic activity in terms of turnover numbers (TON) and turnover frequencies (TOF), as well as a contaminated batch/stream of product. The latter is a critical issue particularly for the

commercial viability of catalytic reactions for the production of active pharmaceutical ingredients (API's), as metal impurities are tightly regulated [64]. The aim of this section is to introduce ways to detect leaching, how leaching may occur, and catalysts designs to mitigate leaching.

2.2 Metal Scavengers

Homogeneous reactions catalysed by molecular Pd catalysts often require workup procedures. This results in an increased cost and poor efficiency, when compared with reactions catalysed by heterogeneous catalysts. The most common workup methods used in removal of residual catalysts from reaction mixtures include crystallisation, solvent extraction and chromatography. These methods often employ high temperatures and large quantities of solvents and materials (e.g. silica gel), which can limit their industrial application. In some cases, metal scavengers can be used to bind with, and precipitate, the catalyst to minimise contamination of the product [65]. Typically, polymer-based resins and silica supports are functionalised with Lewis-bases, such as amines and thiols, which can strongly bind to metal catalysts. Some commercially-available examples of these scavengers which are applicable for Pd removal are Silicycle's SiliaMetS-Thiol [66] and Johnson Matthey's Smopex-103 [67] amongst others (Figure 2.1). These scavengers bear a thiol group grafted onto a silica support and a triethylammonium group on a polymer-based resin respectively.

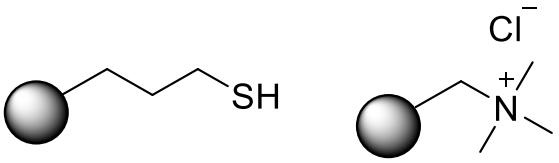


Figure 2.1: Chemical functionalisation of SiliaMetS-Thiol (left) and Smopex-103 (right).

There are some advantages to using silica-based scavengers over polymer-based resins, namely their mechanical stability, as resins can swell in certain organic solvents and break upon mechanical agitation [68]. However, one of the main limiting factors for the industrial scale use of scavengers for Pd removal is their associated cost.

2.3 Conventional Leaching Tests

Little is known about how catalyst leaching occurs, largely due to the lack of methods to observe the process; particularly *in situ*. Most of the experiments that are currently used to test catalyst leaching are either *ex situ*, destructive or invasive, which can only establish the presence of leaching, but not how it occurs. An established method for quantifying trace metals in APIs in industry is inductively coupled plasma (ICP) analysis [69]. Thus, many protocols have been established for assessing leaching as it can quantify the amount of metal residues present in the reaction products. There have been several other methods developed specifically to determine whether the leached catalyst is catalytically active or not. These methods are readily used to discount leaching for newly developed heterogenous catalysts.

1. Hot Filtration

Whilst maintaining reaction conditions, the reaction mixture is filtered once a set time point (or conversion) is reached during the reaction. The filtrate is then subjected to the reaction conditions with leaching being indicated by any observed catalyst activity. This method is relatively easy to execute. However, some homogeneous catalyst may be trapped or altered by the filter media which can skew the results. Another drawback is that hot filtration does not detect inactive leached species as it depends solely on detecting the presence of product formation [70].

2. Mercury Poisoning

Mercury is added to form an amalgam with the heterogeneous catalyst, deactivating it by blocking catalytically active sites [71-73]. The homogeneous portion, if present, will be unaffected and continue to catalyse the reaction. The activity of the leached species can be readily identified by the continuation of the reaction. In contrast, inhibition of a catalytic reaction after treatment with metallic mercury is typically considered to be evidence of a heterogeneous catalytic mechanism. This method depends on the leached species being catalytically active as inactive leached species will go undetected. There are also concerns with handling mercury due to its toxicity especially if it is to be used as a routine procedure. The test is also not applicable to all metal catalysts [74].

3. Three Phase Test

Three phases are present in the reaction: the heterogeneous catalyst, an immobilised reactant and a soluble reactant [75]. Product formation will only occur if there is leaching of an active catalyst as it will be able to react at the site of the immobilised reactant with the soluble reactant. Again, this method does not detect inactive leached species as it depends on monitoring the conversion of the reaction.

Three-phase tests are one of the most conclusive for the detection of intermediates in solutions as describe by Rebek [76, 77]. However, the way they are conducted are critical for correct interpretation. Typically for the Heck reaction, the aryl halide is tethered to an insoluble support to form one of the phases. The heterogeneous catalyst makes up the second phase which is immobilised on a different support to that of the aryl halide. The third phase comprises of the reaction media which contains all other reagents. It is here where the nature of the leaching, which will be discussed later, can have a critical influence on whether leaching is detected or not.

4. Microscopy

Electron microscopes such as scanning electron microscopy (SEM) and transmission electron microscopy (TEM) can sometimes be used as a complementary tool to identify leaching from a heterogeneous catalyst. By comparing images of the catalysts surface and morphology before and after the reaction, any significant changes can be detected and attributed to leaching [78]. Of course, this gives no indication on how the leaching may have occurred, whether it be chemical or mechanical.

The common limitation for the methods discussed in the above is that they can only, at best, identify the presence of leached active catalyst. This can lead to leaching being wrongly dismissed, particularly if the leached species are catalytically inactive. The ‘rate’ of catalyst leaching cannot be determined using these systems.

2.4 Mechanisms of Leaching

The application of the methods discussed in the previous section (2.3) frequently lead to catalyst leaching being wrongly dismissed if the leached species are inactive. For instance, the heterogeneous catalyst can continuously release homogeneous metal species to partake in the reaction. The heterogeneous catalysts are therefore acting as reservoirs of homogeneous particles. With the addition of a 'boomerang' mechanism at play, where the homogeneous particles redeposit onto the metal surface, leaching can easily be overlooked when assessing leaching using these methods.

For Pd-catalysed reactions that are performed in solution, typically cross-coupling reactions, there have been numerous papers and reviews over the years, where the identity of the 'true catalyst' for heterogeneous systems is hotly debated [55, 79-85]. Leaching plays a pivotal role in the interconversion of metal species through the course of a reaction which leads to a dynamic catalytic system. A mutual view on the mechanism of a heterogeneous catalyst leaching can be simplified to two major pathways (Figure 2.2). The first is an erosion process, where the coordination of solute species (solvent, reactant or ligand) with the metal surface particles leads to atom-by-atom detachment. The second leaching process is complete physical detachment of metal clusters or nanoparticles from the surface [82, 86].

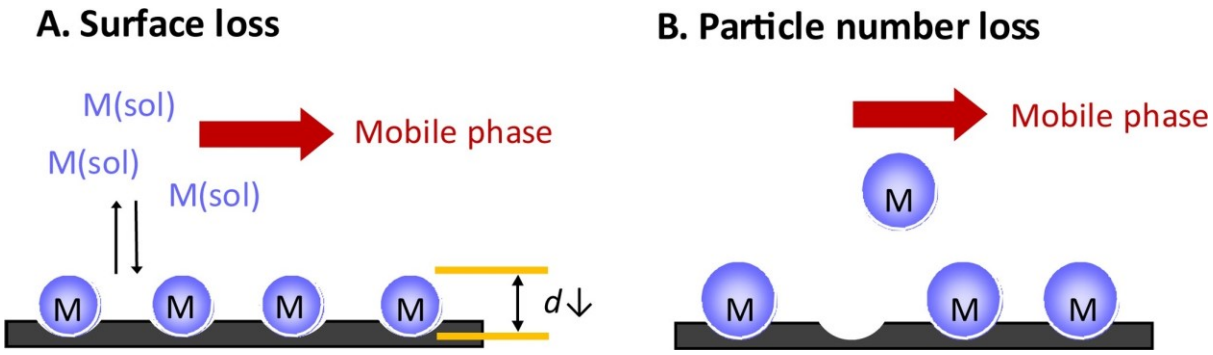


Figure 2.2: Atom by atom detachment and cluster displacement leaching processes reproduced from reference [86].

Further to the two mechanisms described in Figure 2.2, Ananikov and co-workers have proposed a more in-depth picture of what the leaching process may entail, where leaching is categorised into one of four processes: local leaching, leaching of soluble monometallic species, leaching of metal clusters and crushing/destruction of metal nanoparticles (Figure 2.3) [55].

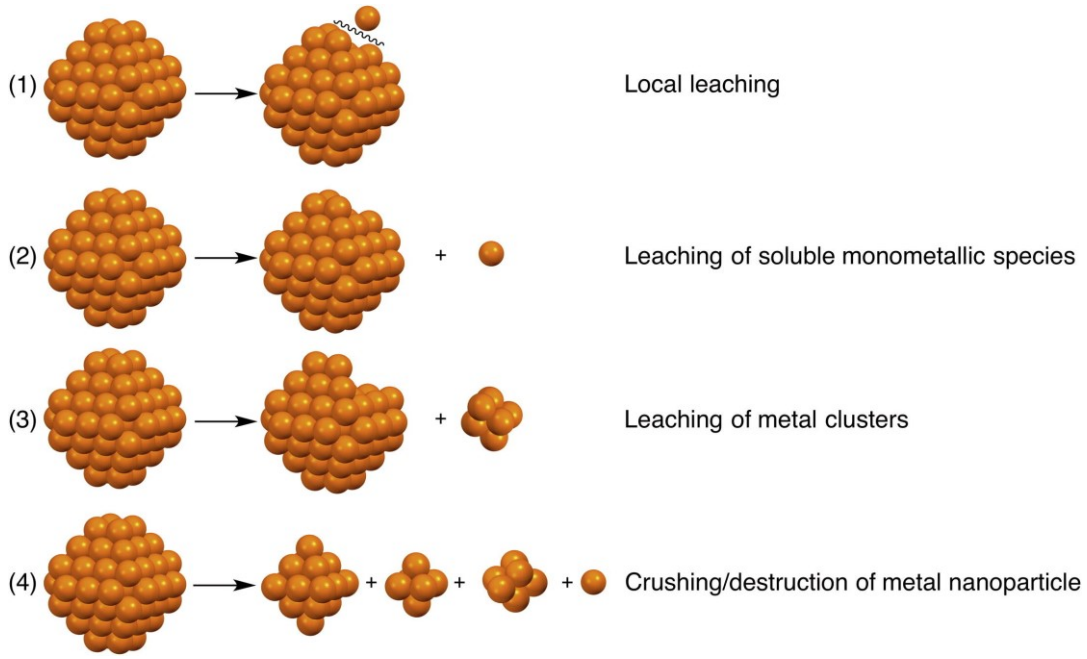


Figure 2.3: Local leaching, leaching of soluble monometallic species, leaching of metal clusters and crushing/destruction of metal nanoparticles. The figure is reproduced from reference [55].

Local leaching is a process which can occur during the reaction where a single atom detaches from the surface of the catalyst but does not leave its local surface site, i.e. it is not transferred to the bulk of the reaction solution. The cause of this leaching is associated with chemical interactions which would be caused by the solvent, ligand and even reactants. Once the cycle is complete, the atom redeposits onto the same particle at the exact same surface site which it originally leached from. As a result, the morphology will be retained, and minimal quantities of the metal will be detected in the liquid phase allowing this process to go undetected by imaging and ICP techniques. As local leaching is so difficult to prove, it is the focal point of many debates on what the true catalyst is for heterogeneous reactions and whether the species leached in this process are even catalytically active.

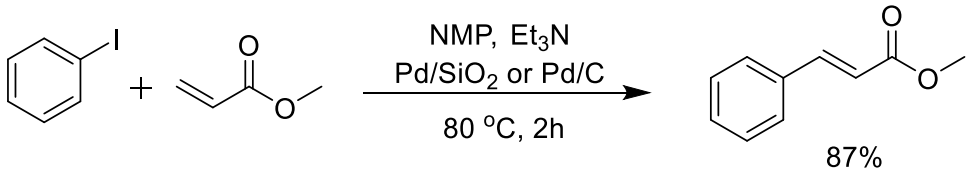
The second leaching process depicted is the solubilisation of a monometallic species. This process consists of a metal atom which has been detached from the catalyst and transferred to the bulk solution. It is a leaching process which can lead to a significant increase in TON from catalysis in the homogeneous phase. Similar to local leaching, the metal atom can redeposit back to the heterogeneous catalysts surface however this is unlikely to be the same site as to where it leached from. This allows for easier detection with imaging techniques due

to changes to the original catalysts' morphology. Since both processes of local leaching and solubilised monometallic share a redeposition step they are often grouped together and referred to more commonly as 'boomerang' catalysis.

The solubilisation of small metallic clusters is the third form of leaching depicted in Figure 2.3. In this mechanism, metal clusters are detached from the heterogeneous catalyst and transferred to the bulk of the reaction solution where they can contribute to the TON in the homogeneous phase. In this case, the electronic properties of the catalyst can be altered significantly through this process, leading to a change in catalytic activity. This change in activity can vary depending on the reaction conditions and how well the clusters are stabilised in the reaction media [87, 88].

The final type of leaching mechanism is the crushing and destruction of the catalyst particle (Figure 2.3). This occurs via different pathways during the activation of the catalyst, which leads to the breakdown of the macro structure to a variety of smaller clusters and atoms. This type of leaching can also be caused mechanically, whereby excessive stirring damages the solid catalyst. Leaching of this kind results in a wide variety of species in the homogenous phase of the reaction which can interconvert further. The homogeneous contribution from the latter three type of leaching can be detected with a combination of hot filtration tests and ICP analysis to unveil if the catalysts are active or inactive in the reaction.

In an effort to uncover the mechanism of leaching in the Heck reaction from the supported Pd catalysts Pd/SiO_2 and Pd/C, Zhao et al. demonstrated, in a series of papers [89-92], that coordination of the solvent (NMP) and/or Et_3N with Pd(0) forms a catalytically active homogeneous species. The Heck reaction between iodobenzene and methyl acrylate were used as a conventional starting point (Scheme 2.1).



Scheme 2.1: Reaction of iodobenzene with methyl acrylate with conventional supported palladium catalysts Pd/SiO_2 and Pd/C in the presence of NMP and Et_3N.

By using a combination of TEM, atomic absorption spectroscopy (AAS) and X-ray diffraction (XRD) it was shown that catalysis for these systems proceeded homogeneously (through leached species) with redeposition of the catalyst onto the surface. Using the recovered catalyst for subsequent reactions showed no loss in catalyst activity, leading to the proposal that the leaching mechanism includes a redeposition step. Figure 2.4 shows XRD patterns from before the reaction (solid line) and after the reaction (dashed line) indicating that the palladium (1 1 1) and (2 0 0) diffraction peaks became sharper and so the palladium particles grew after reaction. The instability of the leached species leads to redeposition of the Pd particles onto the surface sites of the catalyst with an accumulation on the bare support and the residual particles. However, other leaching process cannot be ruled out completely due to the detection, by AAS, of residual Pd (67 ppm) in the reaction mixture.

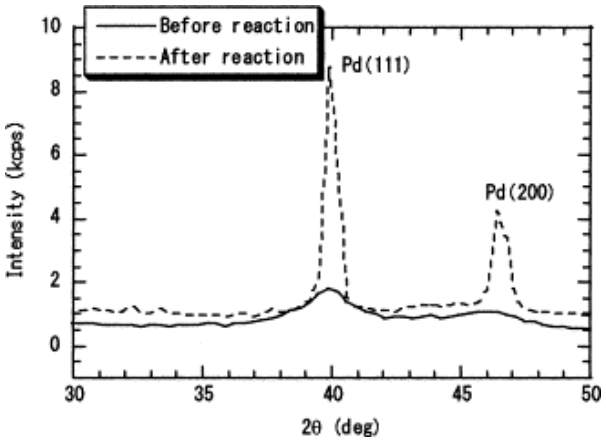
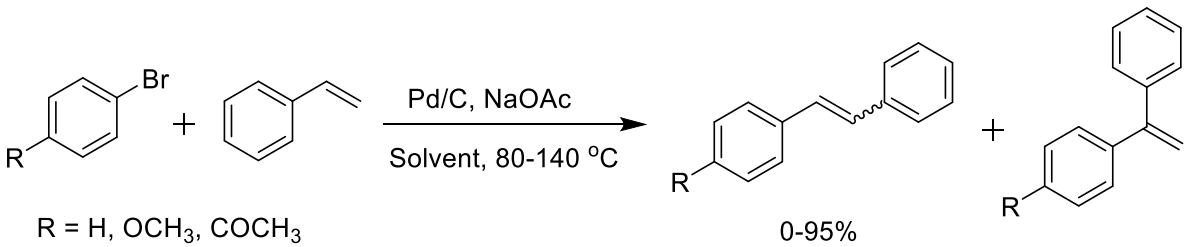


Figure 2.4: XRD of 10 wt.% Pd/C catalyst before and after the Heck reaction between iodobenzene and methyl acrylate at 160 °C in NMP. Reproduced from reference [92].

Using the Heck coupling between bromobenzene and styrene (Scheme 2.2) as a model reaction, Kohler and co-workers investigated twelve Pd/C catalysts varying in Pd dispersion, Pd distribution and oxidation state to uncover relationships between structure, activity and leaching [93, 94].



Scheme 2.2: Heck coupling between bromoarenes and styrene conducted in DMA, toluene or NMP.

By taking reaction aliquots during the reaction for GLC and ICP analysis the catalyst activity and leaching were determined as a function of time (Figure 2.5). It was shown that higher concentrations of Pd were found at the start of the reaction when the concentration of bromobenzene is at its highest, which also correlated to conversion of the reaction product. From these experiments they concluded that the leaching of Pd from the support is initiated by the aryl halide during the oxidative addition step. This result appeared to agree with an earlier report by Reetz et al [52], where the pre-treatment of a previously formed Pd colloid (average particle size 2.2 nm) with stochiometric amounts of iodobenzene was monitored by ^{13}C NMR and UV-Vis spectroscopy. The NMR spectrum showed a clear change in the aromatic region from that of iodobenzene, whilst UV-Vis spectroscopy revealed the continuous decrease of the broad plasmon band between 400-650 nm typical of transition metal colloids and a gradual increase in a peak at 450 nm [95]. The results obtained by Reetz et al suggest that Pd leaching was induced by the oxidative addition of iodobenzene. It was proposed that the formation of complexes such as ArPdI or $[ArPdI_3]^{-2}$ could give rise to these observations. These findings have implications on how the three-phase test should be conducted as the immobilised reactant could be one of the main initiators of the leaching process which never comes into direct contact with the heterogeneous catalyst.

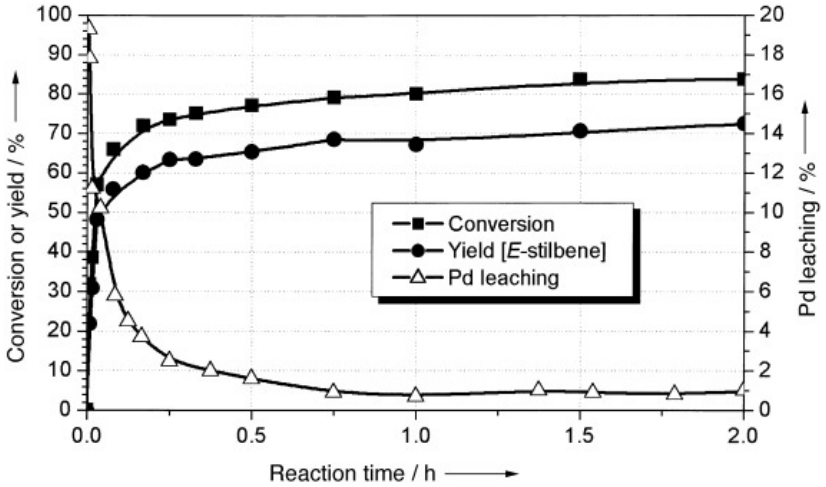


Figure 2.5: Investigation of activity and Pd leaching as a function of time for the Heck reaction between bromobenzene and styrene. The figure is reproduced from reference [94].

In a seminal review, Schmidt and Kurokhtina collated evidence of experimental methods used in distinguishing between homogeneous and heterogeneous mechanisms in the Heck and Suzuki coupling reactions [96]. They concluded that palladium leaching is caused by the

interaction of surface Pd with aryl halide, based on the theory that oxidative addition weakens the palladium-surface interaction. This is thought to result in a simultaneous palladium dissolution and agglomeration process, which may lead to the formation of Pd nanoparticles in solution (Figure 2.6).

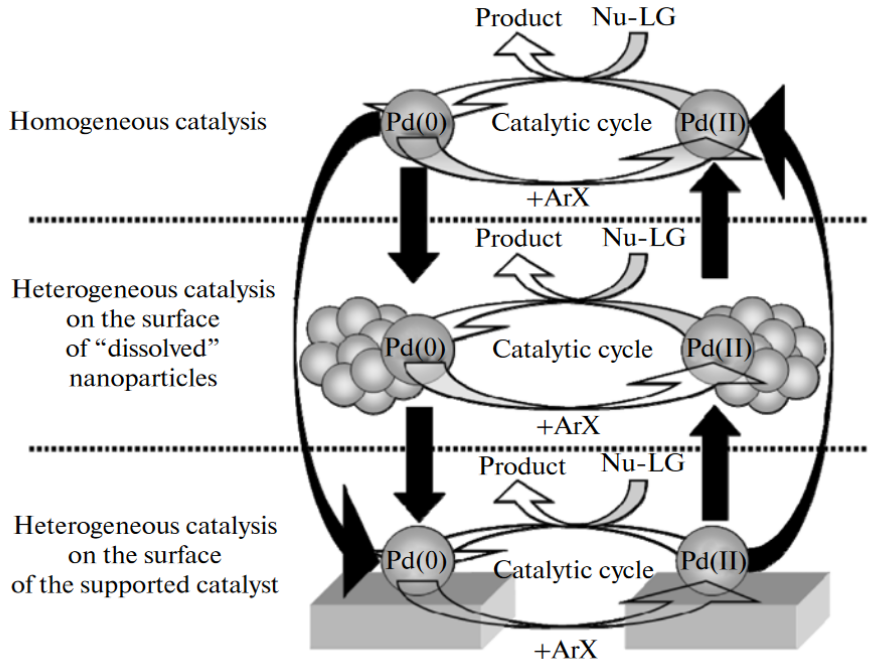


Figure 2.6: Palladium conversions in the Heck reaction as proposed by Schmidt et. al. (ArX aryl halide, Nu-LG nucleophilic coupling partner). Reproduced from reference [96].

Additionally, there is also experimental evidence to suggest that leaching can also occur in the absence of any halide [97, 98]. It was found that 20% of the palladium nano colloids (14 ± 3 nm), prepared by reacting $Pd(OAc)_2$ with tetraoctylammonium glycolate (TOAG) in DMF, underwent dissolution in DMF at 100 °C forming smaller particles (< 5nm) as detected by TEM. As there is no halide present, the dissolution of the clusters was attributed to Pd^0 leaching into solution (atom leaching) rather than Pd^{2+} (ion leaching).

2.5 Development of Heterogeneous Catalysts

The choice of a catalyst support is often motivated by catalyst activity and selectivity, based on the acid/base properties, electronic and geometric effects from the strong metal-support interactions, as well as the surface chemistry, surface area, pore size and porosity. The main purpose of the support is to disperse and stabilise palladium NP's for maximum activity. The most common heterogeneous catalysts for C-C coupling reactions are those dispersed on high

surface area supports such as graphite, carbon, alumina and silica [99-105, 106]. In most studies, catalyst leaching is often only included as an afterthought, rather than been included in the original design, even though many of these factors will also determine how well the catalyst adhere to the support, either chemically or physically.

The method of immobilising the catalyst onto the support is another aspect of the catalyst design which can influence the activity, selectivity and leaching capacity of the catalyst. Many methods of immobilising the catalyst have been established throughout the years, more frequently by covalent bonding, adsorption, ionic bonding or encapsulation (Figure 2.7). Various chemical and physical process can be applied to integrate the catalyst with the support such as impregnation, ion exchange, adsorption, precipitation and co-precipitation [107]. The method of immobilisation of the catalyst to the support influences the catalysts activity and selectivity [108]. Currently there is no evidence to suggest which combination of immobilisation and catalyst support produce the best catalyst to mitigate leaching.

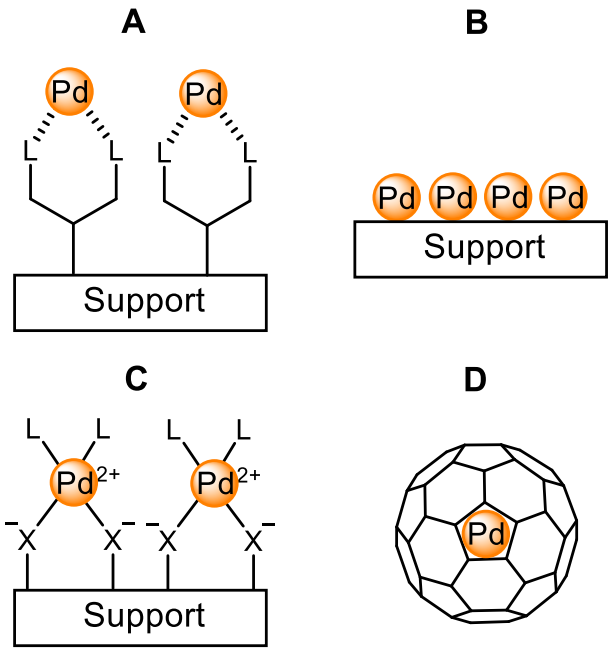
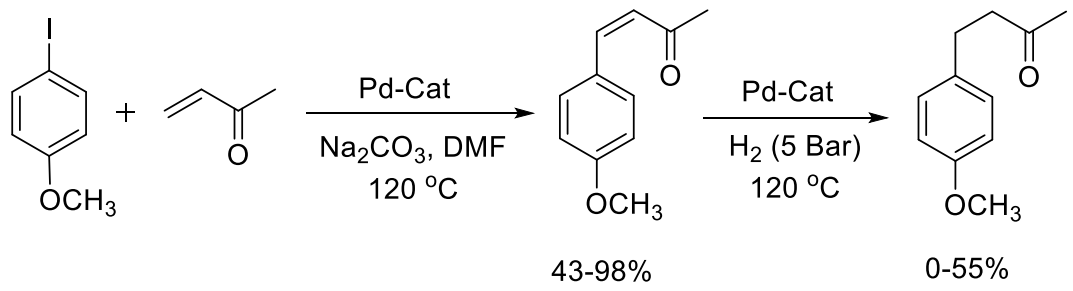


Figure 2.7: Immobilisation methods to secure the catalyst onto solid supports. **A)** Covalent bonding, **B)** Adsorption, **C)** Ionic bonding and **D)** Encapsulation.

A previous study on practical ways to control the leaching from Pd/C during the Heck reaction of bromobenzene with styrene has been conducted by Kohler and co-workers [93]. By using a combination of analytical techniques, ICP-OES, TEM and GC they monitored the Pd concentration in solution along with the reaction progress. It was found that Pd concentration

in solution is the highest at the start of the reaction and decreases after the reaction. Different reaction parameters were then studied to minimise leaching. It was reported that the main parameters which have a direct effect on the quantity of Pd being leached are: the solvent, reaction temperature and reactants used. These findings suggest that the catalyst is re-depositing after the reaction is complete. The parameters which were found to promote Pd re-deposition are increased reaction temperatures, performing the reaction in an inert atmosphere, as well as the addition of reducing agents. By optimising all of the influencing parameters it is possible to minimise leaching and improve the lifetime of Pd on carbon.

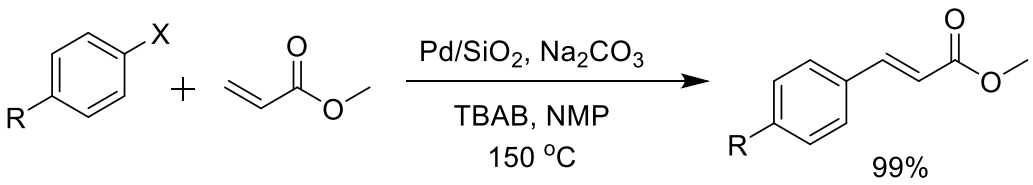
A study carried out by Corma's research group compared the effectiveness of palladium nanoparticles supported on MgO, hydroxyapatite (HA), alumina oxide (γ-Al_2O_3) and titanium dioxide (TiO_2) in the one-pot synthesis of 4-(p-methoxyphenyl) butan-2-one [109]. The reaction proceeded via a Heck reaction followed by a hydrogenation with a single heterogeneous Pd catalyst (Scheme 2.3).



Scheme 2.3: One pot synthesis of 4-(p-methoxyphenyl) butan-2-one using either Pd on MgO, HA, γ-Al_2O_3 and TiO_2.

Of the catalysts screened Pd/TiO_2 had the best performance for both consecutive reactions based on yield and selectivity, even outperforming a homogeneous palladacycle complex. A hot filtration test and TEM imaging were performed subsequently to assess if the Pd/TiO_2 leaches during the reaction. The TEM comparison of the crystallite size distribution before and after the Heck reaction show a redistribution in sizes with an increase at the lower range (5-10 nm) and an increase at the upper range (21-30 nm) suggesting that leaching and agglomeration events are occurring. The hot filtration test offers further evidence that leaching of the catalyst is happening with 0.4 ppm Pd being detected in the filtrate and further conversion being detected. Despite the evidence of leaching, it was still proclaimed as the best 'heterogeneous' catalyst for this system due to its applicability in a one pot reaction.

Silica dioxide (SiO_2) is another extensively used support for Pd catalysts given its excellent chemical and thermal stability [110, 111]. Bucsi et al. prepared silica supported Pd catalysts with extremely low Pd loading containing 0.35% and 0.08% Pd [112]. Their activity was demonstrated with the Heck reaction between methyl acrylate and chloro- and bromo-substituted arenes in NMP (Scheme 2.4).



X = Br, Cl

R = H, OCH_3, NO_2, CN, $COCH_3$

Scheme 2.4: The Heck reaction between haloarenes and methyl acrylate.

Good activity and selectivity of 99% and 99% were achieved with 4-bromo and 4-chloroacetophenone after 3h with the addition of tetrabutylammonium bromide (TBAB). Recycling experiments exposed a significant decrease in activity with each re-use suggesting that the catalysts are deactivating (Figure 2.8). Upon investigation, extensive leaching was confirmed with a hot filtration test with ICP-AES detecting 39 ppm of Pd in the filtrate. This demonstrates the increased activity of Pd when supported on silica whilst also rekindling the question of what the active catalyst is in this system.

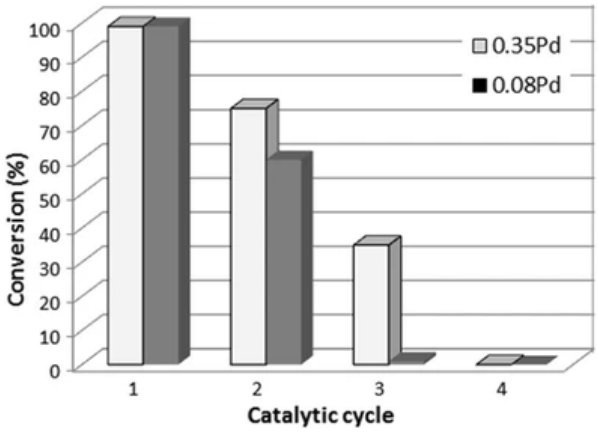


Figure 2.8: Graph of diminishing conversion with each recycle experiment. Recreated from reference [112].

Santa Barbara Amorphous-15 (SBA-15) is a highly stable mesoporous silica sieve, Crudden and co-workers modified the structure by grafting commercially available thiol ligands to develop an effective scavenger which can then be employed as a heterogeneous catalyst with enhanced stability (Figure 2.9) [110, 113, 114]. This resulted in the development of a recoverable catalyst for cross-coupling reactions, such as the Suzuki–Miyaura and Heck reactions (Scheme 2.5). However, when the three-phase test was applied, conversion was observed in the filtered reaction mixture, establishing that leached Pd is likely to be responsible for the catalytic activity [113, 115]. In a separate report, Richardson and Jones demonstrated that by adding SH-SBA-15 (a catalyst poison), the Heck reaction with either homogeneous palladium acetate or Pd-SH-SBA-15 is curtailed; leading them to postulate that the catalytic activity of Pd-SH-SBA-15 (Pd 3-mercaptopropyl-functionalised silica) was solely associated with leached Pd [116].

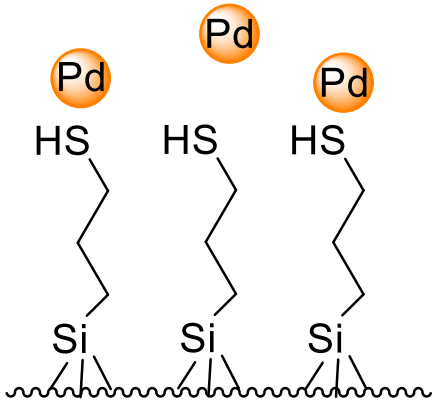
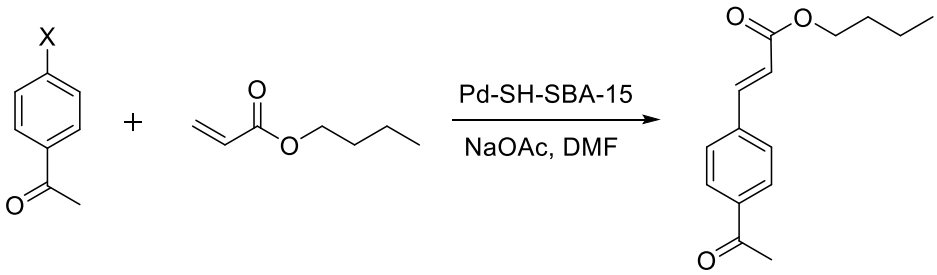


Figure 2.9: Structure of SH-SBA-15 and how it poisons labile Pd.

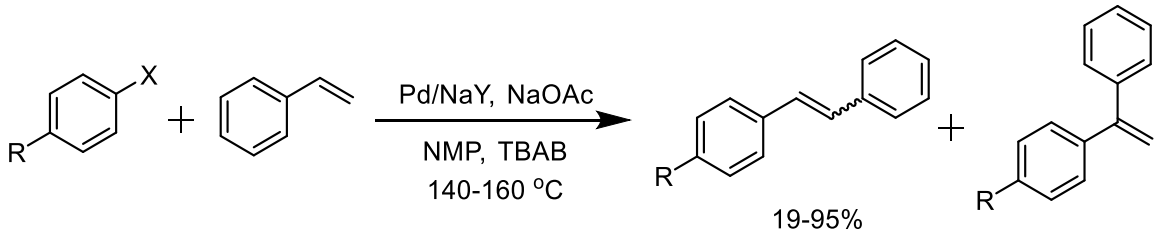


X = I/Br

Scheme 2.5: Heck reaction between iodo/bromoacetophenone and butyl acrylate in DMF catalysed by Pd-SH-SBA-15.

The leaching of active palladium species during the Heck reaction was exploited by Kohler et. al., where a zeolite (Pd/NaY) support has been deliberately modified to allow efficient release

and redeposition of palladium on into the cage (boomerang catalysis) [117]. This is thought to aid in preventing agglomeration thus sustaining the catalysts activity. AAS was used to monitor the amount of Pd present in solution during a Heck reaction between chlorobenzene and styrene (Scheme 2.6). It was reported that during the reaction one third of the Pd leached into solution, which fully redeposited onto the support after the reaction. In this instance, the Pd/NaY functions as a reservoir for molecular Pd species in solution, achieving a TON of 1400.



X = Cl, Br
R = H, CH_3, OCH_3, $COCH_3$

Scheme 2.6: Heck reaction between halo arenes and styrene in catalysed by Pd/NaY in NMP.

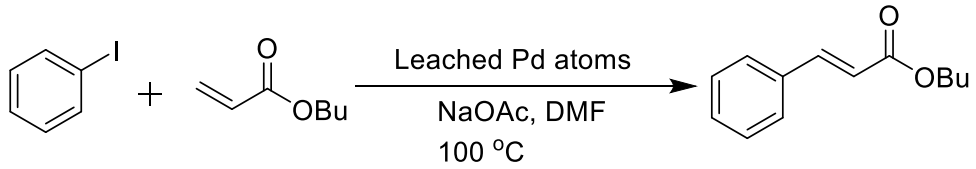
Nevertheless, the activity levels achieved by these catalysts fall short of those observed with homogeneous catalysts. In recognition of the limited applications of homogenous catalysts there has been efforts to immobilise homogeneous catalysts. A notable example of this is PdEnCat®, where the homogeneous catalyst $Pd(OAc)_2$ is encapsulated in a polyurea matrix to retain it in a heterogeneous form during catalysis [118].

It is also important to consider that all the methods for detecting leaching are open to misinterpretation if they are not accurately performed, as different results about the nature of the catalyst can be obtained. For example, it was concluded that a $Pd(OAc)_2$-bis(oxazoline) catalyst on functionalised silica gel did not leach, based on evidence obtained from recycling experiments, hot-filtration, catalyst poisoning and a three phase test [119]. Upon closer inspection, however, although three of the tests supported the argument for a heterogenous catalytic mechanism, the catalyst poisoning test did not support this. Furthermore, none of these tests could distinguish which or if any of the proposed leaching mechanisms were in operation.

The ideal triad of characteristics a catalyst should possess are stability with infinite TON, reactivity with high TOF and robustness to reaction conditions. However, all catalysts will eventually deactivate through processes, such as leaching. This has limited the number of immobilised catalysts to be considered for industrial applications [120].

2.6 Reactors for Assessing Leaching

In addition to the methods described above, there has also been reports of novel reactors that have been used specifically to study catalyst leaching. One of the earlier examples were reported by the research group of Rothenberg, who designed a two-compartment reactor to distinguish the roles of Pd nanoparticles and soluble molecular Pd species in various C-C coupling reactions, including the Heck reaction (Scheme 2.7) [121]. In this reactor, a membrane (with 5 nm pores) separates the two-compartments, keeping the Pd nanoparticles (15 nm) at one side (A), and a heterogenous base on the other side (B) (Figure 2.10). This means that the reaction can only proceed if leached Pd species crosses from compartment A into compartment B of the reactor. Sample outlets on both sides of the reactor allows for reaction monitoring and therefore information as to whether leached species (<5 nm) are participating in the reaction.



Scheme 2.7: The Heck reaction between iodobenzene and butyl acrylate in the presence of NaOAc which is insoluble in DMF.

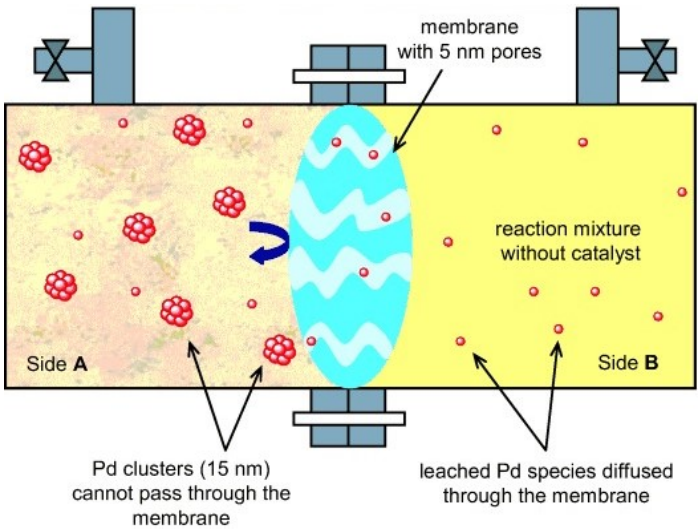


Figure 2.10: Two compartment membrane reactor employed by Rothenberg's group to prove the participation of soluble Pd species in a C-C coupling reactions [121].

The reactor offers easy and simple detection of leaching in reactions with more than one heterogeneous component. However, it is essentially a three phase test and has similar drawbacks as a result. For example, the lack of conversion in compartment B may not necessarily comfirm absence of a homogeneous catalyst. Agglomeration of the leached species to clusters larger than 5 nm in compartment A may also occur before they contact the membrane.

In a following study, Rothenberg and co-workers used the same two-compartment reactor to probe the mechanism of leaching from Pd nanoparticles [97]. Using a combination of ICP, mass spectrometry, UV-Vis spectroscopy, TEM and ^{13}C NMR spectroscopy, three mechanisms of leaching were proposed (Figure 2.11). By assesing the morphology of the catalyst in compartment A with TEM imaging the first mechanism of fragmentation was proposed (Figure 2.11: top). Here the nanoparticles break into smaller Pd^0 clusters which are too large to pass through the membrane.

Under non-oxidising conditions, a suspension of Pd clusters in DMF were placed in compartment A and pure DMF in compartment B, the second mechanism (Figure 2.11: middle) showed that Pd^0 is able to leach and migrate through the membrane.

By adding PhI to both compartments and using mass spectrometry, UV-Vis and ^{13}C NMR spectroscopy they were able to monitor the migration of Pd^{II} ions across the membrane owing to a oxidative leaching mechanism (Figure 2.11: bottom) as reported earlier by Reetz [52] and Schmidt [96]. Practical implementation of this reactor offered a slight improvement on the understanding of leaching for similar catalytic systems when compared to the standard leaching tests. However, as it can take over 150 h for the particles to fragment and diffuse through this membrane, obtaining these results is far from rapid.

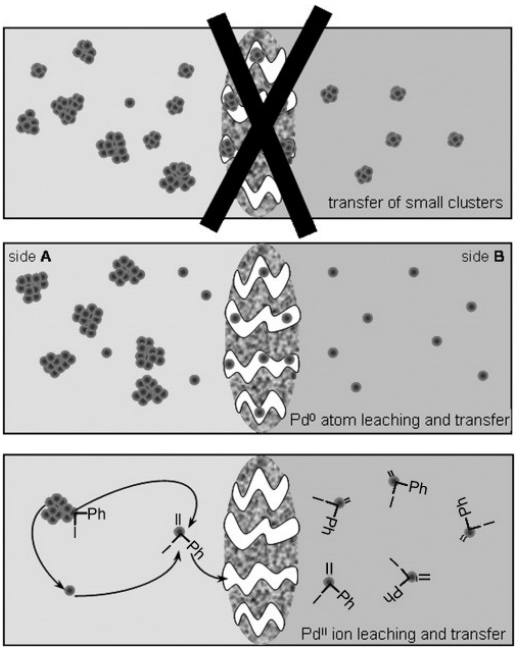


Figure 2.11: Suggested mechanism for the migration of Pd from side **A** to side **B**. Top - nanoparticle fragmentation followed by small cluster transfer; middle – Pd^0 atom leaching and transfer under non-oxidising conditions; bottom – formation and transfer of Pd^{II} species under oxidising conditions. Image recreated from reference [97].

When designed appropriately, flow reactors can offer a much better insight into the leaching mechanism than batch reactors. Critically, batch reactors have a constant reaction volume, where the solvation and re-adsorption of Pd onto the support can occur during the reaction, through boomerang catalysis. In contrast, a continuous reaction stream is passing over the catalyst in a flow reactor, carrying the palladium away from the supports surface preventing redeposition (Figure 2.12). Thus, the behaviour of the catalyst can be drastically different between batch and flow reactors.

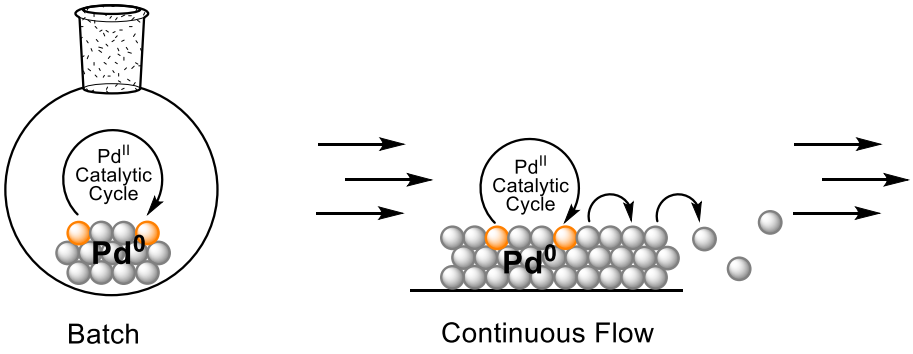
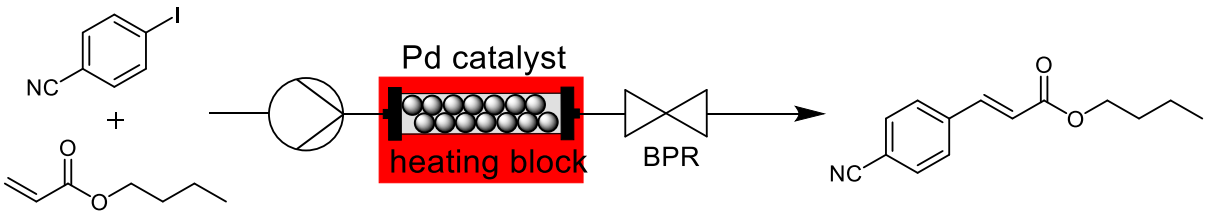


Figure 2.12: A comparison of the possible mechanisms of leaching in a batch reactor compared with a flow reactor.

Leaching of the Heck reaction in a continuous flow reactor was investigated by the Kappe group who, in 2009, using a commercial flow reactor (X-Cube) (Scheme 2.8) [123].



Scheme 2.8: Schematic of the flow set up for the Heck reaction between 4-iodobenzonitrile and butyl acrylate consisting of a pump, catalyst cartridge in a heating block and back pressure regulator [123].

It was found that a significant quantity of Pd was leaching from the heterogeneous catalyst (Pd/C). Insights into the cause of leaching was examined by changing the composition of the reaction mixture passing through the catalyst cartridge, followed by the determination of Pd leaching using ICP-MS (Table 2.2). Based on these observations, it was then proposed with this set up that the catalysis is quasi-homogeneous with small catalytically active Pd^0 species in solution.

Table 2.2: Quantity of Pd leaching from Pd/C under various mobile phase compositions [123].

Entry	Mobile Phase Composition	Leaching [µg Pd]
1	MeCN	1.6
2	MeCN/Et_3N	4.8
3	MeCN/acrylate	1.0
4	MeCN/aryl iodide	17.2
5	MeCN/Et_3N/acrylate	7.2
6	MeCN/aryl iodide/acrylate	46
7	MeCN/Et_3N/aryl iodide/acrylate	220
8	MeCN/Et_3N/aryl iodide	1370

Entries 1 to 3 show very little Pd leaching in the respective mobile phases. Significant leaching was observed whenever the aryl iodide was included in the mobile phase (entries 4, 6, 7 & 8). The highest leaching was observed with a combination of triethylamine and aryl iodide in the solvent (entry 8). By comparing entry 8 with entry 4 it shows that Et_3N has a significant

influence on the extent of leaching. However, in this study it is not clear or evident if the catalyst species is catalytically active or inactive under reaction conditions.

In a similar study, Kappe and co-workers used the same reactor to screen a number of different heterogeneous catalysts which each offer a different solid matrix (Figure 2.13) for the Heck reaction, and also concluded that Pd leached in all cases [124]. A review article on this issue presented the same findings [125]. Indeed, it was proposed that it is more appropriate to perform these types of reactions using a homogeneous catalyst. One reason why many heterogeneous catalysts which are efficient in batch reactors may not be complementary to a flow reactor set up could be due to the fact that they are, effectively, merely acting as reservoirs for active catalysts.

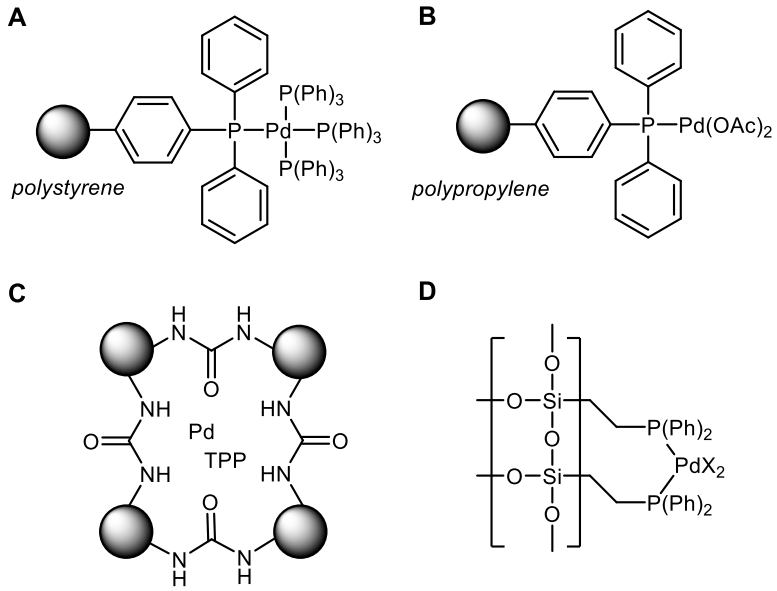
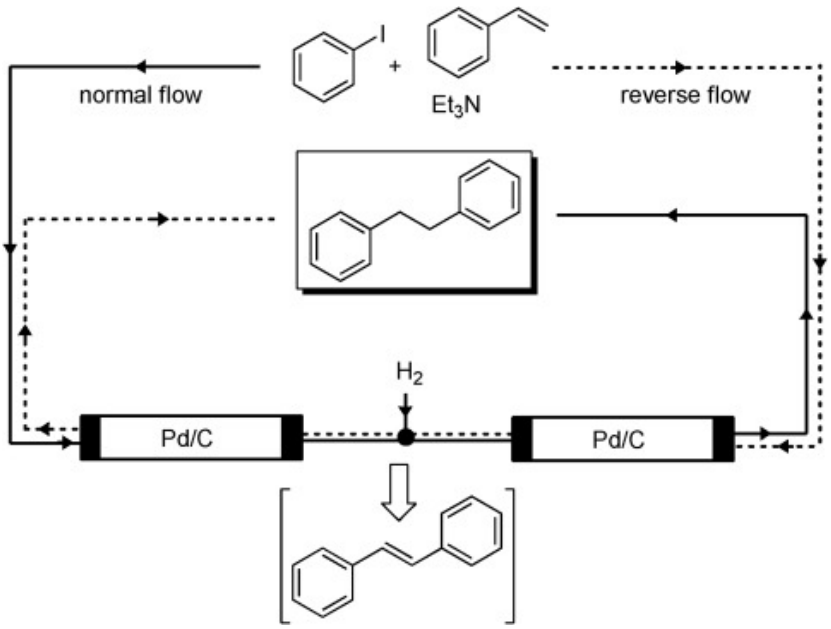


Figure 2.13: Structures of the heterogeneous catalysts which were investigated by Kappe and co-workers **A**) polymer-bound Pd [$Pd(PPh_3)_4$], **B**) FiberCat 1001, **C**) Encat® TPP30 and **D**) SiliaCat DPP-Pd [124].

Conversely, the reactor can be designed to mitigate against the effect of leaching, as demonstrated by Plucinski and co-workers in an interesting report (Scheme 2.9) [126]. In this study, Pd/C was loaded into two PBR's – in the first, the Heck reaction between iodobenzene and styrene produced E/Z isomers of 1,2-diphenylethene, which was subsequently reduced to 1,2-diphenylethane by hydrogenation in the second PBR.



Scheme 2.9: Diagram of the reactor designed by Plucinski and co-workers for the sequential Heck and hydrogenation reactions for the synthesis of 1,2-diphenylethane [126].

By using X-ray photoelectron spectroscopy analysis (XPS), it was found that the Pd content on the carbon surface of the Pd/C catalyst in the second cartridge increases during the reaction. This suggests the Pd that leached from the first PBR during the Heck reaction was captured in the second PBR during the hydrogenation. In the absence of the second catalyst bed, 6% of Pd leached during the Heck reaction (as determined by AAS) to demonstrate that leaching was occurring during the reaction. The 'normal' and 'reverse' flow reactions produced the same reaction profiles, albeit with a slight (5%) decrease between runs, proving to be a resourceful instance which mitigates the leaching process as it is recaptured in the second catalyst cartridge.

X-ray absorption spectroscopy (XAS) is a powerful method for investigating changes in surface and solution metallic species *in situ* [127]. Yuan et. al. carried out *in situ* analysis of various Pd species (Figure 2.14) using XAS to examine catalyst leaching for the Heck reaction (Scheme 2.10) [128, 129]. In order to monitor the reaction *in situ* with XAS a custom reactor was developed (Figure 2.15), this also allowed for the reaction to be simultaneously monitored with powder X-ray diffraction (PXRD).

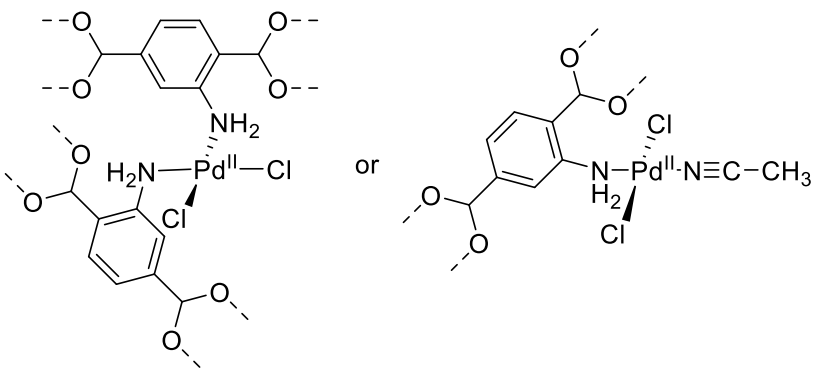
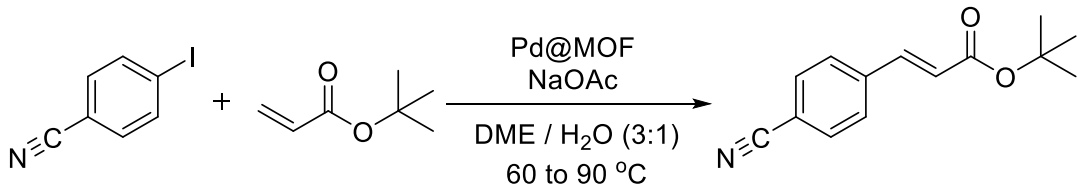


Figure 2.14: Structures of the Pd@MOF complexes used for the catalysis of the Heck reaction for *in situ* XAS experiments [128].



Scheme 2.10: The Heck reaction conducted for *in situ* XAS experiments.

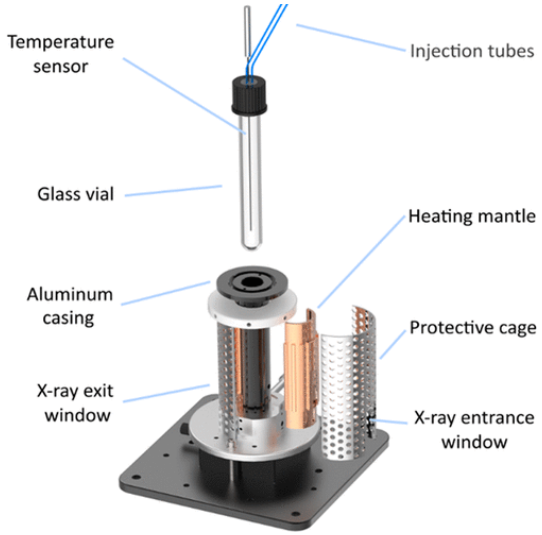


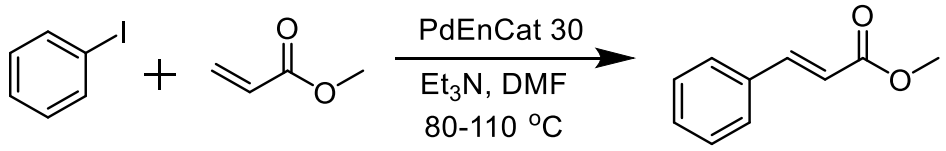
Figure 2.15: Custom reactor for the operando analysis of various Pd species in the Heck reaction [128].

Using this set up they were able to correlate information about the active catalyst species with any changes in the structural stability of the solid support during the Heck reaction. By comparing XAS scans throughout their reactions, an increase in the intensity of Fourier transformed XAS data corresponding to Pd-Pd and Pd-Cl bonds was observed. The results led

them to conclude that the Pd was deactivating by Cl^- ions blocking the active sites of aggregated Pd clusters and nanoparticles as there was a significant drop in activity during recycling experiments. However, as these studies were conducted in batch and the fact that leached species can redeposit on the catalyst the real quantity of leaching and speciation can be suppressed.

Further to this, our research group have previously used XAS for *in situ* monitoring of structural changes in Pd catalysts [130-133]. Of particular interest is the investigation of leaching of Pd in a packed bed reactor, using XAS to map the catalyst bed [134]. During this study the speciation of Pd was observed along the catalyst bed. It was found that when hot EtOH is passed through a Pd/γ-Al_2O_3 catalyst bed, a redistribution of Pd along the bed can be observed, which is accompanied by the reduction to Pd^0, which can be attributed to the partial oxidation of EtOH. When examining the entrance of the catalyst bed, where the solvent first comes into contact with the catalyst, it is mostly Pd^{II} present, whilst the exit of the catalyst bed mainly comprised of Pd^0. This study suggests that: 1) leaching can be caused by using a hot protic solvent (such as ethanol); and 2) the predominate species being leached from Pd/γ-Al_2O_3 is Pd^0, which can be carried along the bed.

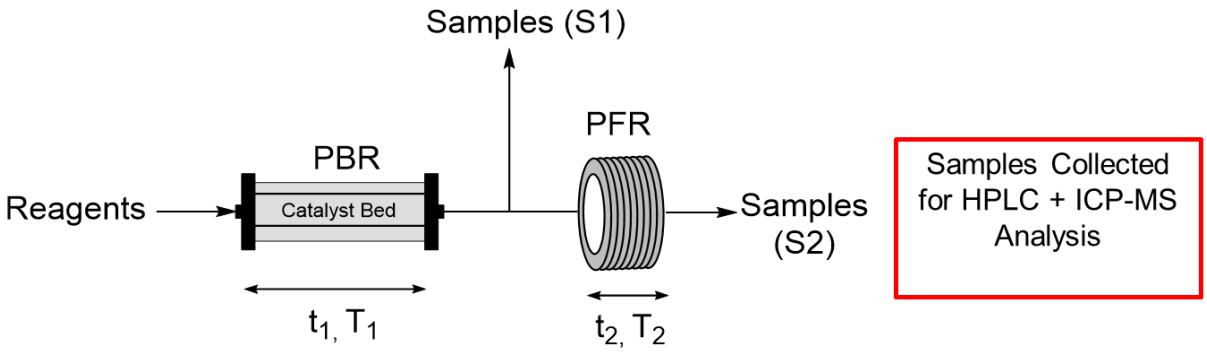
More recently Hii, Hellgardt and co-workers have designed a tandem flow reactor to distinguish between heterogeneous and homogeneous catalytic processes for the Heck reaction (Scheme 2.11) [86].



Scheme 2.11: The Heck reaction between iodobenzene and methyl acrylate catalysed by the polyurea encapsulated Pd catalyst PdEnCat®30 in DMF.

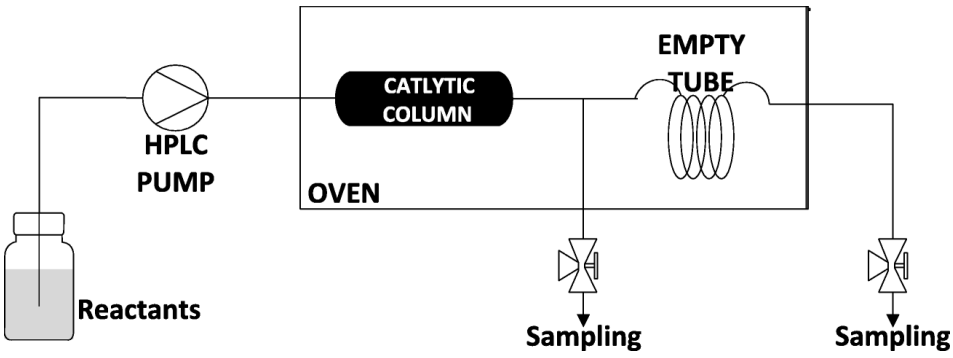
The reactor consists of a PBR which contains the heterogeneous catalyst PdEnCat®30, followed by an empty PFR (Scheme 2.12). Having sample outlets at the end of each reactor enables the extraction of reaction aliquots, thus allowing the progress of the reaction to be monitored by HPLC and Pd content to be quantified with ICP-OES. Using this design, it was possible to have definitive conversions and quantity of Pd leached for both catalytic processes. By comparing the conversion profiles from the PBR and the PFR samples, it was

proved that the majority of conversion (83%) was attributed to leached species catalysing the reaction in the homogeneous phase in the PFR. This was also confirmed with ICP results showing 6.45% of the Pd leaching from the support into the PFR. A multiscale model was subsequently constructed to simulate the activity of the homogeneous and heterogeneous components of the reaction. Reaction rates were then extracted, and it was found that the rate of the homogenous reaction is 10^6 times faster than the heterogeneous reaction. This reactor set-up is comparable to a hot filtration test with continuous filtering and without pause or interference with the reaction.

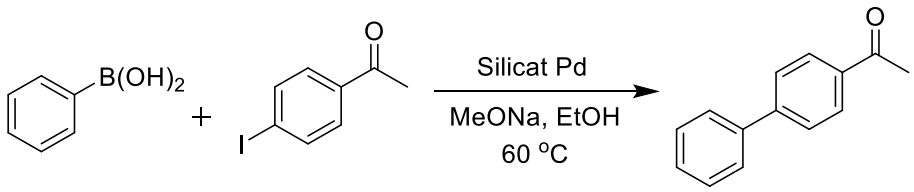


Scheme 2.12: Schematic of the tandem flow reactor used in the study conducted by Hii, Hellgardt and co-workers [86].

Shortly after this publication by Hii [86], Bellefon et. al. implemented a flow reactor to also distinguish between heterogeneous and homogeneous reactions but applied it for the Suzuki-Miyaura coupling (Scheme 2.13) [135]. In their proof of principle studies conducted in ethanol, 4-iodoacetophenone and phenyl boronic acid were catalysed by Silicycle R815-100 and R390-100 as sources of Pd^0 and Pd^{II} respectively (Scheme 2.14). As this reactor is also operated in continuous flow it avoids the complications associated with hot-filtration and ambiguous poisoning tests. Bellefon's results on the major contributing catalyst phase were found to be in line with what Hii reported for the Heck reaction; the catalysis is almost exclusively homogeneous. Overall, these flows set ups offer much faster quantification of leaching than the batch methods discussed previously.



Scheme 2.13: Scheme of the flow reactor designed by Bellefon et. al. for the assessment of leaching in the Suzuki-Miyaura reaction [135].



Scheme 2.14: Suzuki-Miyaura reaction catalysed by Siliacat Pd between phenylboronic acid and 4-iodoacetophenone in the presence of sodium methanolate in ethanol.

2.7 Conclusion

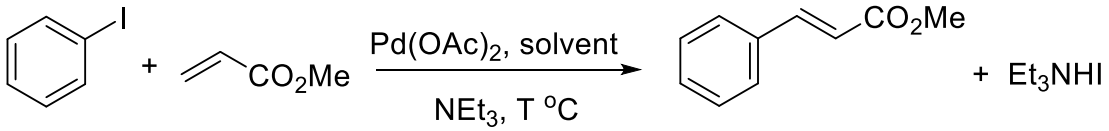
It has been demonstrated throughout this chapter that the mechanism of leaching is not well understood and the activity of heterogenous catalysts is often misinterpreted. All the conventional leaching tests discussed in section 2.2 have their drawbacks, whilst new reactors are assisting with uncovering the true leaching mechanisms there are still gaps in the literature. This thesis sets out to use a novel flow reactor to bridge some of these gaps such as; correlating the quantity of leaching with activity as well as probing each reactant in the Heck reaction for its role in leaching, these results are presented in chapter 4.

2.8 Aims

The aim of this work is to investigate the presence of any 'homeopathic effect' in the Heck reaction between iodobenzene and methyl acrylate in the presence of triethylamine (Scheme 2.15). This reaction was chosen as the model system as it has been studied extensively and is known to proceed using homogeneous or heterogeneous Pd precursors under 'ligand-free' conditions. Very high turnover numbers and frequencies are often observed in this system [21, 86] which provides ideal conditions to investigate the existence of any 'homeopathic effect'.

The progress of the reaction can be easily monitored by using *in situ* FTIR spectroscopy by following the consumption of iodobenzene and the formation of methyl cinnamate. By using this analytical technique large volumes of data will be obtained which can be processed using VTNA to verify the reaction order of each substrate and the reaction order in the catalyst. By performing the reaction at various low concentrations of catalyst it will also be possible to conclude if or when catalyst deactivation becomes a competitive process with the reaction.

While it has been proposed many times that more than one catalytically active species is involved in the Heck reaction it has never been proven experimentally [55]. In this work, RPKA and VTNA methods are utilised to understand the dependence of reactions rates on the concentrations of reactants and catalysts. The data will also be used to generate a microkinetics model to understand how many catalytically active species are involved in the reaction, their relative turnover frequencies and stability against deactivation.



Scheme 2.15: The model Heck reaction applied throughout this study between iodobenzene and methyl acrylate.

In Chapter 2, different studies of Pd leaching in the Heck reaction have been presented, including various methods developed to uncover the mechanism of leaching and the catalyst species involved in the reaction. Various catalysts were used in those studies with the common conclusion that the oxidative addition step is responsible for the solubilisation leaching of catalytic species from a heterogeneous catalyst [122, 123, 124].

The Hii group have previously developed a tandem flow reactor to distinguish surface catalysed reactions from those occurring simultaneously in solution [86]. In this Chapter, this methodology will be applied to study leaching of other heterogenous Pd catalysts in the Heck reaction, to discover if the method of immobilisation and surface characteristics strongly influence the reaction and leaching. This knowledge will provide a better picture of what catalyst characteristics influences leaching and whether the leached species of different heterogeneous catalysts have different catalytic activities.

Another question which can be posed is, what causes leaching? The oxidative addition step is proposed in the literature to solubilise the heterogeneous Pd, one would then assume that the concentration of aryl halide will influence the quantity of Pd leached. In this work, this assumption was tested by modifying the tandem flow reactor to individually examine the roles of the individual components in leaching. This allows for the identification of soluble active species and the quantification of leached Pd correlated to each reaction component. Once the root cause of leaching is understood, better methods can be developed to address the issue of catalyst leaching.

Chapter 3. Experimental Protocol and Methodology

3.1 Introduction

In this chapter all chemicals used throughout the project are first tabulated with their suppliers. Experimental procedures, including batch and flow methods are explained along with computational and analytical methods which will be referred to in later chapters.

3.2 Chemicals

Unless stated otherwise, all chemicals and solvents were purchased from commercial vendors and were used as received without further purification. Table 3.1 lists all the chemicals used in this project with their corresponding suppliers.

Table 3.1: List of chemicals used in this project.

Chemicals and materials	**Supplier**
$Pd(OAc)_2$	Johnson Matthey
FibreCat 1001, 3.97 wt%	Johnson Matthey
Pd EnCat® 30	Sigma Aldrich
Pd/Al_2O_3, 5 wt%	Acros Organics
Pd/C, 5 wt%	Sigma Aldrich
Acetonitrile	Fisher Scientific
Trifluoroacetic acid	Sigma Aldrich
Dimethylformamide	Fisher Scientific
Hydrochloric acid, 37%	Fisher Scientific
Nitric Acid, 65%	Fisher Scientific
Pd ICP Standard 10,000 µg/mL	Sigma Aldrich
Iodobenzene	Sigma Aldrich
Triethylamine	Fisher Scientific
Methyl Acrylate	Sigma Aldrich
Hexane	Fisher Scientific
N,N-Diisopropylethylamine	Sigma Aldrich
Toluene	Fisher Scientific

Dioxane	Fisher Scientific
Diethyl Ether	Fisher Scientific
Chloroform-d 99.8%	Sigma Aldrich
Silica Gel (60 Å, 230-240 mesh)	Fisher Scientific

3.3 Methods

3.3.1 General

Melting points were recorded using a Gallenkamp melting point apparatus (Gallenkamp MPA) with a mercury thermometer and were uncorrected. Gilson micropipettes were used to measure volumes less than 1 mL for sample preparation. Column chromatography was performed on silica gel (60 Å, 230-240 mesh).

3.3.2 Nuclear Magnetic resonance (NMR)

^{1}H, ^{13}C and ^{19}F NMR spectra were recorded on a Bruker AV400 spectrometer at 400, 101 and 377 MHz respectively. ^{1}H, ^{13}C and ^{19}F NMR chemical shifts (δ) are reported in ppm relative to residual solvent peaks of the deuterated solvent used for the preparation of samples ($CDCl_3$ δ_H = 7.26 ppm and δ_C = 77 ppm, $(CD_3)_2SO$ δ_H = 2.50 ppm and δ_C = 39.5 ppm). The multiplicity of the NMR signals is denoted as follows: b = broad, s = singlet, d = doublet, t = triplet, q = quartet, p = pentet, dd = doublet of doublets or m = multiplet. Coupling constants (J values) are given in Hz.

3.3.3 High Pressure Liquid Chromatography (HPLC)

HPLC separations were performed on an Agilent 1100 instrument consisting of an G1322A degasser, G1311A quaternary pump, G1313A ALS, G1315B diode array detector (Agilent, USA) and fitted with a Nucleosil C18 column (100-5C18, 12.5 cm × 4.0 mm, 5 µm). Absorbances at 210, 254 and 280 nm were used for quantification. Unless stated otherwise, a gradient HPLC method was used with the mobile phase consisting of solvent A (acetonitrile acidified with 0.1% TFA) and solvent B (Water acidified with 0.1% TFA) with a flow rate of 1.0 mL/min. The initial mobile phase composition was maintained at 50% solvent A for 0.5 min, changed linearly to 95% (0.5–6.5 min), followed by a return to the initial conditions (6.5–7.5 min). The injection volume was 5 µl. Samples were prepared using a 1:50 dilution with acetonitrile

containing the internal standard cumene (0.001 mM). Chemstation software (version number: B.04.02 SP1) was used to process and analyse all resulting spectra.

3.3.4 Infra-red Spectroscopy (IR)

Infrared spectra were recorded on an Agilent Cary 630 FT-IR spectrometer fitted with an ATR sampling module.

3.3.5 *In situ* Infra-red spectroscopy (ReactIR)

In situ reaction monitoring was performed using a Mettler Toledo ReactIR 15 equipped with a LN_2 MCT detector and a 9 mm DiComp sensor attached to a fibre optic (AgX) probe. Spectra were recorded either every 30 s or 1 min, as stated, comprising of 128 and 256 scans, respectively. The optical range for scanning was 2500 cm^{-1} to 650 cm^{-1}. The FTIR data was processed using Mettler Toledo iCIR 7.0 software with the second derivative mathematical function being applied to all spectra and peak area of the signal being reported using a 2-point baseline.

3.3.6 UV-Vis formation of Pd NP's

Stock solutions of $Pd(OAc)_2$ (0.9 mg or 9 mg) in dry DMF (10 mL) were prepared in volumetric flasks to afford concentrations of 100 and 1000 ppm/mL respectively. UV-Vis spectra of Pd solutions were recorded in 1 cm^{-1} quartz cuvettes with a PTFE stopper on an Agilent Carry 60 UV-Vis spectrometer. Spectra of the solutions were recorded between 200-600 nm after being left for 1, 24 and 48 h at room temperature using DMF as a blank. The formation of Pd NP's was indicated by the increased absorption at 450 nm.

3.3.7 Mass Spectrometry (MS)

All mass spectra were run and recorded by Dr. Lisa Haigh of the Mass Spectrometry Service at Imperial College London. Electrospray ionisation mass spectrometry was conducted using a Waters LCT premier spectrometer in positive ion mode (TOF MS ES+).

3.3.8 Inductively coupled plasma (ICP)

Total metal content was determined by ICP-MS using an Agilent 7900 instrument calibrated with solutions containing 0, 50, 100, 250 and 500 ppb of Pd (prepared from Palladium ICP/DCP standard solution from Aldrich, 10,000 µg/mL Pd in 6% wt.% HCl which was then diluted to

the required standards with a 2% nitric acid solution). All samples were digested in aqua regia to dissolve the Pd and diluted with a 2% nitric acid solution to maintain a homogeneous sample.

3.3.9 Catalyst packing

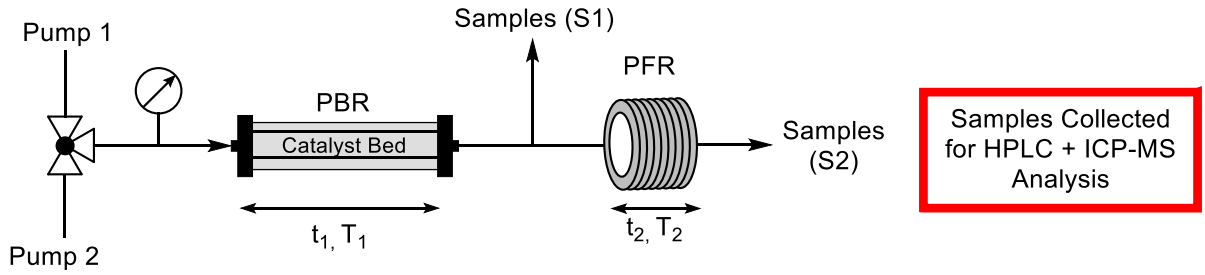
Catalysts (1 mol%, 4 mg Pd content) were dispersed within quartz sand (1 g, <250 µm, Fisher), prior to being packed into a PFA tube (100 x 4 x 6 mm length x inner Ø x outer Ø, Adtech) sealed at either end with glass wool (Figure 3.1). The packed tube was inserted into the aluminium block, and two silicon O-rings (Polymax) were fitted to either end of the cartridge to create a seal between the PFA tube and the Swagelok fittings.



Figure 3.1: Photograph of the packed catalyst cartridge.

3.4 Configuration 1 of the Tandem Flow Reactor

Investigations to distinguish the homogeneous and heterogeneous contributions from a heterogeneous catalyst were performed using configuration 1 of the tandem flow reactor.



Scheme 3.1: Schematic of configuration 1 of the tandem flow reactor.

In configuration 1, the solvent or reagents are delivered to the reactor via a high pressure syringe pump (Chemyx fusion 6000 fitted with a 50 cm^3 stainless steel syringe) through a 3-way ball valve. An additional syringe pump (Graseby 3100 fitted with a 50 cm^3 plastic syringe) is used to purge the reactor initially with the reaction solvent. The pressure of the system is monitored using a pressure gauge (Omega®) positioned between the 3-way ball valve and the

entrance of the PBR. The PBR is an aluminium block (102 x 35 x 20 mm) with drilled cylindrical bores which fit the PFA catalyst cartridge (100 x 4 x 6 mm length x inner Ø x outer Ø, Adtech) and heater cartridges (1/4" x 3", Under Control Instruments Ltd). The heater cartridges are powered and controlled with a PID controller (Sesto D1S-VR-200). A K-type thermometer is fitted to the side of the PBR which provides temperature feedback to the PID controller. Both ends of the PBR are fitted with Swagelok fittings connecting to 1/8" metal tubing. At the top of the PBR a K-type thermometer is fitted through a T-piece to measure the temperature of the fluid immediately exiting the PBR. The outlet of the T-piece is connected to a solenoid valve which splits the flow between a Spectra/Chrom® CF-2 Fraction Collector (S1) and a coil of 1/8" PFA tubing (PFR, 1 m, internal Ø = 1/16"). The PFR is submerged in a silicone oil bath, heated with a hot plate with independent heating controls. The exit of the PFR is connected to the fraction collector (S2) which is programmed to collected samples at set intervals. Each sample is analysed for reactant and product concentration and then all samples are combined and reduced using a BioChromato Smart Evaporator and subjected to ICP analysis for total Pd content.

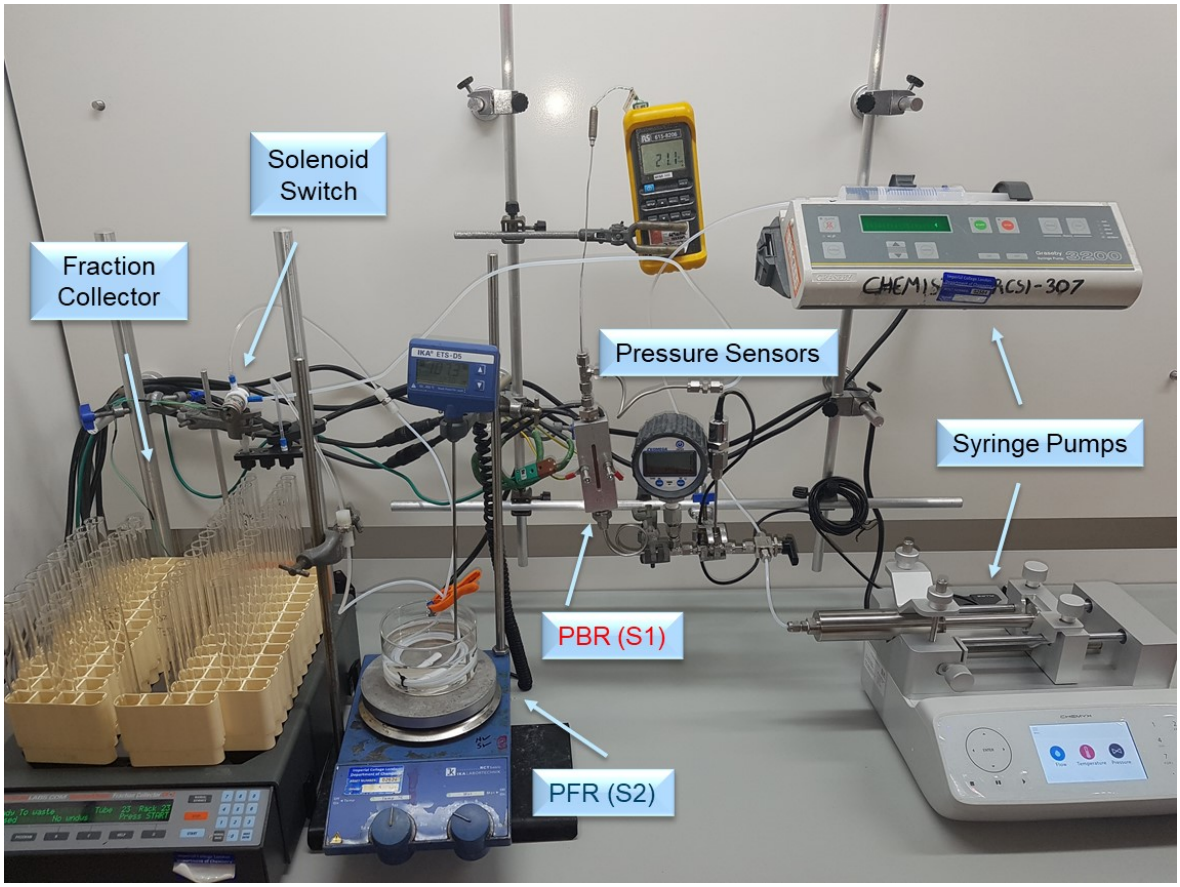


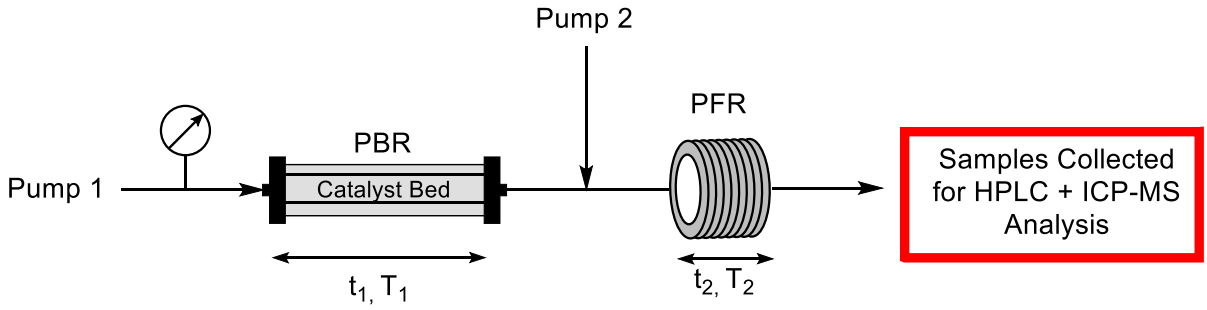
Figure 3.2: A labelled image of the tandem flow reactor set up in configuration 1.

3.5 Standard Experimental Procedure for Configuration 1

A PFA catalyst cartridge (100 x 4 x 6 mm length x inner Ø x outer Ø, Adtech) was packed with the desired heterogeneous Pd catalyst (1 mol %, 4 mg Pd content) and inserted into the PBR. The heating rods attached to the PID controller were then inserted into the PBR along with the feedback k -type thermocouple. A 50 mL syringe was filled with the desired solvent and loaded into pump 1 (Graseby 3100 syringe pump). A second 50 mL syringe was filled with a solution containing iodobenzene (420 µL, 3.76 mmol), methyl acrylate (670 µL, 7.4 mmol) and triethylamine/DIPEA (7.4 mmol) made up to 50 mL with the desired solvent and loaded into pump 2 (Chemyx fusion 6000 high pressure syringe pump). Both syringes were then connected to the reactor via the 3-way ball valve. Prior to the start of each reaction the temperature was set to 25 °C on both the PID controller and on the oil bath. The system was flushed through with the solvent from syringe pump 1 at a flow rate of 0.5 mL/min. The solenoid valve was switched off to direct the flow to S2 only. Once the system is filled, syringe pump 1 was stopped and the 3-way ball valve closed. If required, the temperatures of the PBR and PFR were set to their desired value. Once the desired temperatures had been reached, the 3-way ball valve was opened to the direction of syringe pump 2 which was then set to a flow rate of 0.5 mL/min. The solenoid valve was then switched on (50 Hz), to split the flow between S1 and S2. The eluent was collected using a Spectrum Chromatography CF-2 fraction collector which was programmed to the desired time interval. Fractions from S1 and S2 were analysed using HPLC to quantify the formation of methyl cinnamate and any remaining reactants. Fractions from S1 and S2 were combined, reduced and then subjected to ICP analysis for Pd content.

3.6 Configuration 2 of the Tandem Flow Reactor

Individual components of the Heck reaction were assessed for their influence on leaching of heterogeneous catalysts using configuration 2 of the tandem flow reactor.



Scheme 3.2: Schematic of configuration 2 of the tandem flow reactor.

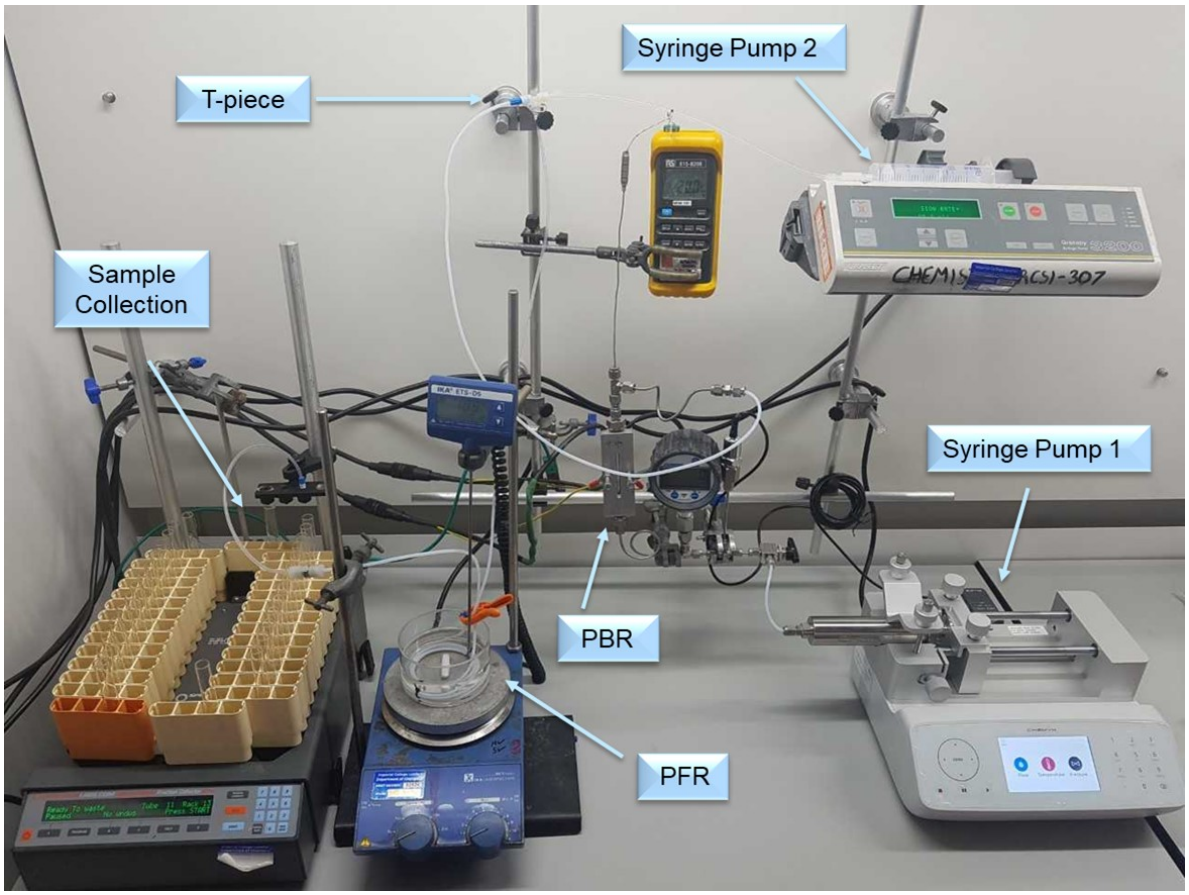


Figure 3.3: A labelled image of the tandem flow reactor set up in configuration 2.

The individual solvent or a mix of solvent and reagents are delivered to the reactor via a high pressure syringe pump (Chemyx fusion 6000 fitted with a 50 cm^3 stainless steel syringe) through a 3-way ball valve. The pressure of the system is monitored using a pressure gauge (Omega®) and a pressure sensor positioned between the 3-way ball valve and the entrance of the PBR. The PBR is an aluminium block (102 x 35 x 20 mm) with drilled cylindrical bores which fit the PFA catalyst cartridge (100 x 4 x 6 mm length x inner Ø x outer Ø, Adtech) and heater cartridges (1/4" x 3", Under Control Instruments Ltd). The heater cartridges are powered and controlled with a PID controller (Sesto D1S-VR-200). A K-type thermometer is fitted to the side of the PBR which provides temperature feedback to the PID controller. Both ends of the PBR are fitted with Swagelok fittings connecting to 1/8" metal tubing. At the top of the PBR a K-type thermometer is fitted through a T-piece to measure the temperature of the fluid immediately exiting the PBR. The outlet of the T-piece is connected to another T-piece which mixes the flow from the exit of the PBR with the remaining reactants for the Heck reaction delivered through an additional syringe pump (Graseby 3100 fitted with a 50 mL luer lock Norm-Ject syringe). The exit stream of the T-piece is connected to a coil of 1/8" PFA tubing (PFR, 1 m, internal Ø = 1/16"). The PFR is submerged in a silicon oil bath sitting on a hot plate with independent heating controls. The exit of the PFR is connected to a Spectra/Chrom® CF-2 Fraction Collector (S2) which is programmed to collected at set intervals.

3.7 Standard Experimental Procedure for Configuration 2

A PFA catalyst cartridge (100 x 4 x 6 mm length x inner Ø x outer Ø, Adtech) was packed with the desired heterogeneous Pd catalyst (1 mol %, 4 mg Pd content) and inserted into the PBR. The heating rods attached to the PID controller were then inserted into the PBR along with the feedback k -type thermocouple. Prior to the start of each reaction the temperature was set to 25 °C on both the PID controller and on the oil bath. The system was then purged at a flow rate of 0.5 mL/min with solvent from pump 1 (Chemyx fusion 6000 high pressure syringe pump). Once the system is filled, syringe pump 1 was stopped and the 3-way ball valve closed. Syringe pump 1 was then loaded with a 50 mL stainless steel syringe filled with a solution containing one out of the three components for the Heck reaction being either iodobenzene (420 µL, 3.76 mmol), methyl acrylate (670 µL, 7.4 mmol) or triethylamine/DIPEA (7.4 mmol) made up to 50 mL with the desired solvent. A 50 mL plastic syringe was filled with a solution

containing the remaining two components of the Heck reaction and made up to 50 mL in the desired solvent and loaded into pump 2 (Graseby 3100 syringe pump). If required, the temperatures of the PBR and PFR were set to their desired value. Once the desired temperatures had been reached, the 3-way ball valve was opened and then set to a flow rate of 0.25 mL/min. Syringe pump 2 was simultaneously set to a flow rate of 0.25 mL/min to deliver a total flow rate of 0.5 mL/min through the PFR. The eluent was collected using a Spectrum Chromatography CF-2 fraction collector which was programmed to the desired time interval. Fractions were analysed using HPLC to quantify the formation of methyl cinnamate. Fractions were combined, reduced and then subjected to ICP analysis for Pd content.

3.8 Flow Reactor Profile - Breakthrough Curve

A series of breakthrough curves were carried out using the flow reactor at different flow rates. Breakthrough curves are important to establish the residence time of reactants and when the solvent or reaction solution will start eluting, which helps to plan reactions.

First, DMF was passed through the flow reactor at a flow rate of 2 mL/min to fill it. Then a solution of Iodobenzene in DMF was passed through the flow reactor at a flow rate of 0.5 mL/min with fractions being collected at 1 min intervals. The concentration of iodobenzene was quantified using HPLC analysis. Breakthrough curves were performed for both S1 and S2 outlets (Figures 3.4 & 3.5).

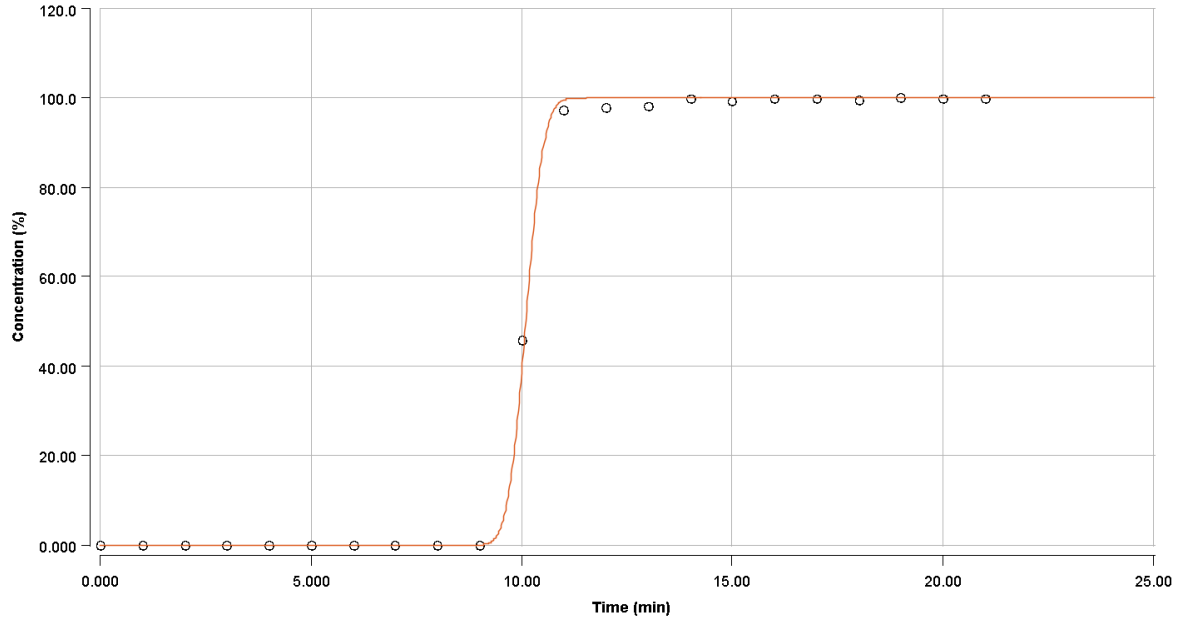


Figure 3.4: Breakthrough curve for the flow reactor eluting from S1 at 0.5 mL/min.

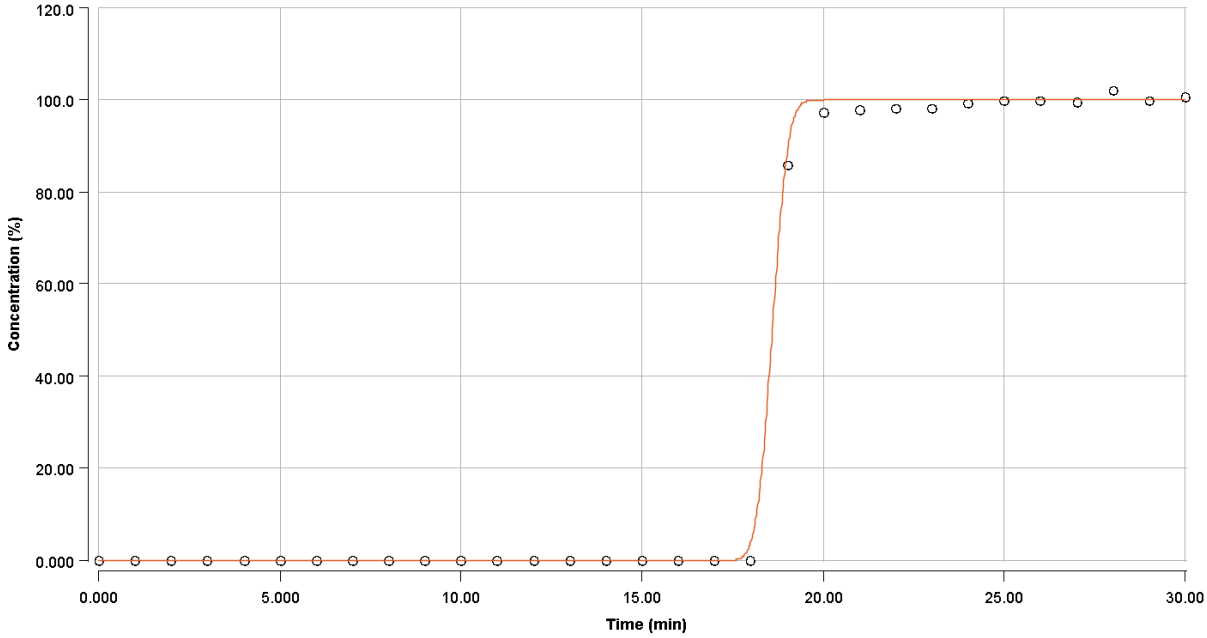


Figure 3.5: Breakthrough curve for the flow reactor eluting from S2 at 0.5 mL/min.

3.9 EasyMax 102 Advanced Thermostat System

Kinetic experiments were performed in a 100 mL glass EasyMax reaction vessel containing a PTFE cross stirrer bar (4 x 4 cm) was purged with N_2 and fitted with a thermocouple, condenser and ReactIR 15 probe (Figure 3.6). The reactions were monitored by *in situ* IR operating in the optical range of 2500 cm^{-1} to 650 cm^{-1}. Reaction aliquots were taken for offline HPLC quantification for orthogonal analysis of iodobenzene and methyl cinnamate.

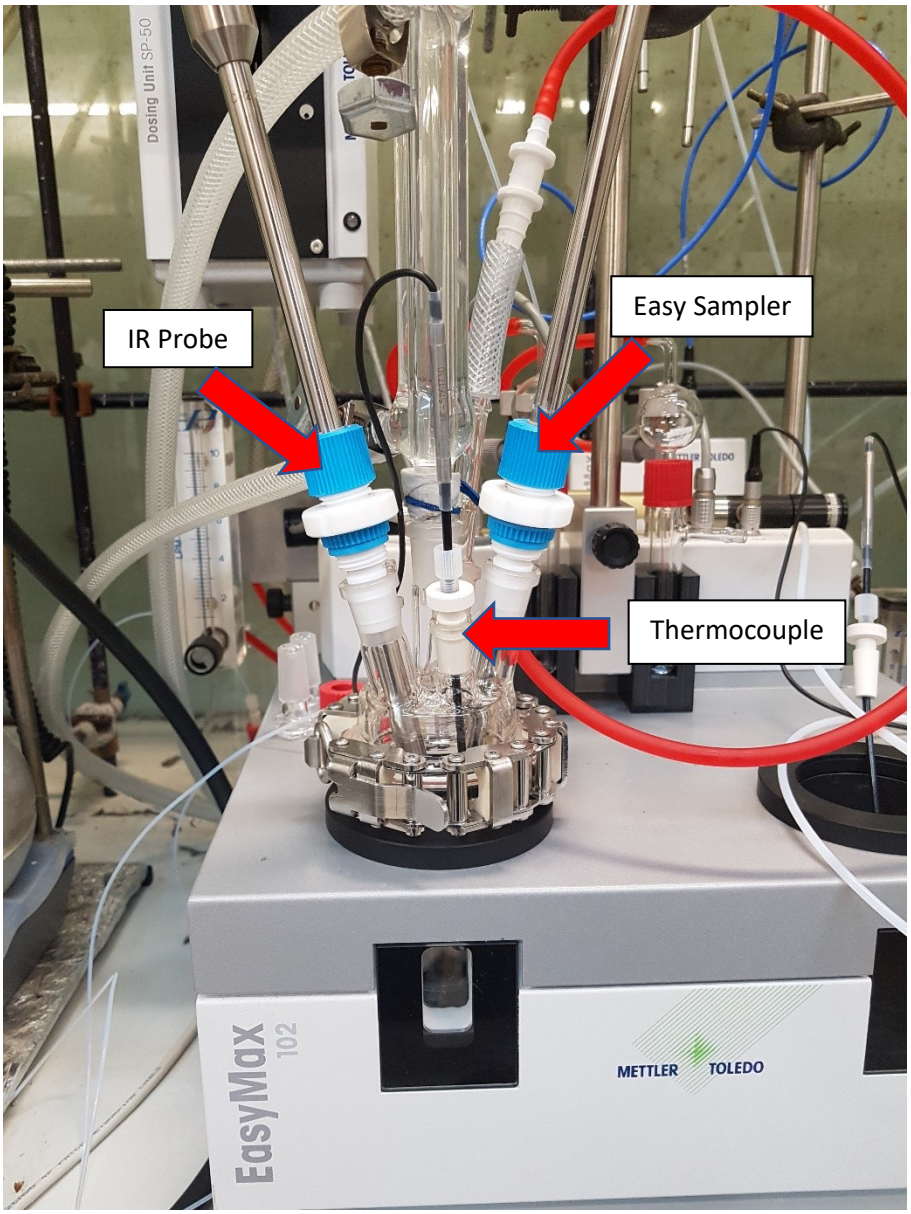
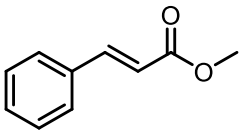


Figure 3.6: Experimental set up in the EasyMax reactor for the kinetic studies.

3.10 Standard Procedure for the Kinetic Analysis of the Pd Catalysed Heck Reaction



A 100 mL glass EasyMax reaction vessel containing a PTFE cross stirrer bar (4 x 4 cm) was purged with N_2 for 20 mins and fitted with a thermocouple, condenser and ReactIR 15 probe. The vessel was then charged with dried DMF (37.2 mL), iodobenzene (0.815 g, 4 mmol, 1 eq.), methyl acrylate (0.516 g, 6 mmol, 1.5 eq.) and triethylamine (0.607 g, 6 mmol, 1.5 eq.). The jacketed reaction vessel was then heated to 80 - 110 °C and stirred at 200 rpm.

A Pd stock solution (typically 100 ppm/mL) was then prepared by dissolving $Pd(OAc)_2$ (0.9 mg) in dry DMF (10 mL) in a volumetric flask. The solution was employed in catalytic reactions within an hour of its preparation. Different amounts of the stock were dispensed, depending on the requisite catalyst loadings (50 µL– 10 mL, corresponding to 5-1000 ppm). A more concentrated Pd stock solution of 1000 ppm/mL was also prepared and used for catalyst loadings between 100–1000 ppm (100 µL – 1 mL). Comparison of the two stock solutions for reactions with a 100 ppm [Pd] loading showed no discernible effect on the reaction profile.

Once reaction temperature had been attained, a portion of the Pd stock solution was injected into the reaction mixture to initiate the reaction. 6 aliquots of the reaction mixture (20 µL) were extracted throughout the course of the reaction for offline HPLC quantification for orthogonal analysis of iodobenzene and methyl cinnamate. The samples were then prepared using a 1:50 dilution with acetonitrile (980 µL) containing the internal standard cumene (0.001 mM) and analysed by HPLC.

The Reaction mixture was then cooled to room temperature and filtered over Celite, which was washed with hexane (~10 mL). The filtrate was evaporated in vacuo, and purification was achieved by flash column chromatography (1:3 Diethyl Ether: Hexane) providing methyl cinnamate (87 %, 3.48 mmol, 564.5 mg) as a white solid.

^{1}H NMR (400 MHz, $CDCl_3$) δ 3.83 (s, 3H), 6.47 (d, J = 16.0 Hz, 1H), 7.37 – 7.44 (m, 3H), 7.52 – 7.57 (m, 2H), 7.72 (d, J = 16.1 Hz, 1H).

^{13}C{^{1}H} NMR (101 MHz, $CDCl_3$) δ 51.73, 117.79, 128.08, 128.90, 130.32, 134.37, 144.90, 167.45

IR (cm^{-1}): 3024, 2993, 1717, 1639, 1536, 1185, 726.

Melting point (°C): 33 – 35 (lit. 33-38).

3.11 Kinetic Reactions (catalyst dosing)

A 100 mL glass EasyMax reaction vessel containing a PTFE cross stirrer bar (4 x 4 cm) was purged with N_2 for 20 mins and fitted with a thermocouple, condenser and ReactIR 15 probe. The vessel was then charged with dried DMF (37.2 mL), iodobenzene (0.204 g, 1 mmol, 1 eq.), methyl acrylate (0.129 g, 1.5 mmol, 1.5 eq.) and triethylamine (0.152 g, 1.5 mmol, 1.5 eq.). The jacketed reaction vessel was then heated to 110 °C and stirred at 200 rpm.

The reaction was initiated with the addition of 1 mL of the Pd stock solution (100 ppm/mL or 1000 ppm/mL), and the reaction progress was monitored by *in situ* FTIR (consumption of iodobenzene and formation of cinnamate product). Once the iodobenzene has been entirely consumed, a further portion of reactants and reagents, consisting of: iodobenzene (0.204 g, 1 mmol, 1 eq.), methyl acrylate (0.129 g, 1.5 mmol, 1.5 eq.) and triethylamine (0.152 g, 1.5 mmol, 1.5 eq.) were added simultaneously using a 1 mL syringe. The process was repeated three times. Aliquots of the reaction mixture were also extracted immediately before and after each addition for HPLC analysis.

3.12 IR Calibration Data

The *in situ* IR data was calibrated with offline HPLC analysis to quantify the consumption of iodobenzene and the formation of the product methyl cinnamate. An internal standard (cumene) was used to account for systematic and random error by monitoring the ratio of the response of the internal standard to the analyte peak areas of interest.

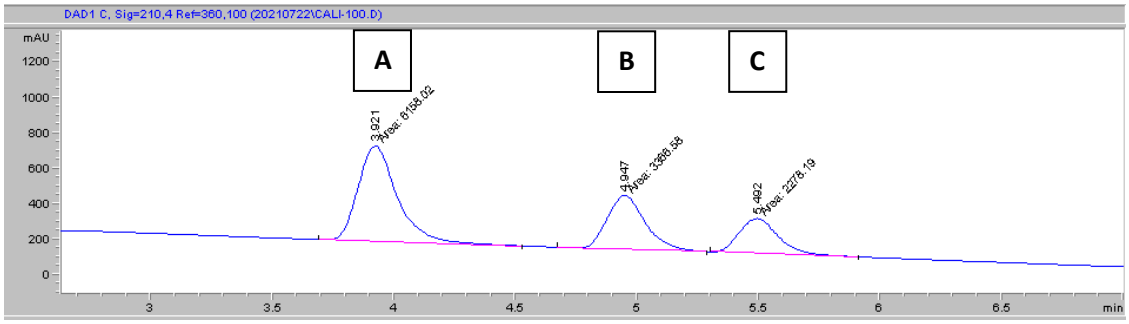


Figure 3.7: Chromatogram of a reaction aliquot showing the elution of the peaks in the following order – A) Methyl cinnamate, B) Iodobenzene, C) Cumene.

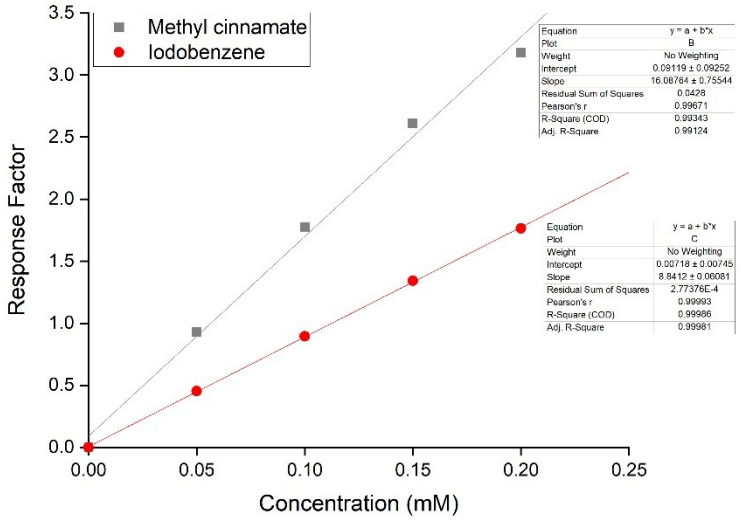


Figure 3.8: Calibration curve constructed from the response factors of iodobenzene and methyl cinnamate.

3.13 Data Processing for *in situ* IR Quantification

Reaction aliquots were taken periodically throughout the reactions and quantified as above using HPLC analysis. This data was then inputted into iC IR 7.0 software in the offline sample table. From the resulting IR spectrum peaks at 739 cm^{-1} and 769 cm^{-1} which corresponded to iodobenzene and methyl cinnamate respectively, full reaction profiles were attained. The data was then exported to a excel file where rate data was extracted and used for VTNA and RPKA analysis.

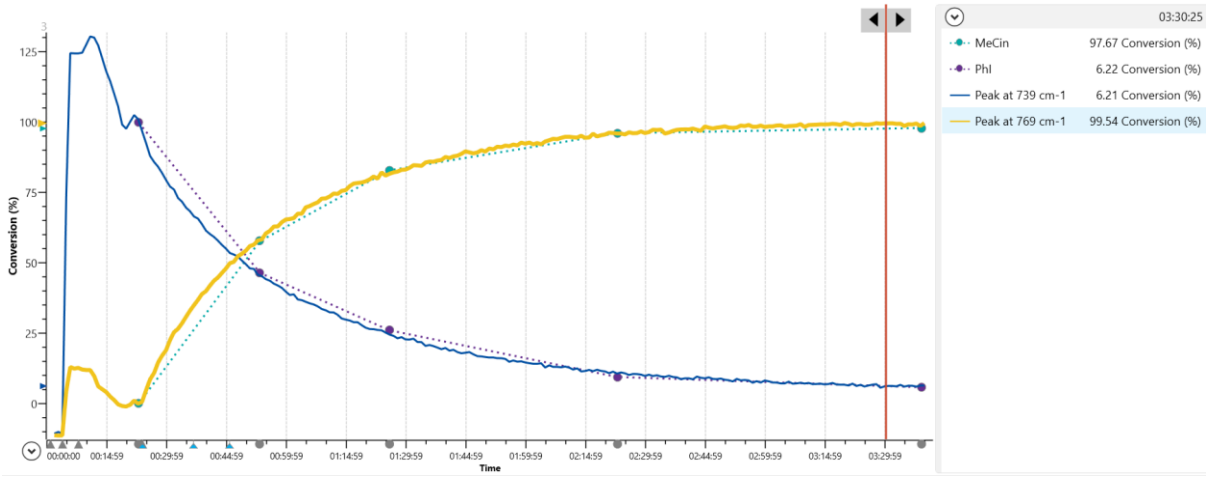


Figure 3.9: Snippet of the IR trends correlated to the HPLC data in the iC IR 7.0 software.

3.14 RPKA and VTNA Data Processing

Concentration profiles obtained from different excess, same excess and different catalyst loading experiments were used for RPKA and VTNA analysis. For same excess experiments the concentration profile was time shifted on the x-axis to achieve overlay with the control and different excess reaction profiles.

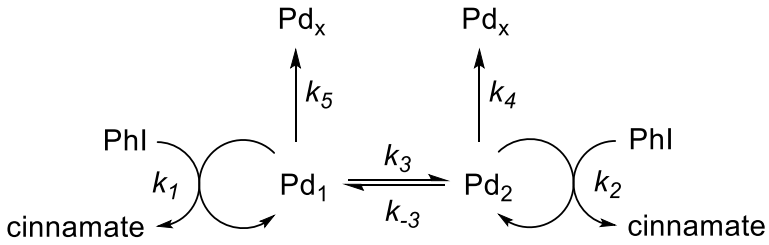
VTNA analysis was used to interpret the order in $Pd(OAc)_2$. The overlay of reaction profiles that differ in the catalyst loading occurs when the correct order in the catalyst is used in the normalization of one of the plot axis. As concentration plots were used the normalization was performed in the time axis. The time axis of each reaction profile for catalyst loadings in the range of 30-1000 ppm were normalised by the initial catalyst loading thus removing any kinetic effects. The order in the catalyst was then attained visually by raising the normalised x-axis to a power which represents the order in the catalyst.

3.15 Kinetic Modelling

Berkeley Madonna™ is a mathematical modelling software developed at the university of California in Berkeley, which can numerically solve differential equations. By building a model based on kinetic equations of proposed reaction steps and inputting the initial conditions the reaction rates can be predicted by the software to give the best fit to the experimental data. Using the curve fit function, a graphical representation of the model was fitted to the experimental data collected from the batch reactions of different catalyst loadings conducted in the EasyMax system.

The code in Table 3.2 was derived from the final model which produced the best fit to the experimental data. In order to superimpose each experimental dataset and model different reaction conditions simultaneously the code in Table 3.2 was duplicated with the letter n being substituted with numbers 1 – 8 used to distinguish each experimental dataset. Importantly, the rate constants do not contain a unique identifier and so are common to every set of differential equations. A total of 8 experimental data sets were used in combination to determine the values of the rate constants (k1, k2, k3, kr3, k4, k5 with the rate constants kr1, kr2, kr4 and kr5 being set to zero).

Table 3.2: Sample code for the final kinetic model.



Code	Function
k1 = 1 kr1 = 0 k2 = 1 kr2 = 0 k3 = 1 kr3 = 0 k4 = 1 kr4 = 0 k5 = 1 kr5 = 0	These define the rate constants (initial values are chosen arbitrarily).
INIT PhI_xx = 4 INIT Pd1_xx = 0.0024 INIT MeCin_xx = 0 INIT Pd2_xx = 0.0008 INIT Pdx_xx = 0	Defines the initial concentrations of the key reactants and reaction intermediates.
RXN1_xx=k1*PhI_xx*Pd1_xx-kr1*MeCin_xx*Pd1_xx RXN2_xx=k2*PhI_xx*Pd2_xx-kr2*MeCin_xx*Pd2_xx RXN3_xx=k3*Pd1_xx*Pd1_xx-kr3*Pd2_xx RXN4_xx=k4*Pd2_xx-kr4*Pdx_xx RXN5_xx=k5*Pd1_xx-kr5*Pdx_xx	Defines each step of the proposed model.
d/dt(PhI_xx)=-RXN1_xx-RXN2_xx d/dt(MeCin_xx)=+RXN1_xx+RXN2_xx d/dt(Pd1_xx)=-RXN3_xx-RXN5_xx d/dt(Pd2_xx)=+RXN3_xx-RXN4_xx d/dt(Pdx_xx)=+RXN4_xx+RXN5_xx	Defines the change in concentration with time for each initial concentration. These are the differential equations which the software solves.

Chapter 4. Catalysis in Flow – Leaching

4.1 Introduction

Heterogeneous catalysts dominate the market share of industrial catalysis and are involved in over 95% of industrial chemical processes [135]. As discussed in Chapter 2, the major advantage of using a heterogeneous catalyst is the ease of separation of the catalyst from the reaction mixture, allowing for simpler process scale up. There are many reports on the recyclability of these catalysts where they can be reused for subsequent reactions without significant loss of catalytic activity [136]. However, catalytic deactivation is a common problem which reduces the turnover frequency with each subsequent reaction (for batch processes), or the reduction in productivity over time (for continuous flow processes). The reasons for catalyst deactivation can be due to several possibilities such as: catalyst poisoning, fouling, thermal degradation, sintering, crushing and leaching [137]. A commonality of all deactivation pathways is the loss of catalytic active sites. There have been many approaches to tackling catalyst deactivation which were discussed in Chapter 2, including: the reactor design, the catalyst design, the addition of reaction stabilisers/additives.

For catalytic reactions involving reactants in a liquid phase, catalyst leaching is a major concern [82]. The drawbacks of leaching pose a particular complication to the separation procedure due to contaminating the product stream. This is problematic for industrial adaptation as metal impurities are strictly regulated in pharmaceutical drugs due to their toxicity [64]. Current methods to assess leaching consist of trace metal analysis (ICP-OES, ICP-MS), imaging techniques (TEM), hot filtration, the three-phase test and the mercury test. However, these are *ex situ* methods and offer little insight into the mechanisms of leaching. More recent advancements in understanding the fundamental mechanics of catalyst leaching are a result of advancements *in situ* analysis techniques and flow technologies for in line analysis. Utilising flow techniques and in line analytics the Kappe group [123, 124] (section 2.6) proposed that the leaching phenomenon for Pd cross-coupling reactions is due to the transformation of Pd^0 species into soluble Pd^{II} species during the oxidative addition step. This means that as the solubilisation of Pd^0 to Pd^{II} is engrained in the mechanism then leaching is a fundamental component of heterogeneous Pd cross coupling reactions, which therefore throws doubt over what the term 'heterogenous catalysis' really means in this context.

4.2 Results and Discussion

In configuration 1, the tandem flow reactor consists of a packed bed reactor (PBR) coupled with an empty plug flow reactor (PFR), each having independent temperature controls and residence times (Scheme 3.1, Figure 3.2). The progress of the reaction was monitored simultaneously at two positions: immediately after the PBR (S1) and after the PFR (S2). An assessment of the catalyst stability and leaching profile can be made by comparing two concurrent samples from S1 and S2; these relate to the 'heterogeneous' and 'homogeneous' catalysed reactions respectively. The amount of Pd leached can also be determined by ICP analysis of the collected samples.

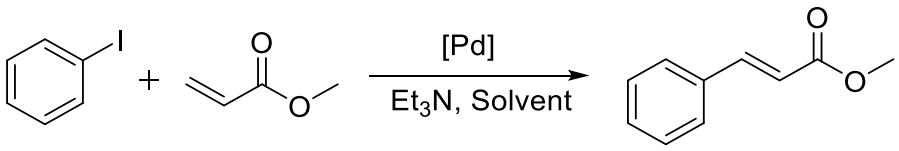
Using configuration 1 of the tandem flow reactor, several possible outcomes have previously been proposed by our group by comparing the product concentration from the sample immediately after the PBR (S1) with those from the outlet of the PFR (S2) (Table 4.1) [86]. The respective outcomes relate to the catalyst's stability, leaching behaviour and activity.

Table 4.1: Proposed conclusions depending on product concentration at each sample outlet [86].

Product Concentrations	Qualitative conclusion
S1=S2	No active catalyst leaching.
S2>S1	Leaching of active catalyst.
S1=S2, but both decreases with time.	Either: 1) The loss of heterogeneous active sites due to inhibition/poisoning; or 2) The loss of surface sites due to leaching of inactive catalyst.
S1=S2, but both increases with time.	Activation of surface catalysis with no leaching of active catalyst.
S2<S1	Reaction is reversible in the homogeneous phase.

4.2.1 Leaching Studies – Configuration 1

The Heck reaction has been previously used in many leaching studies [65, 92, 93, 123, 138] which was why it was selected for this work. The homogeneous base Et_3N was used with the other starting materials iodobenzene and methyl acrylate in the presence of a heterogeneous catalyst (Scheme 4.1). The heterogeneous catalyst initially used for this work was PdEnCat®30 which is an encapsulated form of Pd in an organic polyurea matrix. PdEnCat®30 was developed by the Ley group [118] and has been used in previous studies by our group, which have shown that it leaches active Pd species for the Heck reaction when using the solvent DMF [86]. DMF is a polar aprotic solvent which itself could behave as a stabiliser for any leached Pd species.



Scheme 4.1: The Heck reaction between iodobenzene, methyl acrylate and triethylamine (base) in the presence of a heterogeneous Pd catalyst.

4.2.2 Solvent Screen

In our previous work, DMF was employed as a solvent. In this work, the effect of solvent on catalyst activity and leaching behaviour was examined further, by comparing results obtained with dioxane (polar, aprotic) and toluene (apolar, aprotic), as they are commonly employed in Heck reactions as alternatives to DMF.

Table 4.2: Comparison of solvent properties [139].

Solvent	Dipole moment	Dielectric constant
N, N-Dimethylformamide (DMF)	3.86	36.7
Toluene	0.36	2.38
1,4-Dioxane	0.45	2.25

The dipole moment is a vector measurement of a molecules polarity and is regularly applied to describe the polarity of a solvent. The dielectric constant is the solvents' ability to separate charges which is also used as a measure of a solvent polarity. Previous reports suggest that the polarity of the solvent influence the stability of Pd species in solution [140, 141].

Using configuration 1 of the tandem flow reactor, the Heck reaction in scheme 4.1 was conducted using DMF, toluene and dioxane as solvents with fresh catalyst cartridges packed with PdEnCat®30. For each solvent the PBR was heated to 90 °C and the PFR was heated to 110 °C. The reactants were introduced with a flow rate of 0.5 mL/min through the reactor with S1 and S2 being collected simultaneously. The conversions, determined by HPLC, at S1 and S2 are compared for each solvent along with ICP analysis to attain the total Pd concentration. This provides direct information on the quantity of Pd leaching and the activity of the leached species with each solvent.

4.2.3 Toluene

The first solvent assessed was toluene. As shown in Figure 4.1, the conversions at S1 and S2 are the same (18% conversion to product). Therefore, there was no further catalytic turnover occurring in the PFR and that the conversion must be occurring solely in the PBR in the presence of the heterogeneous catalyst. The results from the ICP analysis showed the presence of 140 ppm Pd residue present in the collected samples, or 1.5% of the initial Pd loading.

These observations imply that while there was leaching Pd from the heterogeneous catalysts PdEnCat®30 in toluene, the leached species was not catalytically active. This is most likely due to the instability of the initial leached species which agglomerate to form Pd black, which was visible at the exit of the PFR.

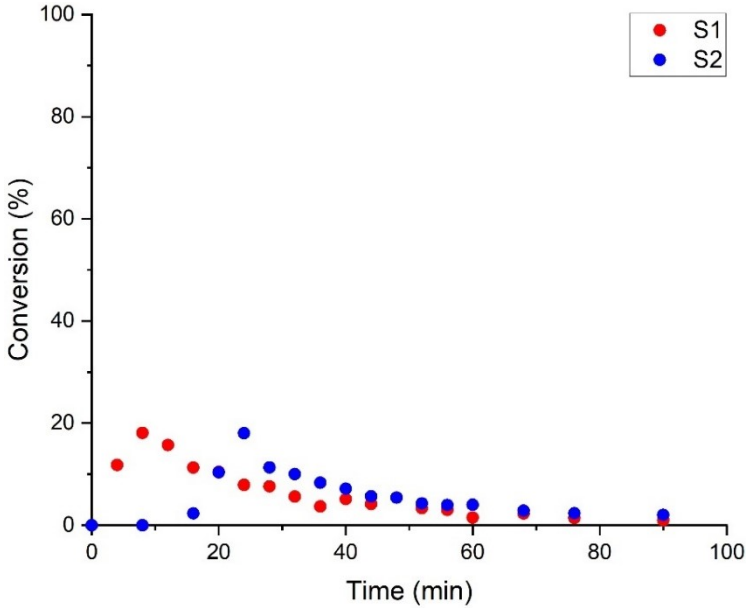


Figure 4.1: Reaction profile of the Heck reaction for the formation of methyl cinnamate in toluene. S1 (red dots) corresponding to the conversion (%) after the PBR and S2 (blue dots) corresponding to the conversion (%) after the PFR.

4.2.4 1,4-Dioxane

The experiment was subsequently replicated with dioxane as the solvent. Once again, similar conversions of the product were observed (16%, S1=S2, Figure 4.2), which also does not show any clear indication that any active species have leached from the catalyst cartridge. The conversion observed at S1 and S2 was 16%, which means that the product was formed on the heterogeneous catalysts surface and there was no further product formation in the PFR. The results from the ICP analysis of all combined samples corresponds to 10 ppm, or 0.11% of the initial Pd loading. This indicates that there was minimal leaching of an inactive Pd species from the heterogeneous catalysts PdEnCat®30 in dioxane. As may be expected with such low level of [Pd], there was no observation of Pd black in any of the samples collected from either S1 or S2.

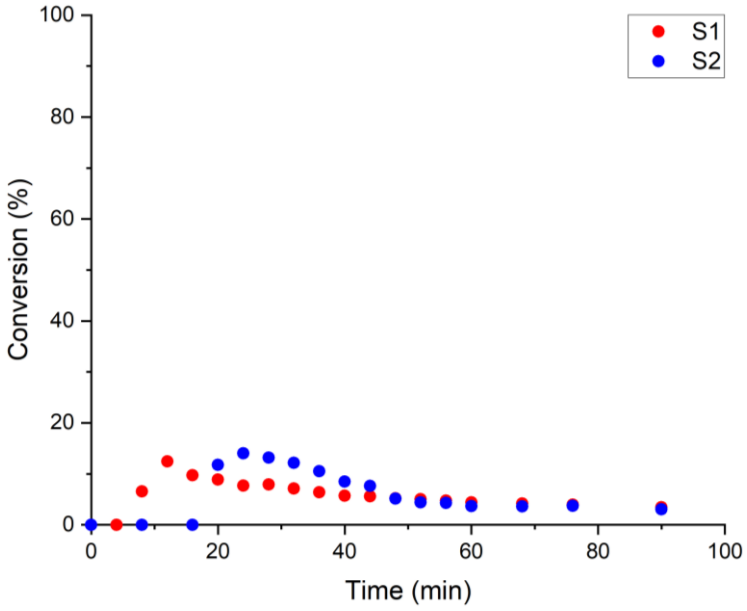


Figure 4.2: Reaction profile of the Heck reaction for the formation of methyl cinnamate in dioxane. S1 (red dots) corresponding to the conversion (%) after the PBR and S2 (blue dots) corresponding to the conversion (%) after the PFR.

4.2.5 Dimethylformamide (DMF)

The final solvent assessed was DMF, which shows a large difference, as S1<S2, indicative of the leaching of active catalyst from the PBR (Figure 4.3). The conversion at S1 was 21% whilst at S2 it was 92%, which means that there was significant conversion occurring in the PFR. The results from the ICP analysis of all combined samples corresponds to a total Pd content of 455 ppm, or 4.9% (0.195 mg) which had leached from the initial Pd loading. This indicates that there was leaching of an active Pd species from the heterogeneous catalysts PdEnCat®30 in DMF.

The homogeneous component of the reaction was accountable for the majority of the conversion, despite only 4.9% of the initial Pd leaching from the catalyst cartridge. This indicates that leached species is much more active than the heterogeneous catalyst.

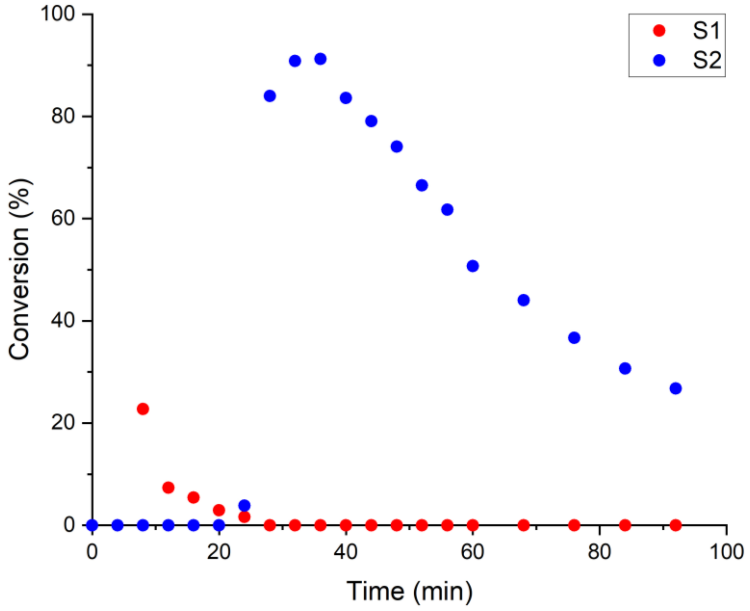


Figure 4.3: Reaction profile of the Heck reaction for the formation of methyl cinnamate in DMF. S1 (red dots) corresponding to the conversion (%) after the PBR and S2 (blue dots) corresponding to the conversion (%) after the PFR.

The reaction profile (Figure 4.3) shows maximum conversion being recorded in the first few samples which decays rapidly with time. This decrease in product formation indicates that there was catalyst deactivation occurring simultaneously during the process. Pd black was also observed at the exit streams of both the PBR and the PFR in samples S1 and S2. This suggests that the deactivation process was initiated in the PBR which was where the observed

Pd black in the PFR could stem from. In comparison to toluene and dioxane the quantity of leaching was the highest for DMF by over 3 and 44 times respectively. Despite leaching occurring in both toluene and dioxane (as indicated by ICP), DMF was the only solvent which produced an active homogeneous species (S2>>S1).

4.2.6 Batch Comparison

In order to verify these results, the Heck flow reaction in scheme 4.1 was replicated in a batch reactor, to assess the activity of the catalyst PdEnCat®30 in each solvent. The same quantity of catalyst, reactants and solvent were used, and the reaction was conducted at 90 °C for 90 minutes, replicating the conditions of the flow reactor. The reaction progresses were monitored by HPLC, which are presented in Figure 4.4. As may be expected, the reaction in DMF was found to reach a much higher conversion (68%) than either toluene or dioxane (both 8%) in 90 minutes, which reflects the conversions in the flow reactor. Notable changes to the reaction mixture were observed in all solvents (Figure 4.5), particularly toluene and dioxane, where the catalyst turned from an initial orange colour to black, indicating Pd deactivation (formation of Pd black). In contrast, for the reaction in DMF, the reaction mixture darkened possibly due to the presence of leached Pd in solution.

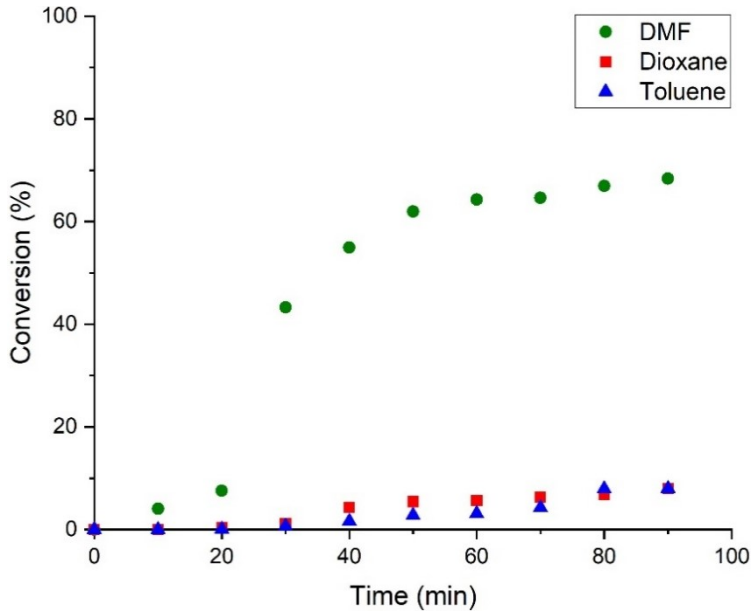


Figure 4.4: Reaction profiles for the Heck arylation of iodobenzene with methyl acrylate performed in the solvents DMF (green dots), dioxane (red squares) and toluene (blue triangles).

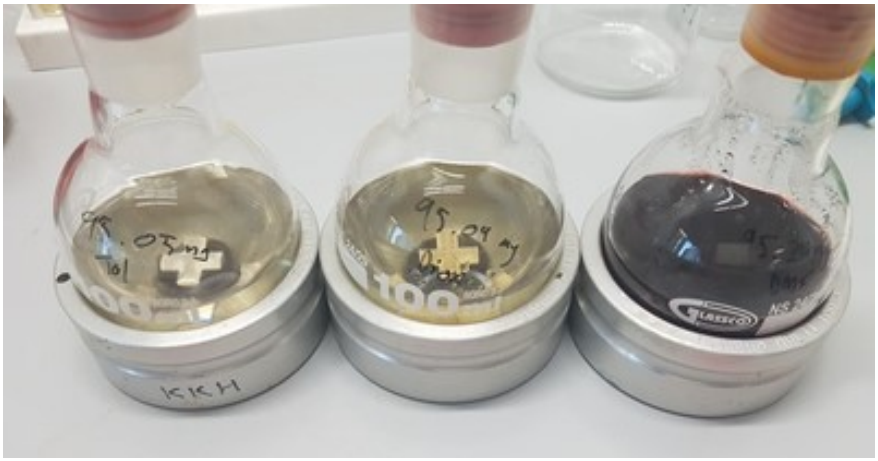
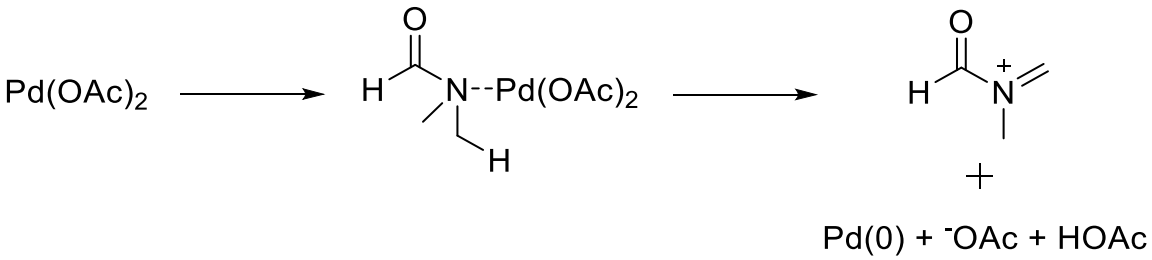


Figure 4.5: Images of the Heck arylation of iodobenzene with methyl acrylate performed in the solvents toluene (left), dioxane (centre) and DMF (right) after 90 minutes.

There was significant leaching of Pd when DMF was employed as a solvent (ICP result from the flow experiments). It had been previously proposed that DMF can ligate to $Pd(OAc)_2$ and reduce it to form a catalytically active Pd(0) species (scheme 4.2) [142]. The high dielectric constant of DMF indicates that it is better suited to stabilising charged species when compared to toluene and dioxane. This could be the reason why a much higher catalytic activity was seen when DMF was used as a solvent.

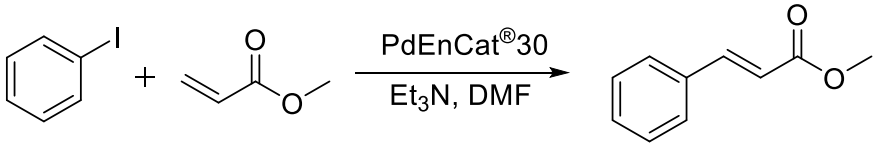


Scheme 4.2: Ligation and reduction of palladium acetate by DMF.

The extent of leaching in these batch reactions is unclear as we cannot rule out a boomerang mechanism, where the catalyst leaches but then redeposits onto the heterogeneous catalyst surface. However, the results obtained from both flow and batch reactions imply that the reaction proceeds heterogeneously in toluene and dioxane. As a result of these findings DMF was chosen as the solvent for further investigations of leaching for PdEnCat®30 and other catalysts.

4.2.7 Effect of Temperature on Catalyst Leaching

Leaching of Pd from PdEnCat®30 is expected to be dependent on the reaction temperature. In this part of the work, the temperature of the PBR was set at 30, 70, 90 and 110 °C, while maintaining the temperature of the PFR at 110 °C. The reaction profiles at S1/S2 were collected to correlate the extent of leaching with catalytic activity.



Scheme 4.3: The Heck reaction between iodobenzene and methyl acrylate catalysed by PdEnCat®30 in the presence of triethylamine in DMF.

Comparing the reaction profiles at S1 (Figure 4.6**A**), product formation was only observed above 70 °C. Below this temperature, very little product formation was formed in the PBR.

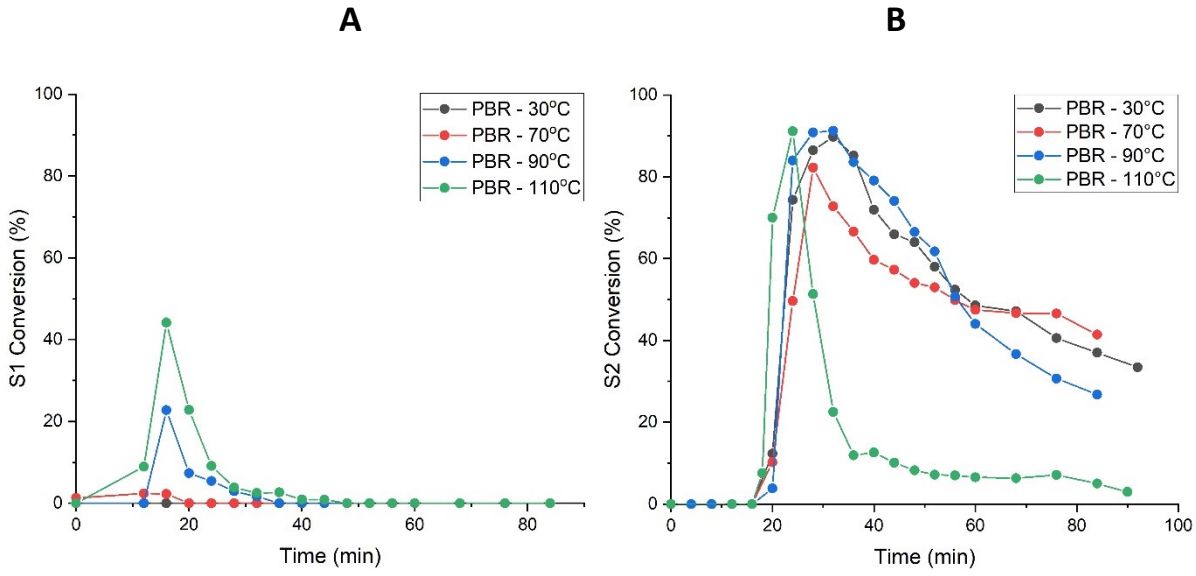


Figure 4.6: Superimposed reaction profiles of the Heck reaction in scheme 3 conducted at various PBR temperatures in the tandem flow reactor using configuration 1. Conversion from S1 sample (**A**) conversion from S2 samples (**B**).

Interestingly, the reaction profiles at S2 (Figure 4.6**B**) show significant product formation, regardless of the temperature of the PBR. This means that there are active catalyst species leaching from the PBR, even when no reaction was occurring heterogeneously. The reaction profiles of the reactions performed at 30-90 °C are similar, displaying high conversions of 90%

for the first few samples which declines steadily to 25-45% by the end of the reaction. In contrast, the reaction profile for the experiment performed at 110 °C displays a rapid decline in conversion after the reaction peak dropping from 91% to 12% in 12 minutes. The observed decline can be attributed to rapid catalyst deactivation, which may be due to faster catalyst leaching of the catalyst bed, as Pd black was observed in the first few samples collected at S2. At higher PBR temperatures (70-110 °C) the catalyst cartridge visibly changes from orange at the start to black at the end of the reaction signifying the formation of Pd black thus catalyst deactivation.

To confirm that there was no Pd contamination in the reactor, the PBR was replaced with a blank cartridge, and all reactants (in DMF) were passed through the entire reactor; with the PBR and the PFR temperatures set to 90 °C and 110 °C, respectively. No product formation was detected at either of the sample outlets (S1 or S2), verifying that there was no background reaction due to residual Pd in the system.

4.2.8 Catalyst Screen

Of the solvents screened leaching was the most prominent in DMF therefore the leaching profile of other catalysts were screened using the same conditions. The selected catalysts were 5% Pd/Al_2O_3, FibreCat 1001 and 5% Pd/C as they have differing characteristics which are summarised in table 4.3. Screening various catalysts with contrasting properties, should give a better insight into the fundamentals of the leaching process and which catalyst properties have the biggest influence on leaching.

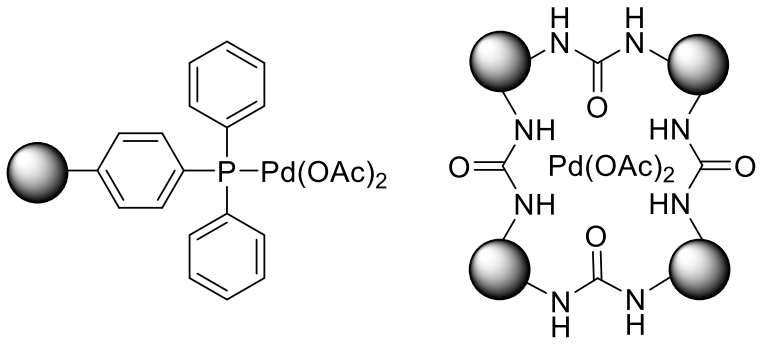


Figure 4.7: (left) structure of FiberCat 1001 covalently bonded to polypropylene and (right) structure of PdEnCat®30 where $Pd(OAc)_2$ is encapsulated in a polyurea matrix.

Table 4.3: Comparison of the type and method of support for the catalysts screened.

Catalyst	Support type [143]	Method of support
PdEnCat®30	Organic	Encapsulation
Pd/Al_2O_3	Inorganic	Adsorption
FibreCat 1001	Organic	Covalent bonding
Pd/C	Carbon	Adsorption

4.2.9 Performance of Pd/Al_2O_3 in Configuration 1

The activity of Pd/Al_2O_3 with the PBR at 90 °C and the PFR at 110 °C was lower of that than PdEnCat®30 for both the heterogeneous (S1) and homogeneous (S2) components (Figure 4.8**A**), however the activity was maintained after the peak of the reaction profile rather than tailing off like PdEnCat®30. This indicates a steady state of leaching where the leached species are consistent in quantity and activity throughout the rest of the reaction. It is also indicative that the catalyst does not deactivate as readily at higher temperatures. ICP analysis of all the samples from S1 and S2 quantified the total Pd which had leached from the catalyst cartridge to be 417 ppm which is similar to that of PdEnCat®30 under the same conditions.

The leaching of Pd/Al_2O_3 was assessed in the absence of a surface catalysed reaction by setting the PBR temperature to 30 °C and the PFR to 110 °C (Figure 4.8**B**). Unlike PdEnCat®30, which showed considerable conversion at S2, Pd/Al_2O_3 does not display any catalytic activity in the samples from S1 or S2, implying that it does not leach any active Pd species in the absence of a surface catalysed reaction. This eludes to the fact that a species other than DMF is responsible for the leaching and is possibly the oxidative addition of the aryl iodide which strips the Pd from the alumina surface. DMF could still play a key role in stabilising the leached species and sustaining its activity in the homogeneous phase.

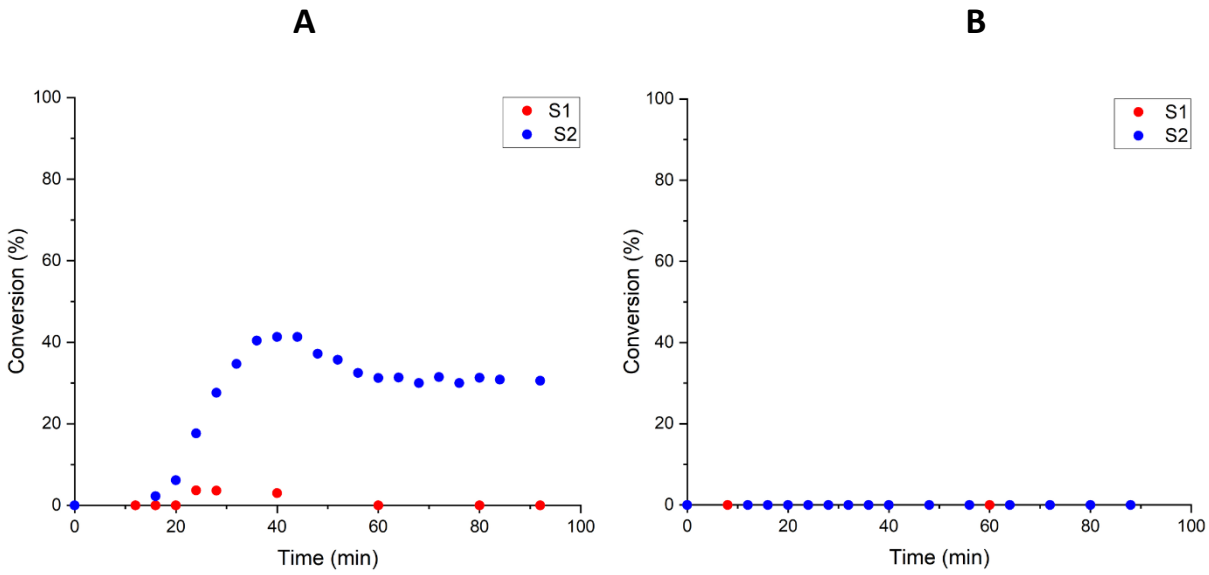


Figure 4.8: Heck reaction catalysed by Pd/Al_2O_3 with the PBR at 90 °C (**A**) or 30 °C (**B**) and the PFR at 110 °C.

By maintaining the PBR temperature at 90 °C and varying the temperature of the PFR between 90 °C and 120 °C, conversions of 15 to 77% were recorded at S2 (Figure 4.9). Even at higher PFR temperatures the catalyst does not deactivate rapidly but maintains its catalytic activity. Although the conversion at S1 was minimal when the PBR was set at 90 °C, it would be wrong to attribute the conversion at S2 exclusively to the leached Pd species but rather view the conversion at S2 as a combination of both homogeneous and heterogeneous catalysis.

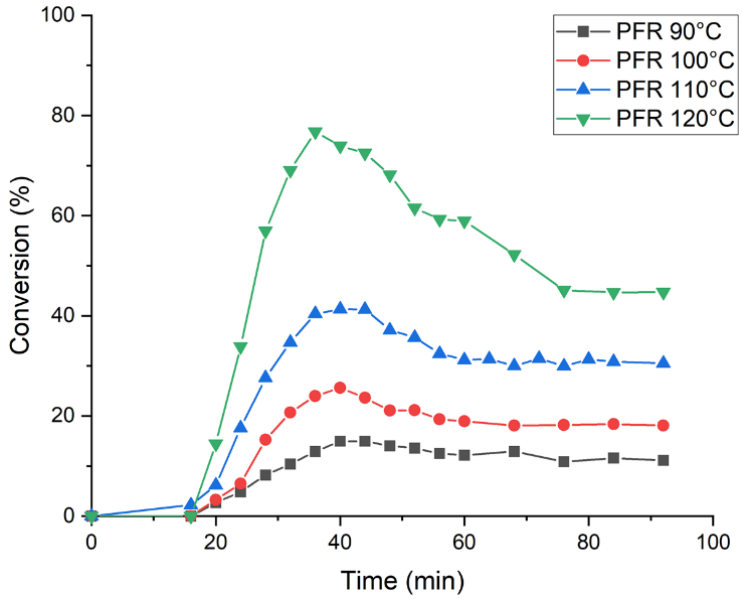


Figure 4.9: Heck reaction catalysed by Pd/Al_2O_3 with the PBR at 90 °C and PFR at 90/100/110/110 °C.

4.2.10 Performance of FiberCat 1001 in Configuration 1

The third catalyst screened was FiberCat 1001 which has a triphenyl phosphine ligand covalently bound to polypropylene and palladium acetate. This was the only catalyst investigated which had a triphenyl phosphine ligand incorporated into its structure. With the PBR temperature set at 90 °C and the PFR reactor temperature varied between 90 and 120 °C, 10% conversion was attained at S1 demonstrating that the reaction proceeds heterogeneously. However, the convesrsion attained at S2 (Figure 4.10**A**) was significantly higher, with conversions reaching 90% indicating that the homogeneous component of the reaction contributes to the majority of the reaction conversion, as was observed with PdEnCat®30. When conducted in the absence of a surface catalysed reaction with the PBR temperature set at 30 °C and the PFR temperature varied between 90 and 120 °C conversion was observed at S2 (Figure 4.10**B**).

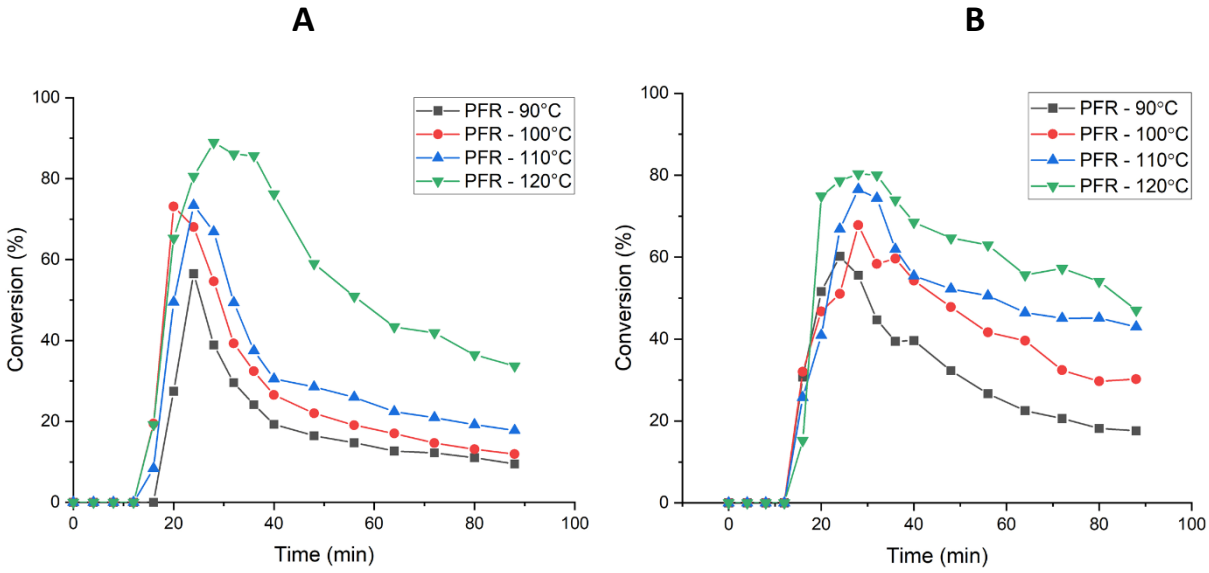


Figure 4.10: Reaction profiles from S2 for the Heck reaction catalysed by FibreCat 1001 with the PBR at 90 °C and PFR at 90/100/110/110 °C (**A**) and with the PBR at 30 °C and PFR at 90/100/110/110 °C (**B**).

When increasing the temperature of the PBR from 30 to 110 °C, a significant decline in conversion was seen at S2 (Figure 4.11). This is linked to the increased formation of Pd black observed in both the catalyst cartridge and in the sample outlet of S2. At higher temperature the heterogenous catalysts deactivates faster and therefore the leached species are inactive in the homogeneous phase.

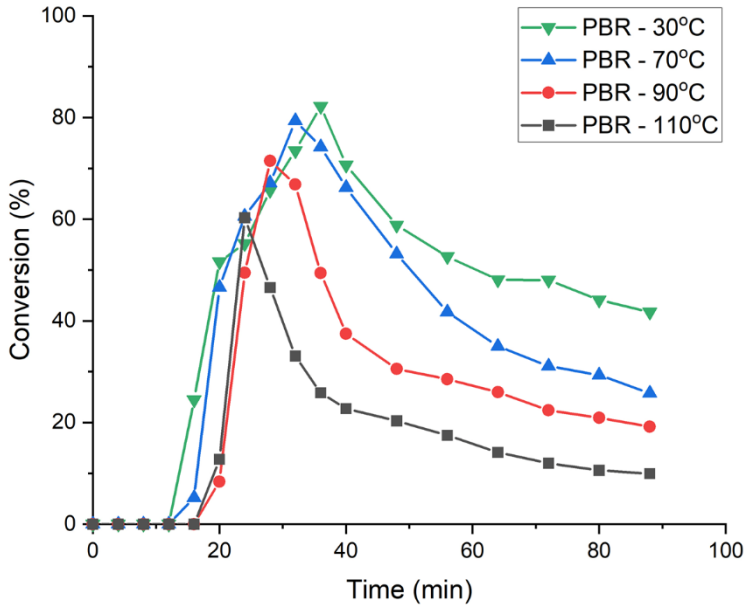


Figure 4.11: Heck reaction catalysed by FibreCat 1001 with the PBR at 30/70/90/110 °C and PFR at 110 °C.

4.2.11 Performance of Pd/C in Configuration 1

Despite Pd/C being one of the most broadly used catalysts for cross coupling reactions, under the present flow conditions it rapidly leached out of the catalyst cartridge when the system was flushed with DMF. The loss of catalyst from the PBR was due to the particle size of Pd/C being too fine to be contained in the catalyst cartridge. Hence, if the reaction solution was passed through the system the conversion at S2 would not be solely due to leached Pd species. As a result, no reaction data was obtained for this catalyst, and it was not further investigated as it was not compatible with the current flow system.

From the catalysts screened two leaching regimes are present: those which only leach active species under surface catalysed conditions (Pd/Al_2O_3) and those which leach active species in the absence of surface catalysed conditions (PdEnCat®30 and FiberCat 1001). The contrasting properties of the supports and methods of entrapment suggest that the organic structures of PdEnCat®30 and FiberCat 1001 are the main influencing factors which affect leaching. The reaction temperature drastically effects the activity of the leached species by causing deactivation to Pd black.

4.2.12 Catalyst Regeneration

In view of the deactivation and loss of activity with time in the tandem flow reactor at elevated PBR temperatures, *in situ* methods to reactivate PdEnCat®30 in the catalyst bed were investigated. Initially the catalyst bed was washed by flowing fresh DMF through the reactor after a 90-minute reaction run (Figure 4.12). By washing the catalyst cartridge with fresh solvent, the conditions at the start of the reaction are replicated (which is where the conversion peaks) as the system was initially primed with solvent. The catalyst cartridge wash should also remove any surface contaminates from the catalyst to renew the activity. The DMF starts eluting after 116 minutes which was evident by the conversion dropping to zero. After 30 minutes of DMF flowing through the reactor the reactants are then passed through. For the second pass the conversion was < 5%, which was the lowest conversion observed at the end of the first pass.

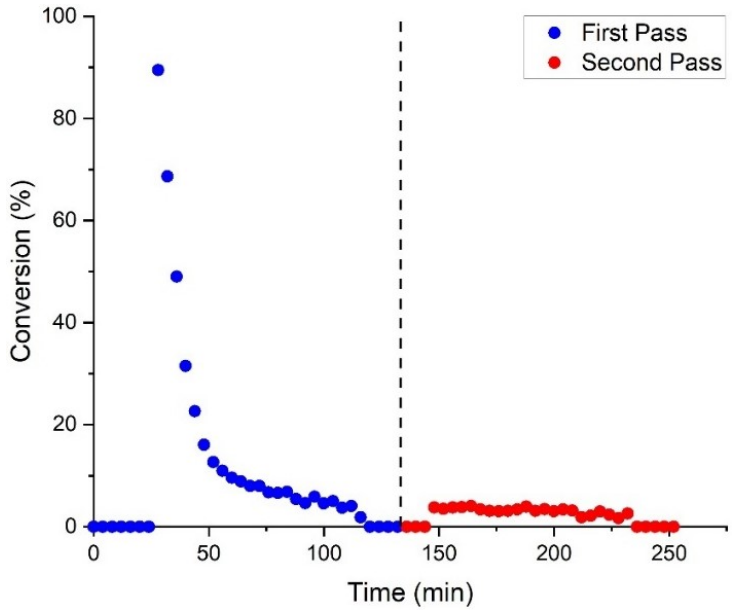


Figure 4.12: Conversion at S2 from the Heck reaction catalysed by PdEnCat®30 before and after washing with DMF with the PBR and PFR set at 110 °C.

The same washing conditions were applied to reactivate Pd/Al_2O_3 (Figure 4.13). The DMF starts eluting after 96 minutes which was evident by the conversion falling to zero. After 30 minutes of DMF flowing through the reactor the reactants are then passed through. For the second pass the conversion did not go above 23%, which was the lowest conversion observed at the end of the first pass. The effect of washing either catalyst had no impact on the catalyst activity and the product conversion at S2 continued to decline in both cases. If anything,

rinsing Pd/Al_2O_3 had a detrimental effect on the catalyst as without any solvent wash the activity reaches a steady state rather than continuing to decline.

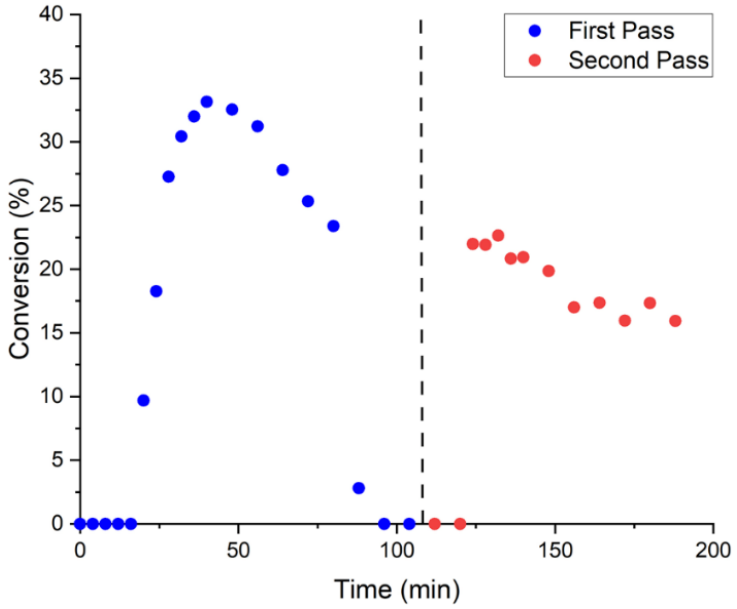


Figure 4.13: Conversion at S2 from the Heck reaction catalysed by $PdAl_2O_3$ before and after washing with DMF with the PBR set at 90 °C and PFR set at 110 °C.

Rather than letting the conversion tail off, the PdEnCat®30 catalyst bed was washed intermittently with DMF to see if the activity could be sustained for longer with the PBR at 90 °C and the PFR at 110 °C. DMF was first passed through the reactor for 20 minutes then the flow was switched to the reactants which were also passed through the reactor for 20 minutes. This process was repeated four times with samples from S2 being analysed (Figure 4.14**A**). The conversion decreased with each cycle from 86% in the first cycle to 21% in the fourth cycle equalling a total reduction of 65% in conversion. This means that washing with DMF had little to no effect on reactivating the catalyst.

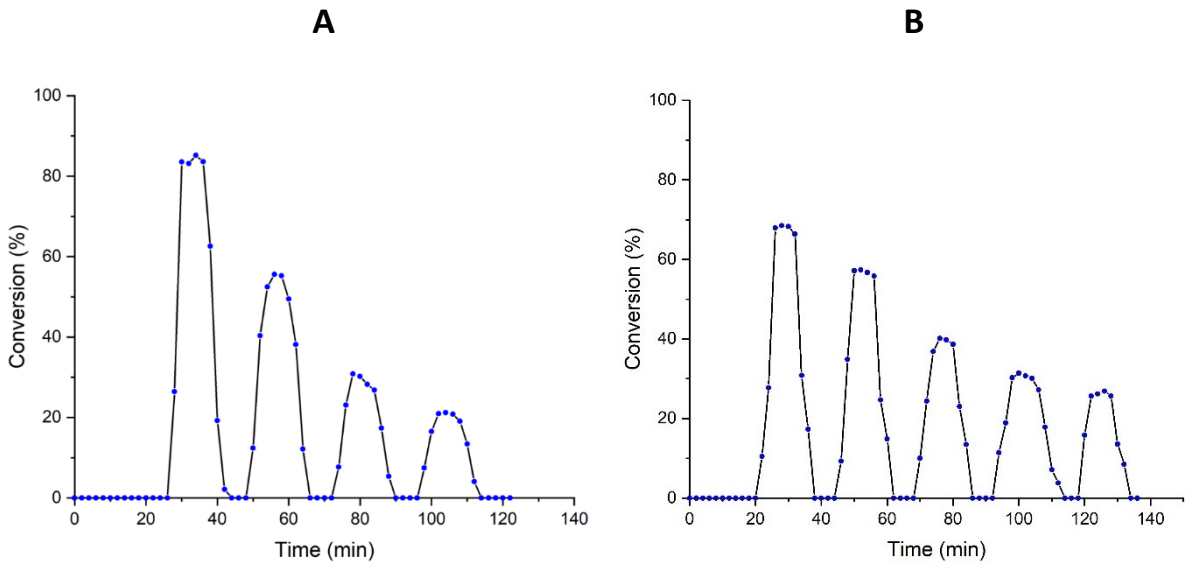


Figure 4.14: Conversion at S2 from the Heck reaction catalysed by PdEnCat®30 washed intermittently with DMF in 20 min reaction cycles when the PBR and PFR are set at 110 °C (**A**) or 30 °C and 110 °C respectively (**B**).

The same intermittent wash was repeated using the PdEnCat®30 catalyst bed with the PBR at 30 °C and the PFR at 110 °C. (Figure 4.14**B**). The conversion decreased with each cycle from 70% in the first cycle to 31% in the fourth cycle. In comparison to the washes with the PBR at 90 °C a smaller reduction in conversion of 39% from the first to the fourth cycle was observed. This is most likely due to a reduction in deactivation of the heterogeneous catalyst due to lower temperatures being used. Overall, the wash with DMF had little to no effect on reactivating PdEnCat®30 or Pd/Al_2O_3. This evidence reinforces the fact that leaching is detrimental to the prospect of reusing or recycling a heterogenous catalyst as it is unlikely to be possible to regenerate the catalyst to its original activity as many sites have leached into the reaction stream.

4.2.13 Reactant screen

For these studies the tandem flow reactor was reconstructed to configuration 2 (Scheme 3.2, Figure 3.3) to assess the roles of the individual components of the Heck reaction on leaching of heterogeneous catalysts. The initial tandem flow reactor was reconstructed with a second flow inlet after the PBR rather than the previous sample outlet (S1). As a result of this modification the experimental set up of configuration 2 involves one flow inlet followed by a PBR of which the outlet mixes with the second inlet at a T-piece. The reaction mixture then passes through an empty PFR, with the outlet leading to an autosampler to collect samples at pre-defined intervals. Each reactor (PBR & PFR) has independent temperature controls and residence times much like configuration 1. However, the progress of the reaction was monitored only at the exit of the PFR (S2). Individual solvents or reactants can be screened for their role in the leaching process by flowing them over the heterogeneous catalyst in the PBR and then mixing the PBR exit stream with the remaining reactants for the Heck reaction through the sample inlet. As a result, conversion will only take place in the PFR if Pd leaches out of the PBR as no heterogeneous catalysis can take place with only one reactant. Therefore, the activity and quantity of leached Pd can be related to individual components of the reaction.

4.2.14 Reactant effects on the leaching of Pd from PdEnCat®30

In this part of the work, the aim was to identify the role each reaction component plays in catalyst leaching. This was achieved by exposing the packed bed of catalyst to individual components of the Heck reaction, including: solvent (DMF), iodobenzene, methyl acrylate, triethylamine and then testing the catalytic activity in the resultant eluent with the rest of the reaction mixture in the PFR. In each experiment, the temperature of the PBR was set at two temperatures: 30 °C and 90 °C.

The first component to be screened for its effect on leaching of PdEnCat®30 was the solvent DMF. The reaction was conducted by having the PBR initially set at 30 °C and then heated to 90 °C with the PFR temperature maintained at 110 °C. The flow rate for each inlet was set at 0.25 mL/min so the rate of DMF passing through the PBR was 0.25 mL/min whilst the flow rate of iodobenzene, methyl acrylate and triethylamine in DMF through the PFR was 0.5 mL/min. Samples are collected periodically from the PFR outlet (e.g. every 4 mins) and then

quantified using HPLC to be plotted as conversion time graphs, with each data point representing a sample.

No noticeable leaching was caused by exposing the PBR to DMF at 30 °C: very little product formation was observed in the collected fraction (between 2-8%, Figure 4.15**A**, blue line). A very similar result was obtained when the temperature of the PBR was raised to 90 °C (Figure 4.15**A**, red line). ICP analysis showed the presence of 30 ppm of Pd in the combined fraction. This indicates that DMF does not cause significant amount of leaching of Pd species.

A very similar result was observed when the PBR was exposed to a solution of methyl acrylate in DMF (Figure 4.15**B**). The total Pd leached was 36 ppm. This indicates that methyl acrylate has little to no influence on the activity or quantity of the leached species.

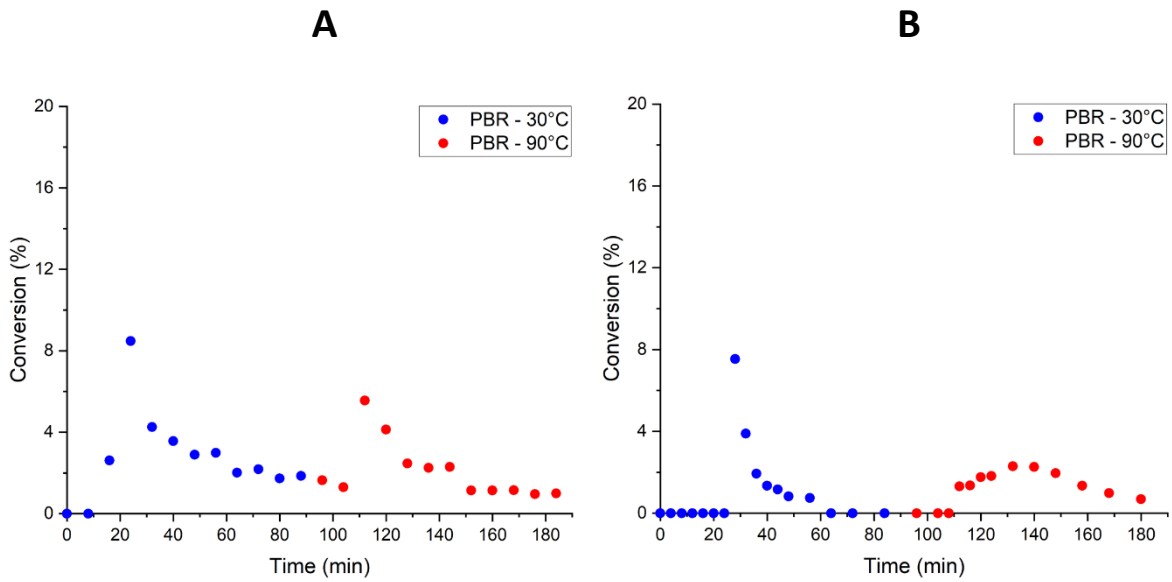


Figure 4.15: Reaction profile from DMF (**A**) and a mixture of DMF and methyl acrylate (**B**) passing through the PBR at 30 °C which was then elevated 90 °C after 90 mins.

Next, a mixture of DMF and iodobenzene was passed through the PBR at 30 and 90 °C (Figure 4.16). Initially, at 30 °C, the reaction output was very similar to that obtained from the previous experiments with methyl acrylate and DMF, i.e. only a small amount of product formation was observed, which declined rapidly to zero. So, it can be concluded that at 30 °C, a minimal amount of leaching occurs for DMF, methyl acrylate and iodobenzene.

When the PBR was heated to 90 °C, a significant increase in conversion was observed, indicating the leaching of catalytically active Pd, which was confirmed by the observation of 65 ppm of Pd residue in the collected eluent.

Comparing the results from these three experiments, it is clear that iodobenzene can induce Pd leaching, but only at 90 °C. This suggests that a chemical transformation is involved in the leaching process. It is known that the oxidative addition step of the Heck reaction involves an aryl halide which reduces a Pd^0 species to a Pd^{II} species. Based on this evidence it can be proposed that the Pd^0 species is leached from the surface of the catalyst by the OA process, in the form of solubilised Pd(II) species.

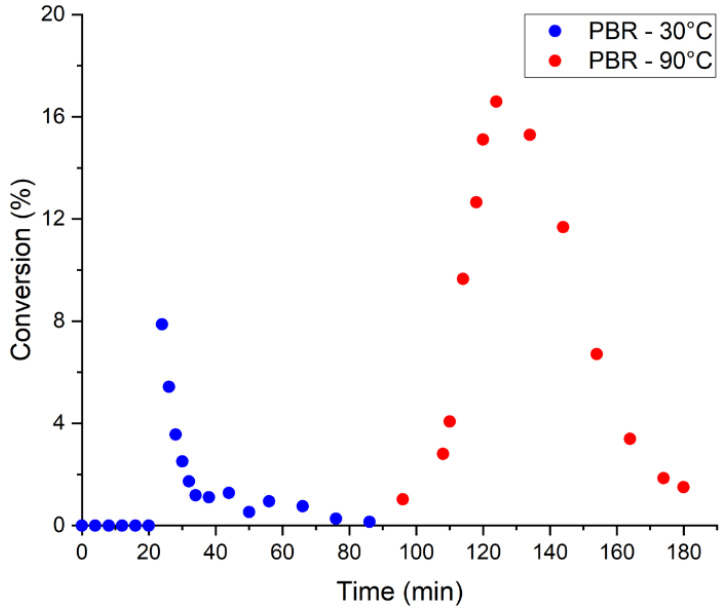


Figure 4.16: Reaction profile from a mixture of DMF and iodobenzene passing through the PBR at 30 °C which was then elevated to 90 °C after 90 mins.

Finally, a solution of triethylamine in DMF was passed through the PBR, before it was combined with a mixture of iodobenzene, methyl acrylate in DMF prior to entering the PFR. Rather surprisingly, significant product formation can be observed at the outlet (Figure 4.17). The substantial amount of product (36%) signifies that leaching of an active Pd species took place at even at 30 °C. It was interesting to see that the product formation declines quite substantially (blue line). Upon increasing the temperature of the PBR to 90 °C, however, there was another notable steep increase in the product formation, followed by a steep decline (Figure 4.17, red line). The total amount of Pd leached was determined to be 182 ppm; the

highest of any reactant. Thus, it can be concluded that the amount of leaching caused by the individual reaction components is in the following order (highest first): NEt_3 > PhI > MeAc.

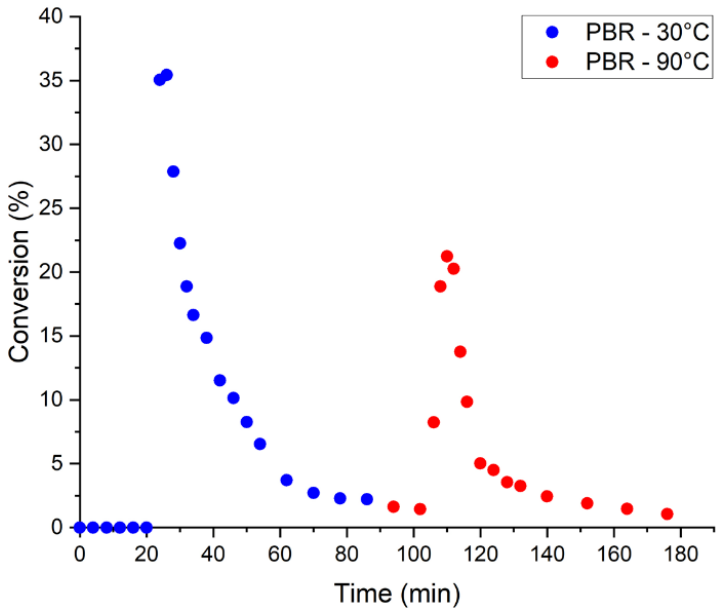


Figure 4.17: Reaction profile from a mixture of DMF and triethylamine passing through the PBR at 30 °C which was then elevated to 90 °C after 90 mins.

Overall, for the catalyst PdEnCat®30, both iodobenzene and triethylamine have been implicated as the major reaction components which causes the leaching of active Pd from the heterogeneous catalyst. At low temperatures, Pd can coordinate to triethylamine and consequently caused the metal to solubilise. In contrast, at elevated temperature, iodobenzene can undergo oxidative addition with the surface Pd to cause leaching. Both DMF and methyl acrylate had little effect on leaching with the lowest conversion and quantity of Pd recorded for these reaction components.

4.2.15 Reactant effects on the leaching of Pd from FiberCat 1001

The ability of each reaction component to cause Pd leaching from FiberCat 1001 was assessed using the same approach as described above (Section 3.4.7), but only with iodobenzene and triethylamine, which had been shown to cause leaching. FiberCat 1001 is a heterogeneous Pd catalyst which has a triphenyl phosphine ligand covalently bound to polypropylene and palladium acetate. This was the only catalyst investigated which has a triphenyl phosphine ligand incorporated into its structure. A comparison with the other heterogeneous catalysts can be found in section 4.2.8 Table 4.3.

First, a solution of iodobenzene in DMF was passed through the PBR containing at 30 °C which was subsequently heated to 90 °C after 90 min (Figure 4.18). An initial peak of 15% in conversion was present at 30 °C which then tails off to 4% after 90 minutes. Upon heating to 90 °C there was a sharp rise in conversion to 30% which then tails off to below 1%. This profile is similar to that obtained for the experiment with PdEnCat®30 and iodobenzene, albeit at higher conversions (Figure 4.16). As a result, the same conclusions were drawn where at 90 °C oxidative addition of Pd into the aryl halide bond solubilises more Pd which leads to a higher product concentration at the exit of the PFR. However, in this case there are noticeable conversions even at 30 °C which suggests a different leaching mechanism is at play. A simple explanation to this could be down to the physical properties of the FiberCat 1001 where the Pd is weakly bound and so more residual leaching occurs. As the conversion tails off to negligible quantities it can be viewed that deactivation is accelerated at higher temperatures.

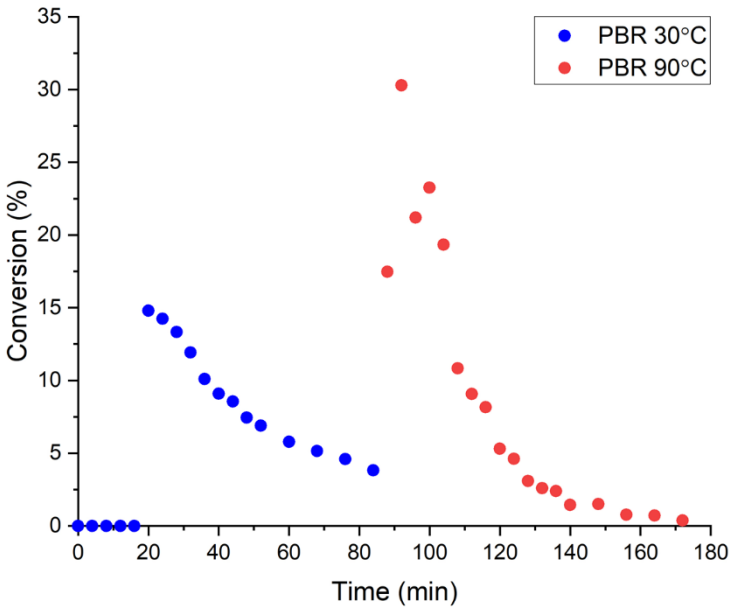


Figure 4.18: Reaction profile from a mixture of DMF and iodobenzene passing through the PBR containing FiberCat 1001 at 30 °C which was then elevated to 90 °C after 90 mins.

Next, a solution of triethylamine in DMF was pumped through the PBR, containing FiberCat 1001, at 30 °C, as described above. The reaction output at S2 revealed an initial product formation of 36%, which tailed off and plateaued at 6% after 90 minutes (Figure 4.19). Upon heating to 90 °C, there was a sharp rise in product yield to 25%, which then tails off to below 17%. Although the conversion tails off, the plateau does not fall to 0% conversion; meaning that some catalytic activity was sustained. This shows that the FiberCat 1001 catalyst

deactivates to a lesser extent that that of PdEnCat®30 when in the presence of DMF and triethylamine. Nevertheless, triethylamine significantly contributes to leaching even at low temperatures.

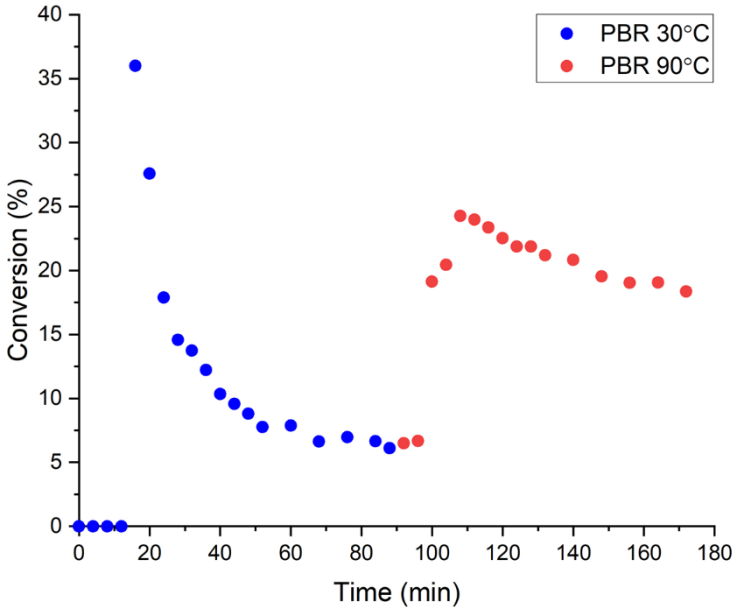


Figure 4.19: Reaction profile from a mixture of DMF and triethylamine passing through the PBR containing FiberCat 1001 at 30 °C which was then elevated to 90 °C after 90 mins.

Overall, for the catalyst FiberCat 1001, moderate conversions were observed at the outlet of the PFR which could only be possible if Pd had leached from the heterogeneous catalyst. Of the two reactants screened, triethylamine led to the highest conversions when the PBR was set at 30 °C whilst iodobenzene produces higher conversions with the PBR set at 90 °C. However, by comparing the slopes of the conversion time graphs of FiberCat 1001 with PdEnCat®30 the catalyst deactivates to a lesser extent due to the plateaus not dropping off to 0%.

4.2.16 Reactant effects on the leaching of Pd from Pd/Al_2O_3

The final catalyst to be investigated for reactant effects on leaching was Pd/Al_2O_3: the only catalyst investigated which had an inorganic support.

To begin, a solution of the reactant iodobenzene in DMF was screened by passing it through the PBR containing the catalyst Pd/Al_2O_3 (Figure 4.20). This was performed with the PBR at 90 °C due to no active species leaching when the reaction was run with the PBR at 30 °C as shown previously in Figure 4.8**B**. The resulting reaction profile is similar to figure 4.8**A** (when all

reactants are passed through the PBR at 90 °C using configuration 1), suggesting that iodobenzene is the main component of the Heck reaction to cause leaching from Pd/Al_2O_3. ICP analysis of the combined fractions quantified that 382 ppm of Pd had leached from the catalyst cartridge into the sample collected at the outlet of the PFR. As the quantity of leached Pd is similar to that observed previously for Figure 4.8**A** (417 ppm) which also employed Pd/Al_2O_3 as a catalyst, it provides further evidence that iodobenzene is the main and potentially the sole contributor to leaching of Pd from Pd/Al_2O_3.

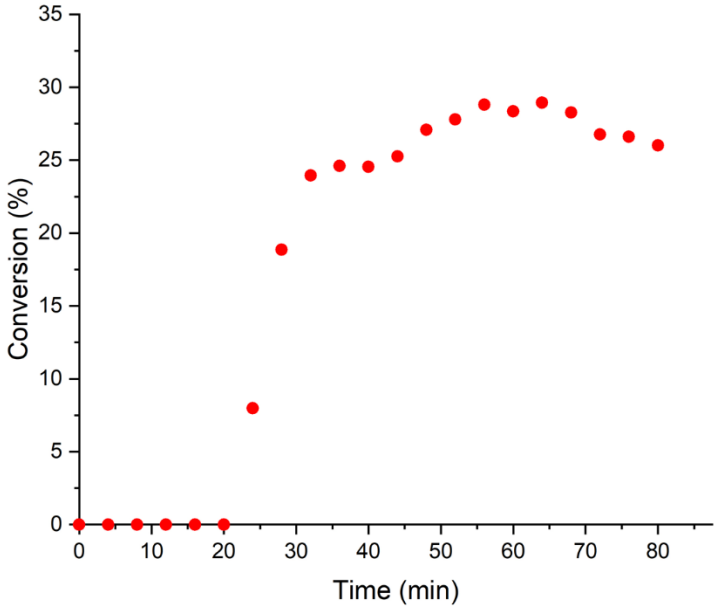


Figure 4.20: Reaction profile from a mixture of DMF and iodobenzene passing through the PBR containing Pd/Al_2O_3 at 90 °C for 90 mins.

Triethylamine was then assessed under the same condition as iodobenzene for Pd/Al_2O_3 and no conversion was obtained at the exit of the PFR, which further supports the theory that oxidative addition is the only method of leaching occurring with the catalyst Pd/Al_2O_3.

4.3 Conclusions

It was shown that leaching is prominent in the Heck reaction when it was performed in the polar aprotic solvent DMF. Using a modified tandem flow reactor, a series of experiments were executed to study the effect of each reaction component (solvent, iodobenzene, methyl acrylate and triethylamine) on the leaching behaviour of three different heterogeneous catalysts: PdEnCat®30, FiberCat 1001 and Pd/Al2O3.

Of the four catalysts investigated, Pd/Al_2O_3 showed the highest resistance to leaching at ambient temperature. In contrast, significant leaching was observed for PdEnCat®30 and FiberCat 1001 at both ambient and reaction temperature. This reflects that the catalyst support employed, and how the method of immobilisation can influence the extent of leaching. As the structure of Pd/Al_2O_3 is a robust and inert support with well-defined active sites, leaching appears to occur in a systematic manner as demonstrated by a steady rate of conversion. However, the structures of PdEnCat®30 and FiberCat 1001 involve polymers which can be distorted and swell in harsh solvents such as DMF. If these structures become distorted, then pronounced leaching may result.

In contrast with batch reactions, simply washing the heterogeneous catalyst with a solvent was not effective enough to regenerate the catalysts activity in a flow regime. This is because leaching is a destructive process in a flow regime i.e. once an active site is lost in flow it is swept away with the mobile phase rendering the leached species unable to redeposit onto the heterogeneous surface.

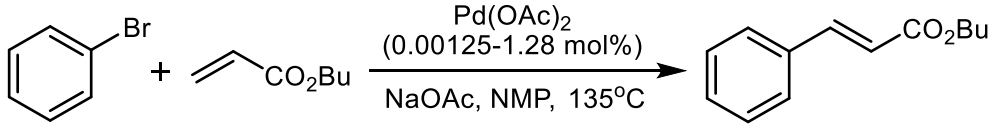
Furthermore, previous reports by the Kappe group state that oxidative addition of the aryl halide with Pd causes solubilisation of the heterogeneous Pd species (polymer-bound Pd Tetrakis, FiberCat 1001, Pd Encat®TPP30 and SiliaCat DPP-PD) [123, 124]. However, triethylamine has been found to be a significant contributor to the leaching process for PdEnCat®30 and FiberCat 1001. There is also evidence that supports the Kappe groups findings that oxidative addition of the aryl halide with Pd causes solubilisation of the heterogeneous Pd species. However, this was only evident at elevated temperatures which reflects the reaction conditions.

Despite very low quantities of Pd leaching from the heterogeneous catalysts the majority of the conversion occurs in the homogeneous phase. Due to these findings the kinetics of ligandless ‘homeopathic’ quantities of Pd were studied to gain a better insight into their activity and speciation. A reaction model has also been established to help identify the dynamics of the catalyst system**.**

Chapter 5. Kinetic analysis of ligandless palladium species using 'homeopathic' quantities

5.1 Introduction

As discussed in section 1.3, Beletskaya and Cheprakov first referred to extremely low quantities of catalyst loadings as 'homeopathic' doses [49]. In the same year, work from our research group showed that very high turnovers of 10^5-10^6 can be attained using $Pd(OAc)_2$ as a pre-catalyst for the Heck arylation reaction between 4-acetophenone or iodobenzene with acrylate [21]. Shortly after in 2003, De Vries and co-workers reported the use of homeopathic levels of ligandless Pd for the Heck reaction with aryl bromide substrates (Scheme 5.1) [51]. Using $Pd(OAc)_2$ as a catalyst precursor, the authors observed an *increase* in TOF with *decreased* Pd loadings down to 0.00125 mol%. At higher Pd loadings, it was proposed that aggregation of Pd occurs, which leads to deactivation of the catalyst in the form of palladium black. In their early work, it was proposed that the catalytically active species is monomeric, supported by the observation of an anionic $PdBr_3^-$ by ES-MS [51].



Scheme 5.1: The Heck reaction between bromobenzene and *n*-butyl acrylate at 135 °C in NMP.

To date, the majority of the mechanistic studies on Pd catalysis focuses on *identification* of discreet molecular entities present in a reaction mixture, which is extremely challenging due to the ultra-dilute conditions. Typically, mass spectrometry has been widely deployed to identify palladium-containing species in reaction mixtures. While the technique is undoubtedly very sensitive, it relies heavily on the mode of ionisation, carrier medium, etc, which can limit what can be detected. Most importantly, as an *ex situ* method, the result has to be interpreted with care, as the detection of such species, separated from the reaction environment, does not necessarily imply that they are kinetically relevant, or that they are directly involved in the catalytic cycle.

In addition, the reaction kinetics of the Heck coupling between iodobenzene, and methyl acrylate have been previously studied under a variety of reaction conditions. Zhao *et al* [144]

first reported the kinetics of this reaction using a catalyst system of $Pd(OAc)_2/nPPh_3$ (1 mol% [Pd] loading; n = 2) which demonstrated that the initial rate is dependent on all the substrates [iodide, olefin and base (NEt_3)]. The metal-to-ligand ratio of the phosphine ligand was subsequently found to have a negative effect on the rate with the highest rate being recorded when n = 0. However, in the absence of the phosphine ligand the 'precipitation of Pd' was noted, which led to the proposition that PPh_3 stabilises the active catalyst (TON) whilst reducing the reaction rate (TOF). The kinetics of several other Pd precursors have since been independently studied which include: a phosphine-free catalytic system $Pd(OAc)_2$/dimethylglycine [57], a PNP pincer Pd complex [145], and a C,N-palladacycle [146]. The authors unanimously concluded that initial Pd complexes act only as reservoirs for highly catalytically active Pd species. Notably, each of these studies were performed with rather high quantities of Pd (0.1-1.5 mol%). To the best of our knowledge, there are no kinetic studies of the Heck arylation reaction performed with Pd loadings of <0.1 mol% without added ligands.

As a result, investigations into the kinetics of the Heck reaction using 'homeopathic' loadings of a 'ligand-free' catalyst were pursued. By using *in situ* reaction monitoring tools, reaction profiles can be plotted using hundreds to thousands of data points with 'real time' accuracy. With these data rich reaction profiles, it would be counter intuitive to disregard the majority of the data points by invoking traditional kinetic analysis methods. Visual kinetic analysis methods, most notably those championed by Blackmond and Bures [147, 61], will be deployed in this work, where data collected over the full course of the reaction will be utilized in the analysis. The significant difference between Bures' and Blackmond's methods are that the latter plots a function of rate against concentration, whilst the former uses concentration against a function of time. When more than one reaction profiles plotted on the same axis simple visual analysis of the data can be made.

5.2 Results and Discussion

5.2.1 Experimental Precautions

The kinetics of the Heck reaction in scheme 2.15 were investigated using a EasyMax batch reactor, equipped with a React IR 15 probe to monitor the reaction *in situ*. Reaction aliquots were also taken periodically which were quantified by HPLC to provide orthogonal reaction analysis. It was necessary to implement precautionary steps for the experimental work to take account for: (1) the requirement to accurately dispense very low quantities of Pd precursors (<0.1 mg) for each reaction; (2) the removal of any Pd contamination which could lead 'phantom' catalysis and an inflation of TON or TOF [148]; and (3) the timings and order of addition of each reaction component to ensure consistency and reproducibility.

The precautionary steps implemented to minimise any variance between reactions were: (1) the use of catalyst stock solutions to reduce error; (2) thoroughly washing all reaction apparatus with *aqua regia* to remove any residual Pd after each reaction; and (3) dispensing the catalyst (as a stock solution) to a thermally equilibrated reaction mixture to initiate the reaction so that an accurate start time (t=0) is recorded, as well as using *in situ* IR to determine the end points of the catalytic reactions much more accurately. This reaction procedure resulted in reproducible kinetic data which was conducted in different laboratories and with different batches of Pd salts.

5.2.2 Catalyst Screen - Choice of 'Ligandless' Palladium Precursors

$Pd(OAc)_2$ and $Pd(dba)_2$ are used commonly as precursors for Pd catalysis. In the former, the initial oxidation state of Pd is +2, which has to be reduced *in situ* to form the active Pd(0) catalyst, and the acetate ligand can remain bound to the metal centre [149]. In the case of the $Pd(dba)_2$, the Pd is already present in the reduced form, but it is also known for some time, that dba can bind strongly to the metal centre to inhibit its catalyst activity [150]. In practice, many 'ligandless' or 'ligand-free' Heck reactions are performed using $Pd(OAc)_2$ as a precursor [54].

It is also important to note that neither of these palladium precursors exist as monomers in the solid state – the solid-state structure of $Pd(OAc)_2$ is reported to be trimeric [$Pd_3(OAc)_6$], while $Pd_2(dba)_3$ can also exist as a dimer [$Pd_2(dba)_3 \cdot CHCl_3$] [151, 152]. The precursors may

retain their nuclearity, or dissociate to form monomeric species, each with different catalytic behaviours. Conversely, the deactivation of the catalyst occurs through the agglomeration of Pd to form oligomers, colloids, nanoparticles – all of which may be catalytically active; eventually forming catalytically inactive bulk metal. This picture of a 'cocktail' of catalysis was proposed by Ananikov [55].

Using 100 ppm of catalyst loading (0.01 mol%), both catalyst precursors were found to be highly active in the Heck coupling, able to achieve up to 9,800 turnovers. However, the reaction profiles (Figure 5.1) clearly show very distinct differences. The reaction with the Pd(0) precursor was much slower, requiring 15 h to attain the same level of conversion that the Pd(II) can achieve in 2 h. The reaction catalysed by the dba complex has a sigmoid curvature, indicating the presence of an induction period, typically associated with the slow generation of an active catalyst, which is attributed to the slow dissociation of the dba, as was previously reported by Fairlamb et al. [150]. In contrast, the reaction with the acetate salt proceeded instantaneously, leading us to select it as the precursor in the rest of this work.

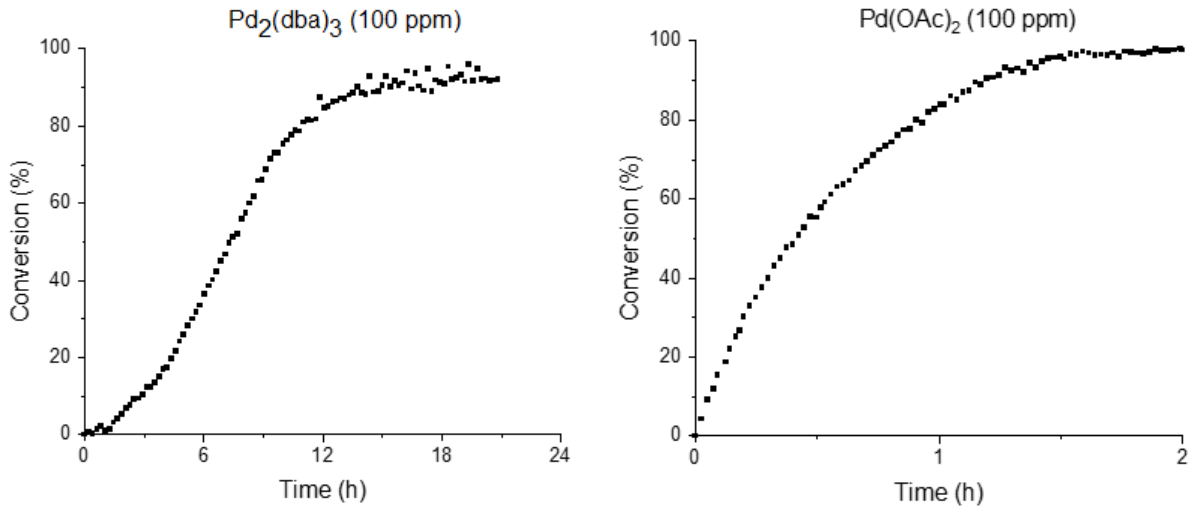


Figure 5.1: Reaction profiles of $Pd(dba)_2$ vs $Pd(OAc)_2$. Iodobenzene (1 eq.), methyl acrylate (1.5 eq.) and triethylamine (1.5 eq.), 110 °C, 1 mL of catalyst stock solution (100 ppm, corresponding to 0.01 mol%). Graph constructed from *in situ* IR data quantified with offline HPLC samples.

5.2.3 Solvent Screen

The choice of solvent not only has an environmental impact, but it is also known to have a profound effect on the catalyst performance [141]. This was demonstrated by comparing reactions conducted in the three common solvents for Heck reactions: DMF, toluene and acetonitrile – As shown in Figure 5.2, the reaction proceeds very efficiently in DMF, with a much higher conversion (turnover number), compared to the other two solvents, *i.e.* the active catalyst is more stable in the polar aprotic solvent.

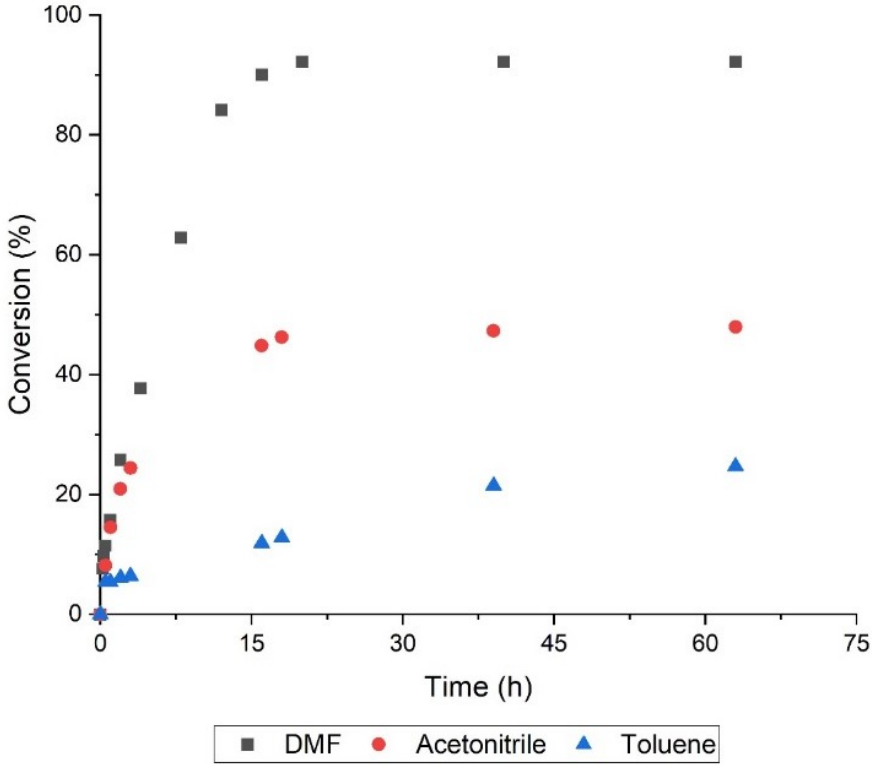


Figure 5.2: Reaction profiles of the Heck reaction catalyzed by $Pd(OAc)_2$ (100 ppm, corresponding to 0.01 mol% Pd loading). Reaction conditions: Iodobenzene (1 eq.), methyl acrylate (1.5 eq.) and triethylamine (1.5 eq.), reactions performed at 80 °C (monitored by quantitative HPLC).

5.2.4 UV-Vis Analysis of the Stability of Pd in DMF

As catalyst stock solutions were being used in this study, it was important to establish the stability of $Pd(OAc)_2$ in DMF, in order to ensure reproducibility and reliability of results. It was initially noted that there was an observable colour change in the stock solutions (100 & 1000 ppm) when left overnight (Figure 5.3). The aged Pd solutions were subsequently used for repeat reactions with good reproducibility for the 100 ppm solution but slight variance for the 1000 ppm solution.

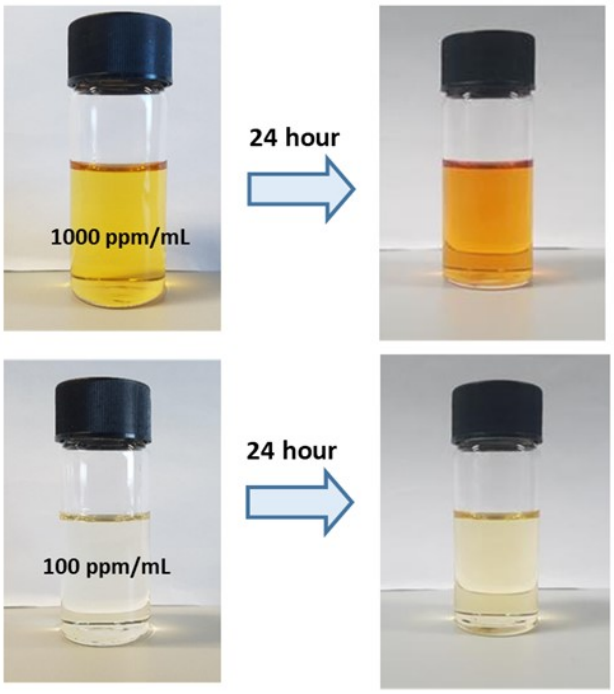


Figure 5.3: Visual identification of Pd nanoparticles in DMF over a 24 hour period at room temperature.

In a previous study, our group established that $Pd_3(OAc)_6$ dissociates reversibly in DMF to form monomers and dimers. Under certain conditions, DMF can reduce Pd(II) to form nanoparticles (NPs) [142]. Pd nanoparticles in solution scatter light differently to monomeric species due to their nanometric dimensions which can be verified by a characteristic UV-Vis absorption at 450 nm, corresponding to surface-plasmon resonance of the NPs [153, 154]. During the preparation of the Pd stock solutions (1000 and 100 ppm of $Pd(OAc)_2$) in DMF for the kinetic study, the formation of Pd NPs can be detected visually at 450 nm after a certain period of time (Figure 5.4).

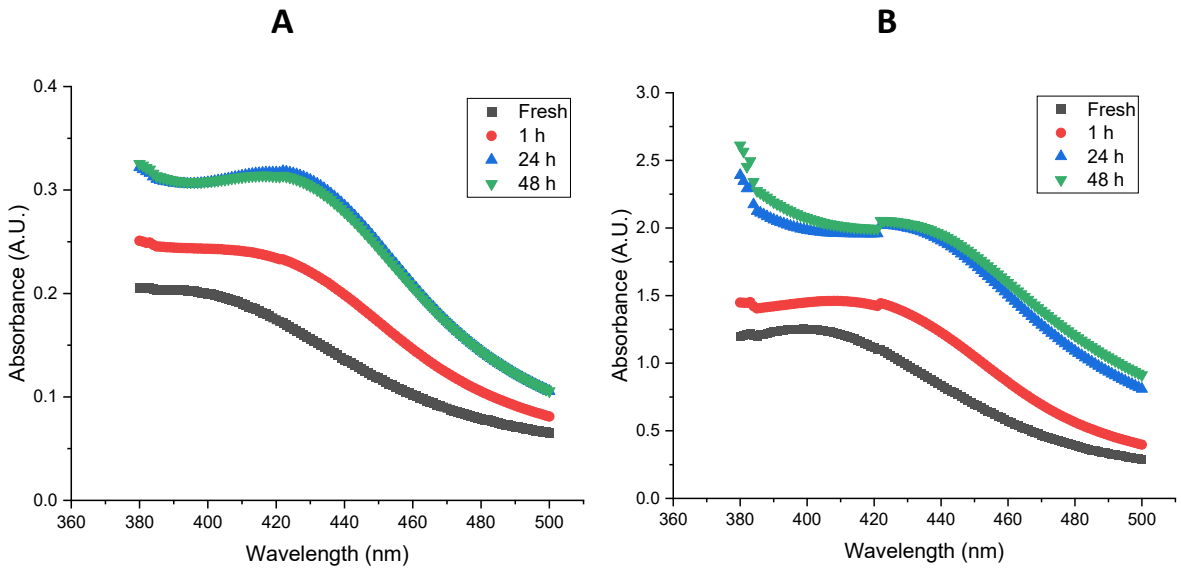


Figure 5.4: UV-Vis spectra of 100 ppm (**A**) and 1000 ppm (**B**) stock solutions monitored over a 48 hour period at room temperature in DMF.

Both 100 and 1000 ppm solutions show an increase in the region of 420 - 450 nm on their respective absorbance graphs (Figure 5.4). For the 100 ppm solution (Figure 5.4**A**) the absorbance increases to its maximum in 24 h. The 1000 ppm solution (Figure 5.4**B**) follows a similar trend, as the absorbance reached a maximum after 24 hours. These observations suggest that, for both catalyst concentrations, there is a gradual reduction of Pd(II) to Pd(0), with the formation of Pd np's over 24 hours. By plotting time vs absorbance for both stock solutions (Figure 5.5) it is clearer to see that there is a sharp increase in absorbance over the first 8 hours which then plateaus after 24 h.

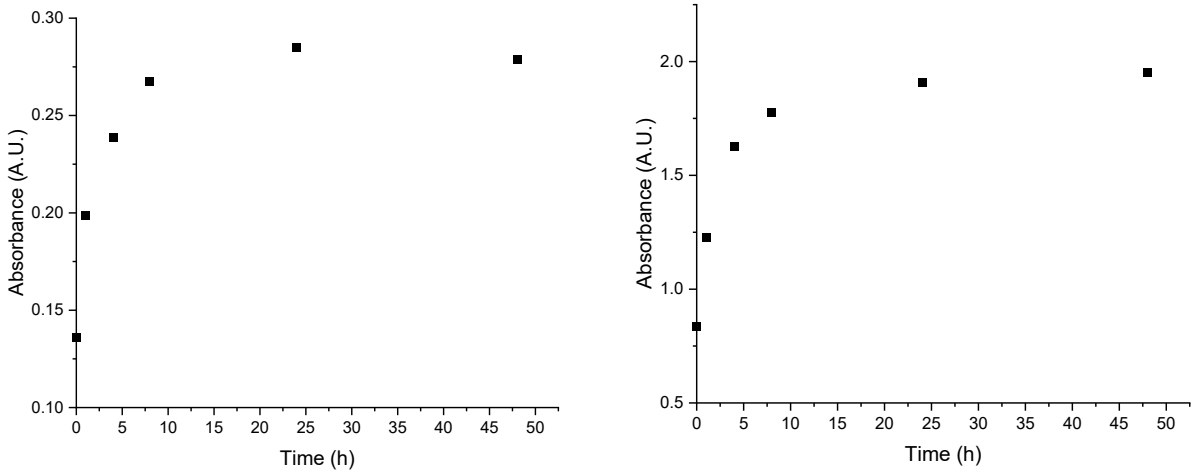


Figure 5.5: Absorbance at 450 nm vs time graphs for 100 ppm (left) 1000 ppm (right) stock solutions over a 48 hour period at room temperature in DMF.

5.2.5 Catalyst Stability

The agglomeration of reduced Pd(0) to form colloids, clusters and NP's are known to form a complex mixture ('cocktail') of catalysts, [55] eventually leading to the formation of catalyst inactive bulk metal (palladium black). As may be expected, the process is more pronounced in more concentrated solutions as shown by the higher absorbance for the 1000 ppm solution.

The catalyst stability of the 100 ppm and 1000 ppm stock solutions were then assessed under reaction conditions. This was done by the addition of four equal doses of a mixture of the reactants (iodobenzene, methyl acrylate and triethylamine) to a solution of DMF containing 100 ppm or 1000 ppm of $Pd(OAc)_2$. Judging by the reaction half-life, each fresh dose of reactants to the 100 ppm solution was consumed at a similar rate with no sign of significant catalyst deactivation throughout the reaction (Figure 5.6**A**). In contrast, the addition of the first dose of reactants to the 1000 ppm solution was consumed within 10 minutes (Figure 5.6**B**). The formation of Pd black was very apparent after the consumption of the first dose with subsequent reaction profiles being distinctively different as each reactant dose took longer to be consumed (from <10 min, to 2h, to 11 h, to >20 h), indicating significant catalyst deactivation. A direct correlation between the catalyst loading and deactivation was established through these experiments. This concurs with the predominant theory that Pd aggregation is a primary route to catalyst deactivation. An interesting observation from this study is that the aggregation process can be suppressed by effectively lowering the catalyst loading.

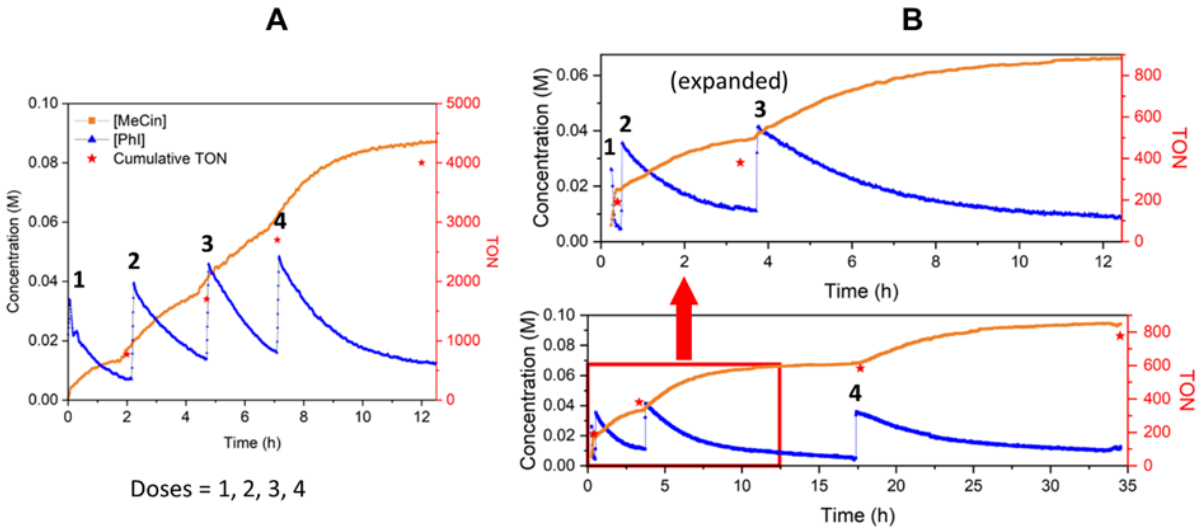


Figure 5.6: Consecutive dosing experiments to determine deactivation. **A**: 100 ppm $Pd(OAc)_2$ (no catalyst deactivation), **B**: 1000 ppm $Pd(OAc)_2$ (catalyst deactivation).

As no Pd black was observed for the duration of the 100 ppm reaction, it can be assumed that the $Pd(OAc)_2$ was sufficiently stabilised in DMF at low concentrations without any significant loss in activity. However, as a precaution for the kinetic analysis the catalyst solutions were used within 1 hour of being prepared.

5.2.6 Temperature Dependence (Arrhenius Plot)

Reactions were conducted at four different temperatures (80, 90, 100 & 110 °C) using a 100 ppm catalyst stock solution and the first 10 minutes of these reactions were plotted to obtain the k_{obs} (Figure 5.7).

An Arrhenius plot - $\ln(k_{obs})$ versus T^{-1} - was produced (Figure 5.8) from the k_{obs} obtained from the first 10 minutes of these reaction profiles. The plot yields a straight line, revealing an activation energy of 56.8 kJ mol^{-1} (or 13.6 kcal mol^{-1}) with a pre-exponential factor (A) of 4.78 x 10^6 s^{-1}.

An Eyring plot was also produced (Figure 5.9) from the initial rates data from the reactions conducted with 100 ppm of Pd at 80-110 °C to obtain the enthalpy of activation ($\Delta H^{\ddagger}$ value). The enthalpy of activation was found to be 53.8 kJ mol^{-1} (or 12.9 kcal mol^{-1}).

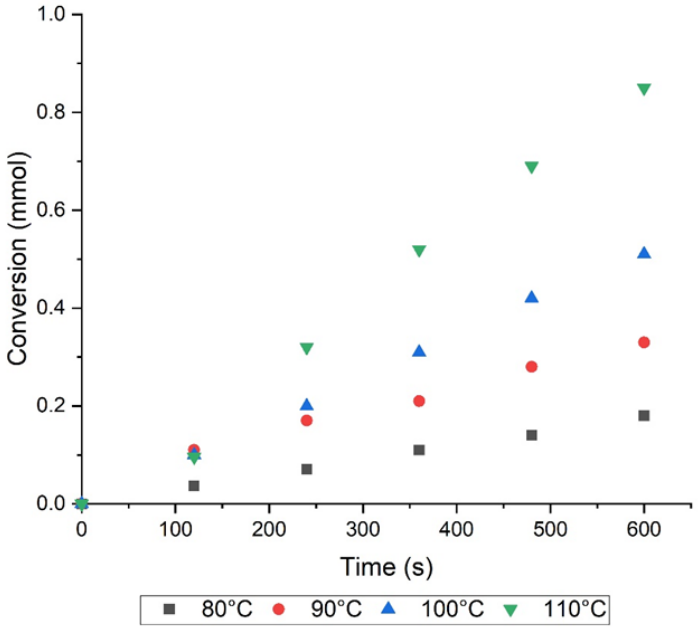
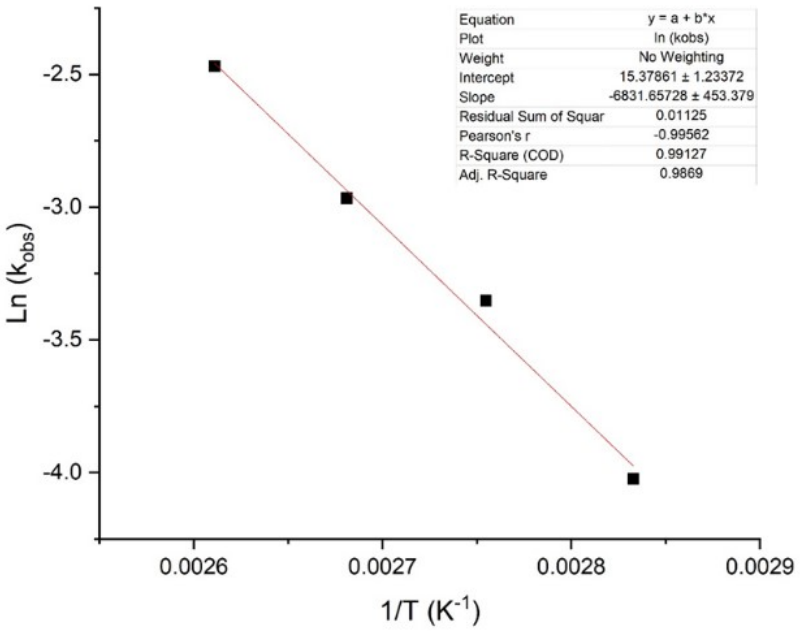


Figure 5.7: Initial rates of the Heck arylation reaction using 100 ppm of $Pd(OAc)_2$ between 80-110 °C.



$$k = Ae^{\frac{-Ea}{RT}}$$

$$Ln\ k = LnA - \frac{Ea}{RT}$$

$$Ln\ k = \frac{-Ea}{R}\left(\frac{1}{T}\right) + Ln\ A$$

$$y = mx + c$$

$$y = -6831.7x + 15.379$$

$$\frac{-Ea}{R} = -6831.7\ \pm 453.4$$

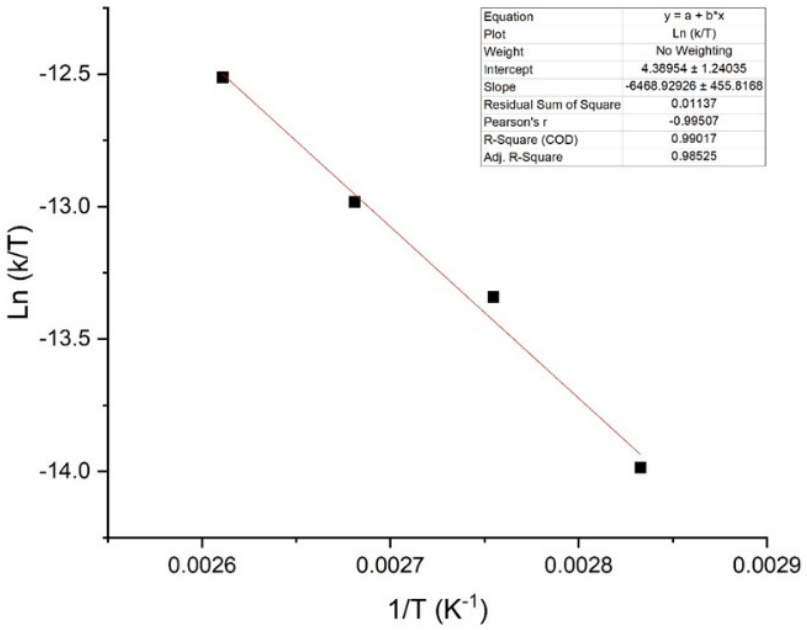
$$-Ea = -6831.7 \times 8.315$$

$$-Ea = -56805.5\ \pm\ 453.4$$

$$Ea = 5.68 \times 10^4 J\ mol^{-1}$$

$$56.8\ \pm 0.5\ kJmol^{-1}\ (13.6\ kcal\ mol^{-1})$$

Figure 5.8: Arrhenius plot of the Heck arylation reaction catalysed by $Pd(OAc)_2$ and associated activation energy.



$$\ln\frac{k}{T} = -\frac{\Delta H^{\ddagger}}{R}\frac{1}{T} + ln\frac{k_B}{h} + \frac{\Delta S}{R}$$

$$\mathrm{y} = \mathrm{m}x + c$$

$$\mathrm{y} = -6468.9\mathrm{x} + 4.3895$$

$$-\frac{\Delta H^{\ddagger}}{R} = -6468.9 \pm 455.8$$

$$\Delta H^{\ddagger} = 53788.9 \pm 455.8\, J\, mol^{-1}$$

$$\Delta H^{\ddagger} = 53.8 \pm 0.5\, kJ\, mol^{-1}\ (12.9\, kcal\, mol^{-1})$$

$$ln\frac{k_B}{h} + \frac{\Delta S}{R} = 4.4 \pm 1.2$$

$$\Delta S^{\ddagger} = -161.0 \pm 1.2\, J\, K^{-1}\, mol^{-1}$$

$$\Delta S^{\ddagger} = -0.161 \pm 0.0012\, kJ\, K^{-1}\, mol^{-1}$$

Figure 5.9: Eyring plot of the Heck arylation reaction catalysed by $Pd(OAc)_2$ and associated enthalpy of activation.

The values obtained for the activation energy and the enthalpy of activation are considerably lower than previous reports of catalytic systems which include $Pd(OAc)_2/PPh_3$ (E_a = 96.2 kJ/mol) [32] and for a [CN]-palladacycle ($\Delta H^{\ddagger}$ = 69 kJ/mol) [33]. This indicates that the active species from the simple Pd precursor $Pd(OAc)_2$ is highly active, more so than these ligated complexes.

5.2.7 Dependence of TON and TOF on Catalyst Loading

Catalyst stability and activity are regularly quantified by the turnover number (TON = [mol of product]/[mol of catalyst]) and turnover frequency (TOF = TON/reaction time) of a catalytic reaction. Therefore, in this work the stability and activity of $Pd(OAc)_2$ was assessed by comparing the TON's and TOF's across different catalyst loadings (30-1000 ppm) for the Heck arylation reaction between iodobenzene and methyl acrylate (Scheme 5.2), the results are shown in Table 5.1. By comparing the resulting TON's from these reactions (Figure 5.10) there is a clear trend; as the catalyst loading decreases the TON increases, indicating that the catalyst is not deactivating. As the reaction goes to near completion (>95%) for each reaction above 50 ppm high TON can be achieved, but it does not necessarily mean that the catalyst is stable across the concentration range of 50-1000 ppm. At 30 ppm and below it was harder to attain complete conversion, possibly due to the presence of very small amounts of catalyst poisoning or deactivation.

Table 5.1: Calculated TON and averaged TOF values at 95% conversion (Figures 5.10 and 5.11).

[Pd] (ppm)	Pd (mmol)	Conversion (%)	time (min)	TON	TOF (min^{-1})	Rate (mmol/min)
5	$2*10^{-5}$	82 (3.28 mmol)	1086	164000	151	0.0030
30	$1.2*10^{-4}$	79 (3.16 mmol)	430	26333	61	0.0073
50	$2*10^{-4}$	95 (3.8 mmol)	313	19000	61	0.0121
100	$4*10^{-4}$	98 (3.92 mmol)	95	9800	105	0.0413
200	$8*10^{-4}$	98 (3.92 mmol)	28	4900	175	0.1400
400	$1.6*10^{-3}$	97 (3.88 mmol)	14	2425	173	0.2771
600	$2.4*10^{-3}$	98 (3.91 mmol)	9.5	1629	171	0.4116
800	$3.2*10^{-3}$	98 (3.92 mmol)	7	1225	175	0.5600
1000	$4*10^{-3}$	97 (3.88 mmol)	5.5	970	176	0.7055

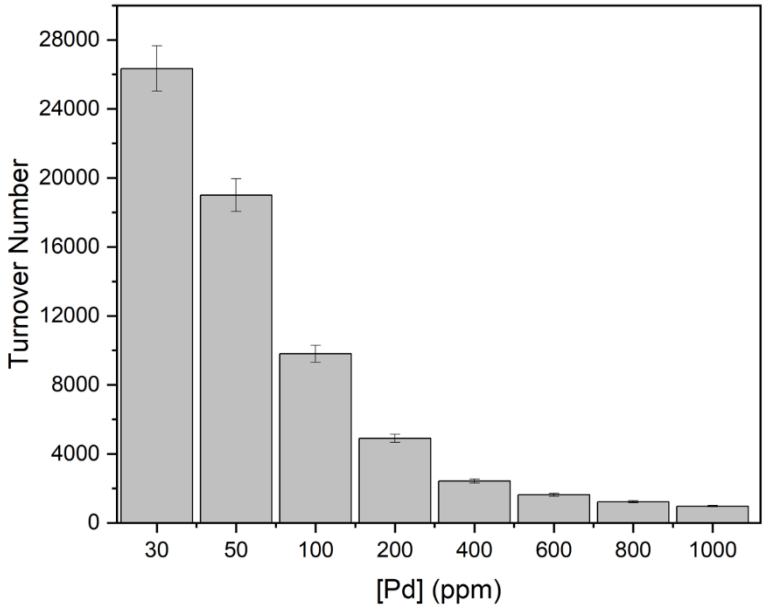


Figure 5.10: Dependence of TON's on catalyst loading from 30-1000 ppm of [Pd].

When assessing and comparing the TOF's of different catalytic reactions of near quantitative yields, it is vital that the end point of the reaction is recorded accurately otherwise a window of uncertainty may be present in the calculation. For example, if eight samples were taken throughout a reaction each hour, and the conversion between the penultimate sample and the final sample changes from 93% to 99%, then it is likely that the reaction was completed in under eight hours and therefore the TOF would be an underestimate. However, by using *in situ* reaction monitoring precise reaction times can be recorded to eliminate any uncertainty. *In situ* infra-red spectroscopy was used to monitor these reactions therefore providing exact timescales for each reaction and therefore precise TOF's. When plotting the TOF against catalyst loading from 30-1000 ppm (Figure 5.11) it can be shown that the TOF was constant at about 175 min^{-1} for Pd loadings above 200 ppm (≥ 0.02 mol% catalyst loading). There was then a notable decrease in the TOF to 105 min^{-1} and then 61 min^{-1} for the Pd loadings at 100 ppm (0.01 mol%) and 50-30 ppm (0.005-0.003 mol%) respectively. This change in catalyst activity indicates a change in the nature of the active catalyst or a shift to a different catalytic mechanism.

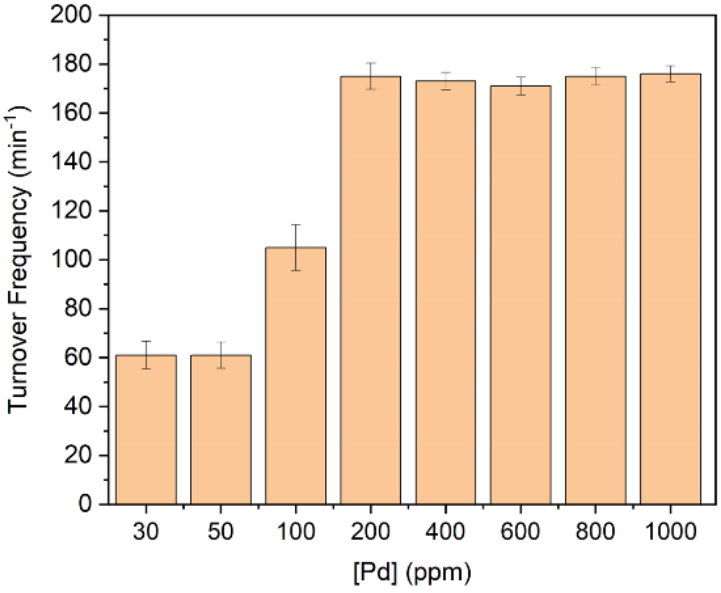


Figure 5.11: Dependence of TOF's on catalyst loading from 30-1000 ppm of [Pd], assuming a monomeric catalytically active Pd species for model reaction.

A significant observation was that at lower catalyst loadings the TOF also decreases due to the longer reaction times required to achieve high conversions which directly challenges the 'homeopathic effect' proposed by de Vries [51], where the opposite effect was reported based on product yield at set time points. This motivated us to perform further kinetic studies to better understand the nature of 'homeopathic' (<0.1 mol%) Pd catalysis; specifically in the range of 30-1000 ppm of Pd.

As mentioned earlier in section 5.2.1, precautionary steps were taken to rule out any 'phantom' catalytic activity from residual Pd contaminating any part of the reaction apparatus by treatment with *aqua regia*. To help confirm that the TON's are solely from the addition of catalyst for these 'homeopathic' loadings the reaction mixture was allowed to equilibrate thermally to identify any turnover prior to the addition of the catalysts (Figure 5.12). Using an *in situ* monitoring technique made this process very easy and viable for each experiment.

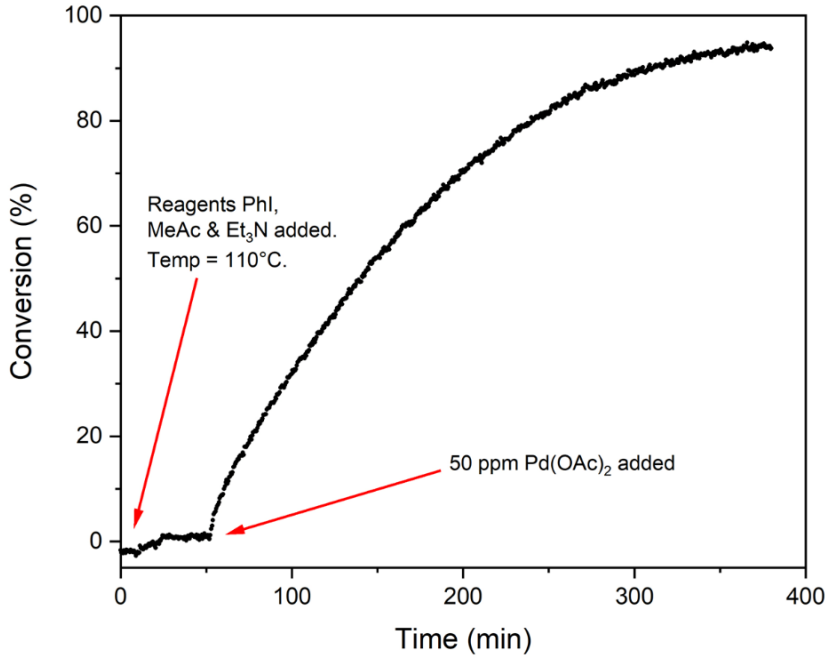


Figure 5.12: Pre-equilibration of the reaction mixture before the addition of 50 ppm of the Pd stock solution.

5.2.8 Kinetic Analysis – Order in Reactants

In this section of the study, kinetic experiments have been carried out to probe the mechanism of the Heck reaction when conducted using ppm quantities of $Pd(OAc)_2$. A particular emphasis was placed on understanding if there is a change in reaction order when transitioning from 1000 ppm to 30 ppm. The kinetic analysis performed to determine the reaction order in catalyst was done using both the initial rates method and reaction progress kinetic analysis (RPKA). Both methods were employed to ensure that no relevant kinetic information was left unexplored and to have a reference point for one another. As its name implies the initial rates method only utilises the initial portion of a reaction profile which can result in linearity being forced to allow the rate to be extracted. Furthermore, any changes in the rate dependencies at a later stage of the reaction will not be detected when using the initial rates method. In contrast, the data collected over the full course of the reaction was utilised when applying reaction progress kinetic analysis (RPKA), a set of techniques developed by Blackmond [147, 155].

5.2.9 Order in Iodobenzene

A set of RPKA experiments were initially performed to determine the individual order in reactants and establish a global reaction order. Using 50 ppm catalyst loading (0.005 mol%) a control experiment was first performed, followed by a same excess and a different excess experiment with the reactant iodobenzene. The resulting reaction profiles were then time normalised, which produced a good overlay for each of the control, same excess and different excess experiments (Figure 5.13). The overlay of the same excess plot with the control plot further confirmed that the reaction was not hindered by catalyst deactivation or product inhibition. Whilst the overlay of the different excess experiment with the control shows that there is a zero-order relationship between iodobenzene and the reaction rate.

Table 5.2: Concentrations of each reactant used for the control, same excess and different excess experiments.

Runs	Experiment	[PhI]/M	[MeAc]/M	[Et_3N]/M	[Pd]/ $x10^{-5}$ M
1	'Control'	0.15	0.1	0.1	0.5 (50 ppm)
2	Same excess	0.1	0.05	0.05	0.5 (50 ppm)
3	Different excess	0.2	0.1	0.1	0.5 (50 ppm)

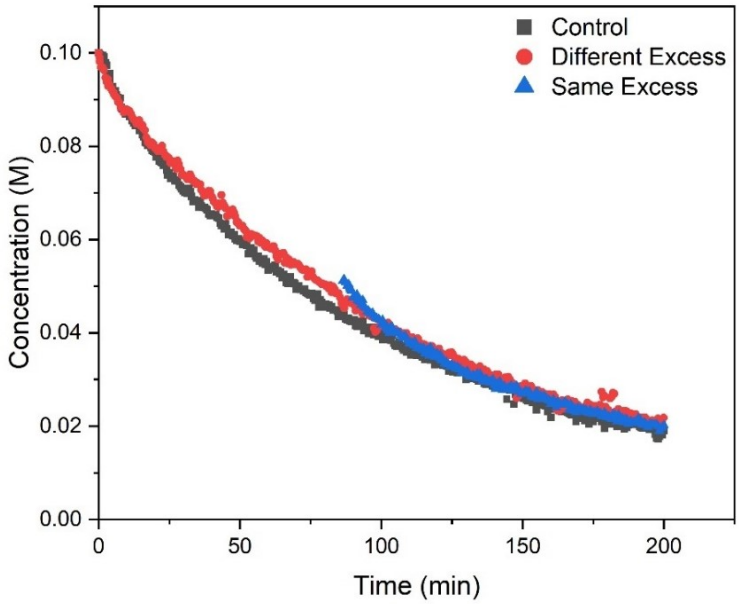


Figure 5.13: Visual plots showing the consumption of the limiting reagent (methyl acrylate) for the 'control', 'same excess' and 'different excess' RPKA experiments which show no catalyst deactivation and zero order dependency of global reaction rate on [PhI].

5.2.10 Order in Methyl Acrylate & Triethylamine

The reaction order in methyl acrylate and triethylamine were also established using RPKA. By performing a control, same excess and different excess experiments with 100 ppm of $Pd(OAc)_2$ (0.01 mol%) and then time normalising the resulting reaction profiles, the order in reactants were determined visually. A good overlap of reaction profiles was obtained for both sets of experiments with methyl acrylate and triethylamine (Figure 5.14 & 5.15). These results show that the reaction also has a zero-order dependency in both methyl acrylate and triethylamine as well as iodobenzene from the previous experiments.

Table 5.3: Concentrations of reactants and reagents used for 'control', 'same excess' and 'different excess' of methyl acrylate (MeAc).

Experiment	**[PhI] /**M	**[MeAc] /**M	**[Et_3N] /**M	**Excess of [MeAc] /**M
Control	0.1	0.15	0.1	0.05
Same XS	0.05	0.1	0.05	0.05
Different XS	0.1	0.2	0.1	0.1

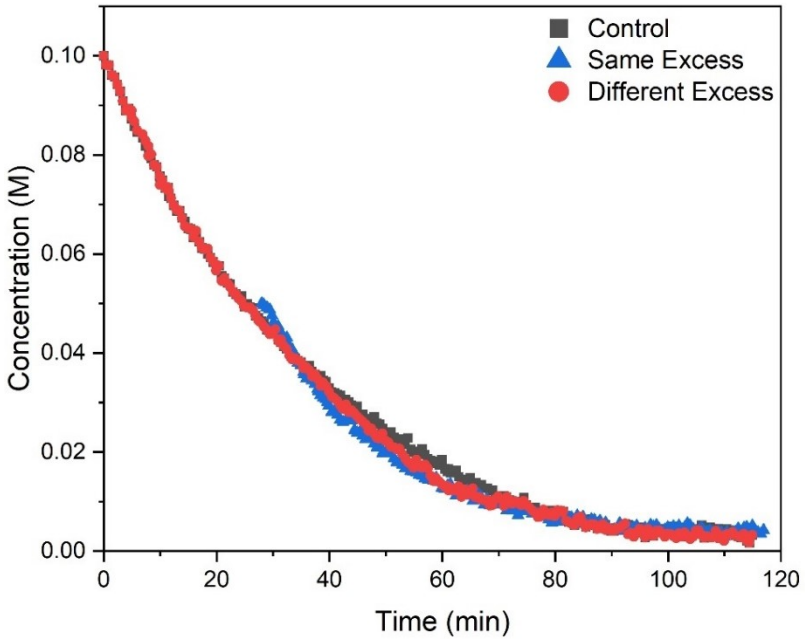


Figure 5.14: Concentration vs time profiles showing the consumption of iodobenzene for 'control', 'same excess' and 'different excess' of methyl acrylate (MeAc). Time shift applied to the same excess profile to achieve overlay indicating a zero-order dependency in MeAc.

Table 5.4: Concentrations of reactants and reagents used for 'control', 'same excess' and 'different excess' of triethylamine (Et_3N).

Experiment	[PhI] /M	[MeAc] /M	[Et_3N] /M	Excess of [Et_3N] /M
Control	0.1	0.1	0.15	0.05
Same XS	0.05	0.05	0.1	0.05
Different XS	0.1	0.1	0.2	0.1

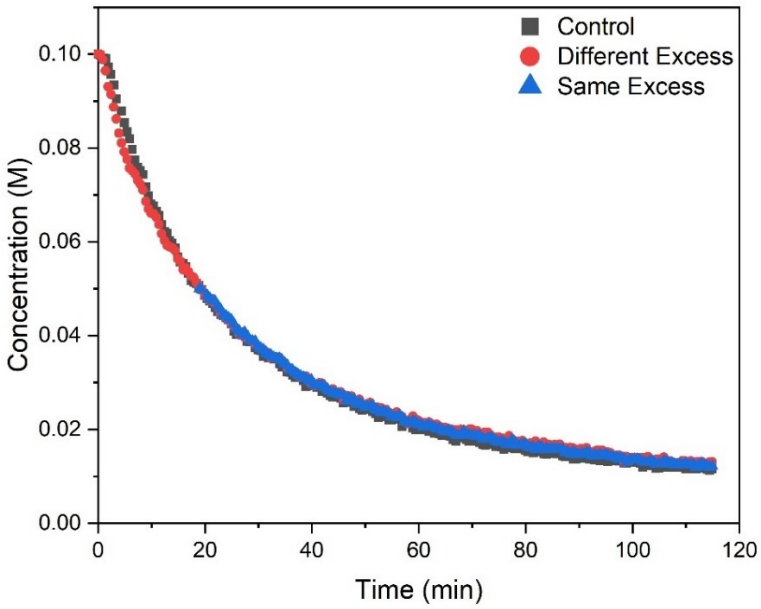


Figure 5.15: Concentration vs time profiles showing the consumption of iodobenzene for 'control', 'same excess' and 'different excess' of triethylamine (Et_3N). Time shift applied to the same excess profile to assess overlay which indicates a zero-order dependency in Et_3N.

Considering these findings, the TOF of the system can exclude all reactant parameters and be simply written as:

$$TOF = k[Pd]^x \qquad \text{[eqn 1]}$$

When considering the elementary steps of the Heck catalytic cycle it may seem surprising that each reactant has a zero-order rate dependency, as each elementary step involves the participation of a reaction component. However, when applying such low catalyst loadings of 0.01 mol% (which equates to a 10,000-fold excess of the limiting reactant with respect to the Pd catalyst), it is unlikely that any noticeable changes in the reaction rate would be observed when changing the initial reactant concentrations.

5.2.11 Kinetic Analysis - Initial Rates Method

Our initial kinetic studies were aimed at gauging the order of the reaction with respect to the catalyst, $Pd(OAc)_2$. Using the concentration vs time data obtained from the reactions conducted at catalyst loadings from 30 to 1000 ppm (Figure 5.16), the order with respect to catalyst was investigated. The time required to complete the reaction varies from under 10 minutes for a 1000 ppm Pd loading to over 7 hours for a 30 ppm catalyst loading at 110 °C therefore, only the first 5 minutes of each reaction profile was used to gather the initial rate data which was then plotted against [Pd] (Figure 5.17). For the range of catalyst concentrations between 30 and 1000 ppm a linear fit was achieved which implies that the reaction is first order in Pd, which may lead to the conclusion that the active catalyst is a monomeric species.

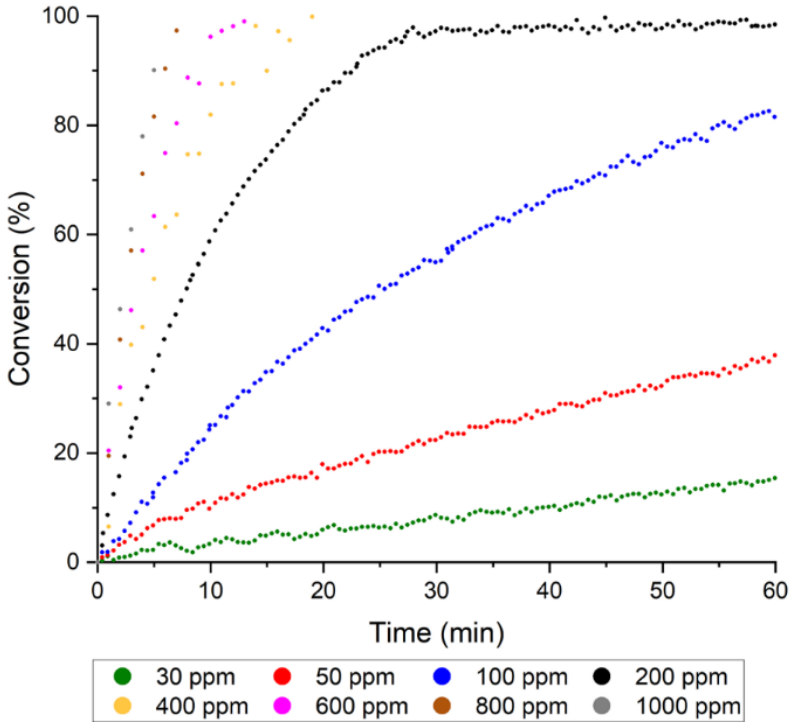


Figure 5.16: First 60 minutes of each reaction profile for the Heck reaction with catalyst loadings from 30 to 1000 ppm.

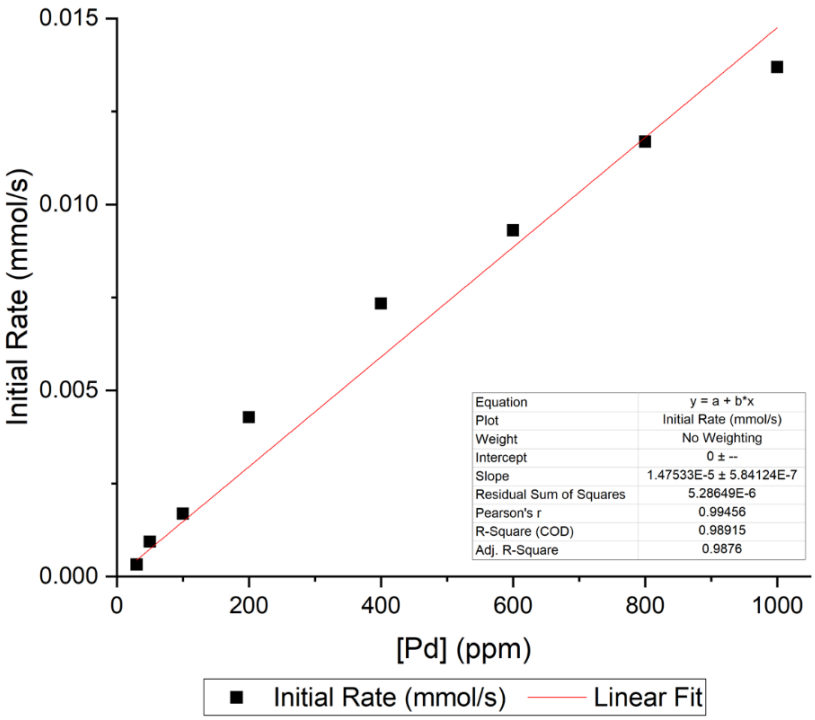


Figure 5.17: [Pd] vs initial rate constructed from the data obtained in the first 5 minutes of the reaction. ([Pd] = 30, 50, 100, 200, 400, 600, 800, 1000 ppm)

However, there are a few caveats with this approach. First of all, if the previous proposal of 'cocktail of catalysts' is correct, it can be expected that the [Pd] order will change across the different loadings. At ultra-low catalyst loadings (between 30-100 ppm), the initial rate method was also unsatisfactory, as the error can be significant when conversion is low, which can mask any effects at low catalyst loadings. As discussed earlier, the method of initial rates only uses the first portion of the reaction to describe the kinetics, and so may not be used to study the onset of catalyst deactivation which was only visible towards the end of a reaction. To check that the observed first order kinetics for the catalyst persists throughout the whole reaction visual time normalisation analysis was applied.

5.2.12 Kinetic Analysis - Virtual Time Normalisation Analysis (VTNA)

The virtual time normalisation analysis (VTNA) method reported by Bures [61] derives the catalyst order from the entire reaction profile by fitting the power rate law to attain overlap of different catalyst concentrations. *In situ* IR was used to monitor these reactions generating large data sets. The application of VTNA to the concentration vs time profiles can more accurately determine the global reaction order in the rate equation [eqn 1]. In addition, any changes in the catalyst active species or in its speciation throughout the catalytic reaction will be exposed whilst also offering a direct comparison to the first order observed using the initial rates method. By normalising the time axis by the catalyst concentration and rising it to a power an overlap can be obtained from the original reaction profiles in Figure 5.16. Using visual fitting and adjusting the value of the power no overlap was attainable across all catalyst concentrations. However, taking the observed drop off in TOF below 200 ppm into account the catalyst loadings were split into a 'low loading' group (30, 50, 100, 200 ppm) and a 'high loading' group (200, 400, 600, 800, 1000 ppm). By splitting the data into 'low loading' and 'high loading' groups, a clear overlap was achieved for each data set when adjusting the power on the x-axis (Figure 5.18). For the 'high' catalyst loading reactions the best overlap was observed when the power was set to 0.9. This result was very close to that obtained when applying the initial rates method. In contrast, for the 'low' catalyst loading reactions the best observed overlap was achieved when the power was set to 1.7. This indicates a clear change in the behaviour of the catalyst below 200 ppm which alludes to a change in the catalytic active species.

It was surprising to observe a change to a higher Pd order at lower catalyst loadings, as this implies that a multinuclear catalyst has a larger contribution to the rate of reaction at lower catalyst loadings. In earlier studies which involve a monomer-dimer equilibrium the dimer was often reported to be inactive or at least kinetically non-competitive with its main role being a reservoir for a catalytically active monomeric Pd species [62, 156]. Experimentally, the existence of more than one active species has never been demonstrated.

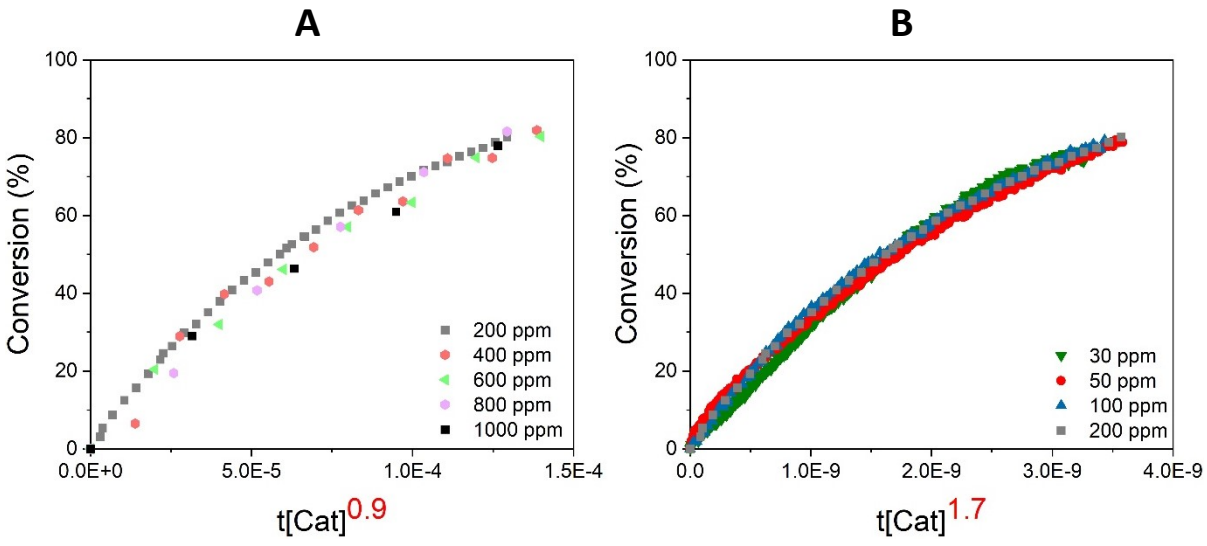


Figure 5.18: Catalyst order determined by VTNA for 'high' (**A**, 200-1000 ppm) and 'low' (**B**, 30-200 ppm) catalyst loading groups.

It is important to highlight an alternative explanation for what could cause the observed change to a higher order in Pd – that is, the presence of a persistent amount of impurity which poisons the catalyst. This was tested by fixing the power on the x-axis to 1 and deducing a fixed amount from the initial catalyst loading. The best attainable overlay was achieved when 33 ppm of catalyst was removed from the initial catalyst loadings. In the case where 33 ppm of catalyst is poisoned in each reaction, it will have a larger percentage impact on the catalyst loadings at the lower concentration range adjusting the effective catalyst loadings from 50, 100 and 200 ppm to 17, 67 and 167 ppm, respectively. However, the resulting overlay was fairly poor (Figure 5.19). Additionally, catalytic activities can still be observed at loadings of ≤ 30 ppm in this system which lead us to rule out the presence of a persistent catalyst poison. Impurities present in $Pd(OAc)_2$ can also be ruled out as this would correlate directly with Pd loading which does not improve the observed overlay.

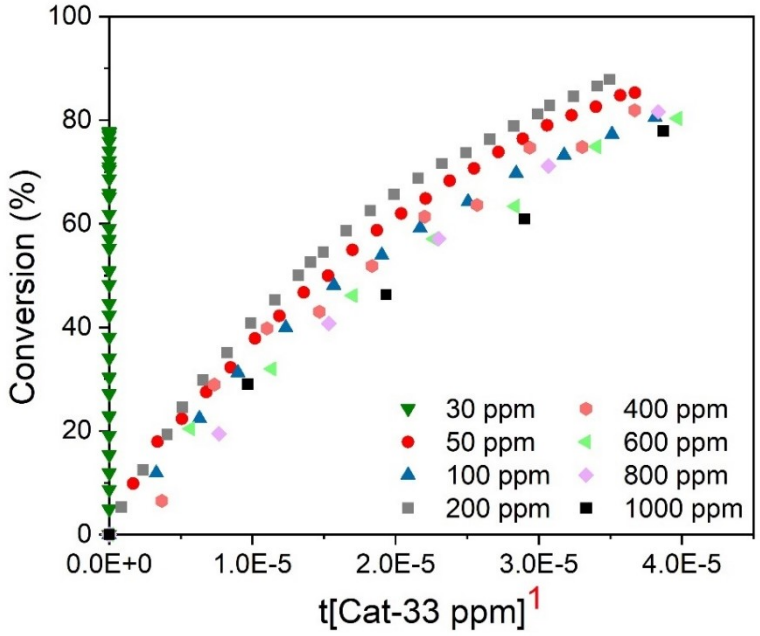


Figure 5.19: VTNA reaction profiles fitted to first order Pd, assuming presence of 33 ppm of catalyst poison.

The Heck arylation reaction was also conducted using a lower catalyst loading of 5 ppm to see if the reaction was still feasible. The resulting reaction profile is a stark contrast to that of higher catalyst loadings, by exhibiting a sigmoid shape. This sigmoid reaction profile has a long induction period, which is possibly when the active catalyst forms, but nevertheless demonstrates that the reaction is conceivable at even lower concentrations.

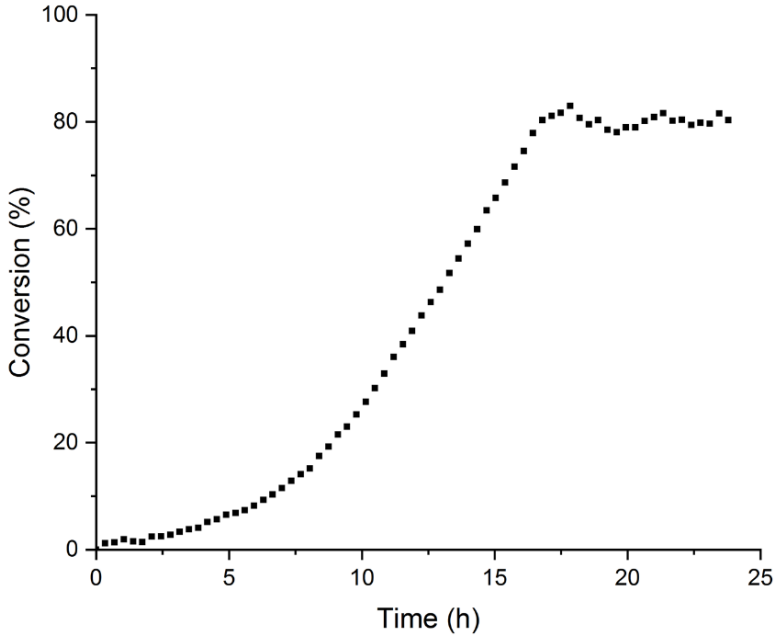


Figure 5.20: Conversion vs Time profile for the Heck reaction between iodobenzene and methyl acrylate at 110 °C using 5 ppm (0.0005 mol%) of $Pd(OAc)_2$.

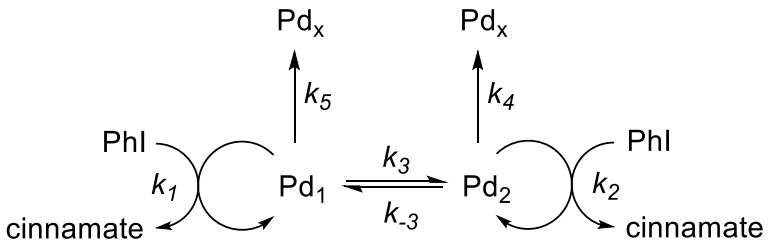
5.2.13 Kinetic Modelling

Kinetic modelling was used to construct viable catalytic pathways, based on the experimental observations. With relation to this work, a kinetic model is a set of differential equations which describe the changes in reactant, product and catalyst concentrations over time. By using suitable software, the differential equations can be solved which produces a simulation of the reaction profiles based on the calculated concentrations and rate constants. Chemical engineers and process chemists use such models to predict the effects of altering reaction components. As well as this, kinetic modelling can be used as a mechanistic tool to establish if the proposed mechanism fits with the experimental data. A model which can accurately simulate the experimental data offers strong evidence that the proposed catalytic cycle accurately describes the observed kinetics.

Before constructing a kinetic model some initial assumptions were made based on the experimental data:

- An experimental catalyst order of 1.7 for the concentrations between 30-200 ppm indicates that the involvement of a higher order species hence two catalytically active species are incorporated into the model.
- The two catalytically active species were modelled as a monomer and dimer to reduce the complexity of the model and prevent overfitting. As the catalyst deactivation (Pd agglomeration) is expected to be a highly complex process involving several Pd species, [62] these were modelled simply as first-order processes.
- The visual appearance of palladium black in the reaction mixtures suggests that there is catalyst deactivation at catalyst loadings >200 ppm, which was therefore included as a possible pathway in the model.
- Same excess experiments show that there was no catalyst deactivation throughout the reaction for catalyst loadings <200 ppm. Therefore, the rate of formation of palladium black must be slower than the rate of product formation (TOF).
- An initial ratio of 3:1 monomer to dimer was reached as the stock solution was always prepared in the same way and this ratio provided an enhanced fit across all reaction concentrations. Other ratios were tested from 5:1 to 1:5.

Taking these initial assumptions into account, a minimal model was constructed to describe the key steps of the reaction based on the experimental observations (Scheme 5.3). A set of differential equations were written to describe the change in concentration for each of the following reaction components: PhI, cinnamate, Pd_1 (monomer), Pd_2 (dimer) and Pd_x (deactivated Pd). The Pd monomer and dimer were both modelled as catalytically active species in equilibrium (k_3), each contributing to a TOF with their rates represented as k_1 and k_2 respectively. The aim of the kinetic modelling was to extract specific values for the rate constants k_1, k_2, k_3 and k_{-3} which should be fixed and applicable across our experimental catalyst concentration range (30-1000 ppm). Meanwhile, the remaining two constants k_4 and k_5, which describe the rate of catalyst deactivation, were allowed to float between different catalyst concentrations as these are expected to be independent to the initial catalyst concentration.



$[Pd]_{total} = Pd_1 + 0.5\ Pd_2$

$Pd_2 = Pd_1 + Pd_1$

PhI = iodobenzene

cinnamate = Heck product

Pd_x = catalytically inactive Pd species

(1) $\frac{d[PhI]}{dt} = -k_1[PhI][Pd_1] - k_2[PhI][Pd_2]$

(2) $\frac{d[cinnamate]}{dt} = k_1[PhI][Pd_1] + k_2[PhI][Pd_2]$

(3) $\frac{d[Pd_1]}{dt} = k_{-3}[Pd_2] - k_3[Pd_2] - k_5[Pd_1]$

(4) $\frac{d[Pd_2]}{dt} = k_3[Pd_1] - k_{-3}[Pd_1] - k_4[Pd_2]$

(5) $\frac{d[Pd_x]}{dt} = k_4[Pd_2] + k_5[Pd_1]$

Scheme 5.2: Kinetic model and associated differential equations incorporating two catalytically active species and two (independent) deactivation rates.

The differential equations were compiled into code (see Appendix Table 6.1), in order to be read and solved in the ODE solver software Berkeley Madonna (BM). It is important to note at this juncture that the elementary step of the monomeric Pd_1 converting to the dimer Pd_2 requires two monomers and is thus second order in [Pd_1], i.e. $Pd_2 = 2 * Pd_1$. Once the model was devised, the rate constants which most accurately replicate the experimental data were found using the curve-fit function in BM. Eight experimental datasets which represent the catalyst loading from 30 to 1000 ppm were used to fit the model. The initial catalyst concentrations were defined independently which required a set of differential equations to be written for each catalyst loading (eight sets of equations). Critically, the same rate constants (k_1, k_2, k_3, k_{-3}) were fixed for each set of differential equations. Only the rate constants which describe the rate of deactivation were allowed to float (k_4, k_5) as it was anticipated that the rate of deactivation is faster at higher catalyst loadings due to the observation of deactivation in the dosing experiments and the presence of Pd black. As a result, the curve fit function of BM will have determined the values of 6 rate constants, to fit 8 datasets, using 40 differential equations (based on 5 differential equations per data set). Table 5.5 displays the parameters used to set up the model.

Table 5.5: A description of set up of the kinetic model.

Experimental Data	Differential Equations	Rate Constants
• 8 reaction profiles obtained by *in situ* IR and offline HPLC sample. • The experimentally derived rate equation ($TOF=k[Pd]^x$) only depends on the catalyst concentration hence, unnecessary reactants are omitted.	• 8 sets of differential equations which define the change in concentration with time of the reaction components PhI, Cinnamate, Pd_1 (monomer), Pd_2 (dimer) and Pd_x (deactivated Pd).	• BM varied 6 rate constants (shown in Scheme 5.3) to fit the simulated data to the experimental data. • The rate constants themselves were fixed across all differential equations apart from k_4 and k_5 as the rate of deactivation may vary from low to high catalyst loadings.

The best fit between the simulated data and the experimental data was achieved with the rate constants shown in Table 5.6 along with the respective root mean square (RMS). These were extracted in two steps: initially the rates constants (k_1, k_2, k_3, k_{-3}) for the catalyst loadings between 50-200 ppm were obtained as approximate values, the deactivation steps (k_4 and k_5) were omitted as the experimental data suggests that deactivation is negligible at low catalyst loadings. Subsequent fittings refined these values and expanded the data set to all loadings between 30-1000 ppm before including the deactivation rates (k_4 and k_5).

Table 5.6: Kinetic rate constants and RMS values extracted from fitting the kinetic model (Scheme 5.2) to the experimental data.

$[Pd]_0$	k_1	k_2	k_3	k_{-3}	k_4	k_5	RMS
30	8.61	790.96	366.9	0.96	$1.39*10^{-16}$	$4.97*10^{-19}$	0.106
50					$1.16*10^{-4}$	$8.76*10^{-12}$	0.072
100					0.00761	$6.15*10^{-15}$	0.069
200					0.0296	$1.73*10^{-15}$	0.093
400					0.46	$3.17*10^{-15}$	0.273
600					0.929	$2.27*10^{-15}$	0.311
800					1.31	$1.58*10^{-16}$	0.409
1000					1.92	$1.06*10^{-15}$	0.344

The accuracy of the kinetic model was assessed by comparing the simulated data to the experimental data obtained from *in situ* IR (Figure 5.21). A visual comparison of the reaction profiles can be made due to the simplicity of the plots along with the RMS values reported in Table 5.6 to assess how well the model fits. Visually the experimental and simulated data show good overlap, meaning that having two catalytically active species help accurately reproduce the experimental data. The RMS values are larger for the higher catalyst loadings due to having less data points in their respective experimental data sets. It should be noted, however, before arriving at this model, simpler models were tested which involve only one catalytically active species and others which only have one deactivation pathway. These models are summarised in Table 6.1 of the Appendix but none of them produced a good fit with the experimental data.

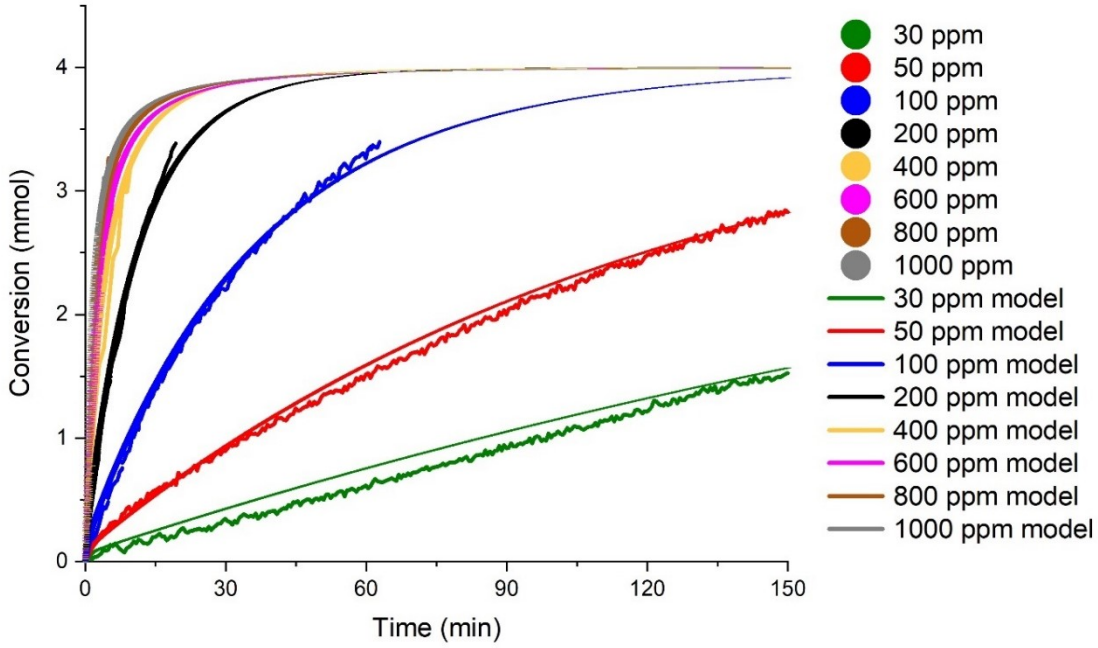


Figure 5.21: Expansion of the fit of the model to experimental data (full fitting was performed between 0-400 min). Dots represent the experimental data; solid lines represent the simulated data from the model.

The rate constants can be discussed with respect to their influence on the simulated data with several key insights being revealed, which are summarised below:

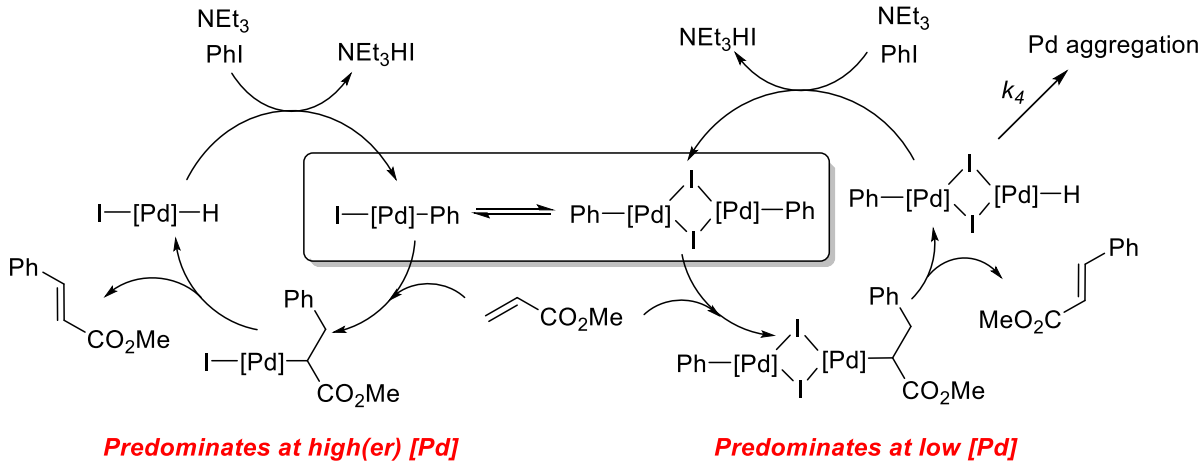
1. With just two catalytically active species, Pd_1 and Pd_2 modelled as a monomer and a dimer respectively, a reasonably good fit can be achieved between the experimental and the simulated data from the model. The involvement of a mixture of higher order Pd species (trimers, multimers, etc) cannot be ruled out at this juncture as k_2 may represent an average TOF of several higher order species combined. In fact, a better fit may well be attainable if additional active Pd species were included, but this could risk overfitting without necessarily adding any new insight. The introduction of off-cycle Pd species which behave like catalyst reservoirs were either unsuccessful or had little effect, *i.e.* the total Pd ($[Pd]_{total}$) speciates into catalytically active species (Pd_1 and Pd_2) upon addition to the reaction mixture.

2. The activity of the Pd_2 species was found to be nearly two orders of magnitude higher than that of the monomeric Pd_1 (k_2/k_1 = 91). This may account for the observed change in catalyst order (from 0.9 to 1.7) at lower catalyst loadings. The thermodynamic stability of Pd_2 is also greater than that of Pd_1 (k_3/k_{-3} = 382). To the best of our knowledge this is the first time that a greater catalytic activity has been associated to a Pd species of higher nuclearity.

3. On the contrary, the rate of deactivation of the dimer Pd_2 species is much higher than that obtained for the monomeric Pd_1 species (k_5 is negligible compared to k_4). The hypothesis that catalyst agglomeration is the primary source of deactivation is supported by the fact that the rate of deactivation of Pd_2 (k_4) increases significantly with higher catalyst loadings.

4. As mentioned previously the catalyst was introduced as a stock solution to a solution of the reactants in a heated reactor at the required temperature. In nearly every case, there was an absence of an induction period with the reaction starting immediately. However, there was one exception with the 30 ppm Pd loading reaction profile displaying the onset of an induction period at the initial stage of the reaction (Figure 5.21). As a result, for reactions catalysed by <50 ppm (<0.005 mol%) of Pd, additional processes may need to be considered to account for the *in situ* formation of the active catalyst species.

The 3:1 ratio of the active species Pd_1:Pd_2 was perhaps one of the most surprising features of the kinetic model, which is consistent across the fitting of the 8 datasets. Efforts to alter this ratio involved changing the initial Pd concentration of the catalyst stock solution, or by using a different solvent to make the catalyst stock solution, such as toluene which is less polar and known to alter the equilibrium between monomeric, dimeric and trimeric Pd species [140]. Neither attempt had an influence the observed rate. It can be speculated that this 3:1 ratio could stem from within the catalytic cycle as a partitioning of reactive intermediates rather than from the pre-catalyst. A mechanism is tentatively proposed based on the resting state being an oxidative adduct which is often the thermodynamically more stable reaction intermediate (Scheme 5.4). Pd_1 and Pd_2 are represented in the proposed mechanism as two catalytically viable oxidative addition adducts. Similar anion-bridged adducts have been previously proposed for the Suzuki-Miyaura cross coupling reaction, including dimers and trimers which support this hypothesis [156, 157].



Scheme 5.3: Proposed catalytic cycles involving Pd_1 and Pd_2 in a 'ligandless' system.

There is strong evidence from this work to propose that, for the Heck arylation reaction, high-order Pd species can have catalytic activities which are several orders of magnitude faster than those observed with monometallic species. However, based on this work, this can only be true/observed at low catalyst loadings, where there is adequate suppression of the competitive catalyst deactivation (via aggregation) process.

Finally, the activation energy obtained previously from the Arrhenius plot was 56.8 kJ/mol and the Eyring plot gave a $\Delta H^{\ddagger}$ of 53.8 kJ/mol (Figures 5.8 & 5.9). As the reactions to produce the plots were carried out at 100 ppm of [Pd], the model suggests they will be predominantly

catalysed by the Pd_2 dimer. The values obtained are considerably lower than previous reports for $Pd(OAc)_2/PPh_3$ (E_a = 96.2 kJ/mol) [144] and for a [CN]-palladacycle ($\Delta H^{\ddagger}$ = 69 kL/mol) [158] which consolidates the idea that Pd_2 is considerably more active than these ligated complexes.

5.3 Conclusions

To summarise, the presence of more than one catalytically active species has been identified in the Heck arylation reaction between iodobenzene and methyl acrylate. Two distinct kinetic regimes have been deduced by using a combination of RPKA, VTNA and kinetic modelling for this system. Catalyst deactivation was identified to be non-competitive within the reaction timescale for low catalyst loadings between 30-200 ppm, with the global rate equation showing an order of 1.7 for [Pd]. Conversely, catalyst deactivation started to predominate above 200 ppm which was accompanied by a decrease in the order of Pd to 0.9.

Further to this, kinetic modelling uncovered the presence of an equilibrium between more than one catalytically active species. The best fitting model concluded these species to be a Pd monomer and a dimer in a 3:1 ratio with the latter being over 90 times more active than the former whilst also dominating the equilibrium. The observed turnover can be primarily attributed to the catalytic activity of the monomeric species above 200 ppm, due to the rapid deactivation observed (likely through agglomeration to form Pd black). To the best of our knowledge, this is the first time that such a system has been observed in Pd catalysed reactions.

It must be acknowledged that the experimental data deviates from the model at the lowest catalyst loading of 30 ppm (0.003 mol%). Reproducible kinetic data became difficult below this threshold, with a significant induction period present at 5 ppm [Pd] loading which changes between experiments. As the predominant catalyst at low concentrations is the higher order Pd_2 species the induction period could indicate the presence of a pre-activation process (Figure 5.22). At such loadings trace amounts of impurities from the reactants, solvent or even H_2O or O_2 [157] have an amplified effect on the catalyst activity and the exact conditions become difficult to replicate between experiments.

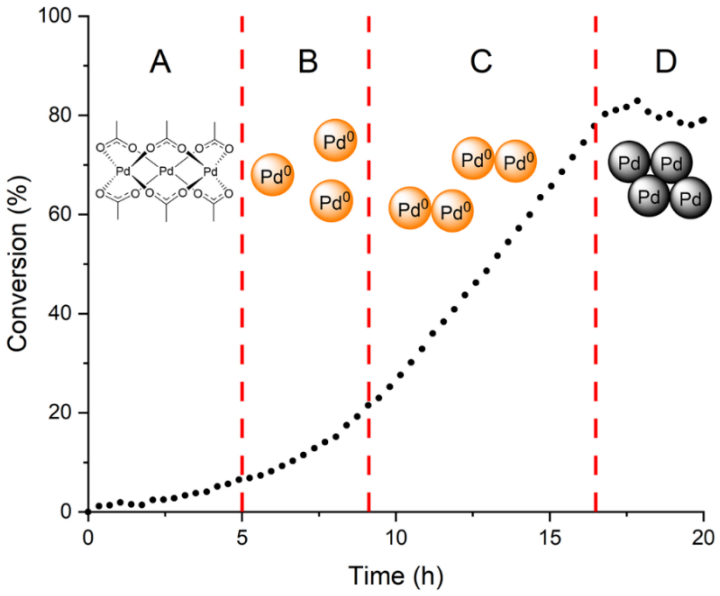


Figure 5.22: Possible catalyst activation pathway at low concentrations superimposed on the reaction profile obtained with 5 ppm [Pd] loading.

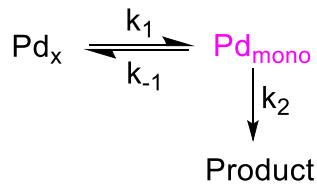
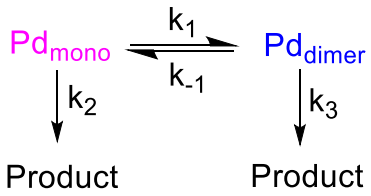
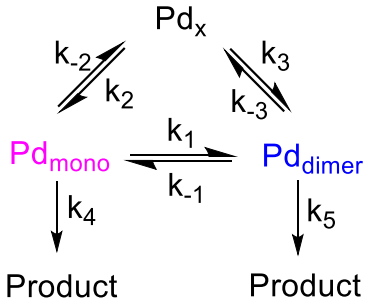
In this work it has been established that by lowering the catalyst loading, the catalyst deactivation can be suppressed. Perhaps of even more significance is the discovery of a specific catalyst loading regime, which has a much lower activation energy in comparison to ligated Pd complexes and where a dimeric Pd species was modelled to be over 90 time more active than the monomeric Pd species. This offers a new, interesting alternative to the common practice of palladium catalysis; rather than suppressing the catalyst degradation at the expense of reaction rate with the addition of specific ligands, such as PPh_3, it can be accomplished by simply lowering the catalyst loading. This will have significance implications for process optimisation, as less Pd is required with the additional advantage of simplifying the workup procedure and thus, improving the overall sustainability of the process.

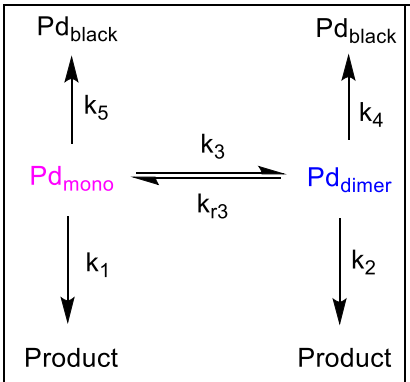
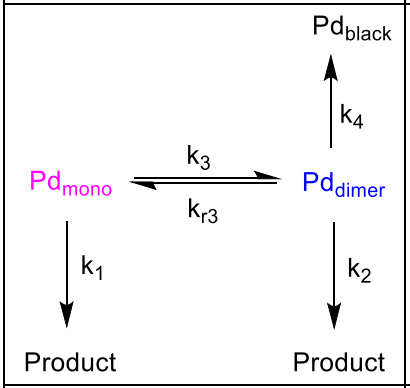
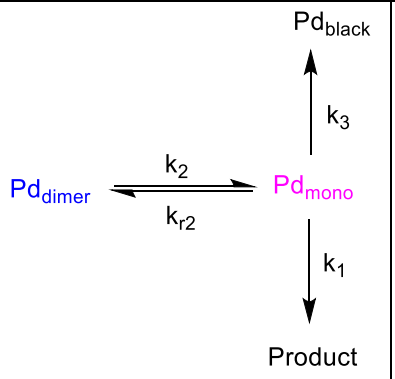
5.4 Future Work

It will be interesting to extend the work to other Pd catalysed cross coupling reactions, such as the Suzuki-Miyaura reaction, as this is known to also proceed using ultra-low levels of Pd [159]. Further work could also be undertaken to study and obtain activation energies at higher catalyst loadings in this specific system to observe if they differ with different catalytic loadings. This would allow us to correlate the activity of the catalyst with catalyst concentration.

6. Appendix

Table 6.1: visual representation of previous models with their associated assumptions and outcomes.

Model	Assumption	Outcome
	Model 1 has only one active catalytic species, Pd_{mono}. Pd_x represents an inactive palladium species in equilibrium with the active species Pd_{mono}.	Unable to fit with the experimental data across the whole concentration range.
	Model 2 incorporates the fact that there was no significant catalyst deactivation detected when same excess experiments were performed. Therefore, Pd_{mono} and Pd_{dimer} are both catalytically active but have different initial concentrations. Pd_{mono} in this instance is incorporated in the model as a monomer and Pd_{dimer} is incorporated as a dimer.	The fit improved from model 1 but there was an over estimation for the reaction rate. This overestimation indicates that there is a degree of deactivation in the experimental data.
	Model 3 incorporates an off cycle Pd_x species which behaves as a reservoir for the active palladium species Pd_{mono} and Pd_{dimer}. This model is like model 1 but with two catalytically active species. Again, Pd_{mono} and Pd_{dimer} are incorporated into the model as a monomer and a dimer respectively.	Poor fit with low values for the interconversion between Pd_x, Pd_{mono} and Pd_{dimer}. Also, the fact that there isn't a hard deactivation parameter means there was no improvement from the previous model 2.

	Model 4 consists of a monomer and a dimer in equilibrium which are both catalytically active. This model allows for both active species to deactivate independently of each other. The addition of the deactivation parameters is hoped to circumvent the downfall of overestimation in model 2.	Excellent fit with the experimental data across all palladium concentrations. However, the rate constant for the monomer deactivation (k_5) is insignificant and essentially zero. This suggests overfitting and that the deactivation pathway for the monomer is simply by aggregating to form the dimer.
	Model 5 is the same as model 4 but without the monomeric palladium species deactivating. This should help prevent overfitting.	Good fit with the experimental data across all palladium concentrations. High degree of under and over estimations for the 30 ppm profile.
	Adapted Rothenberg model where the dimer is inactive and the monomer which is now the only active species can deactivate. Need to note that the initial concentration of palladium is pre-equilibrated between the dimer and monomer due to making a stock solution.	Poor fit as the model overestimates the reaction rate.

7. References

[1] A. Biffis, P. Centomo, A. Del Zotto and M. Zecca, *Chem. Rev.*, 2018, **118**, 2249–2295.

[2] J. Rayadurgam, S. Sana, M. Sasikumar and Q. Gu, *Org. Chem. Front.*, 2021, **8**, 384–414.

[3] C. Valente, S. Çalimsiz, K. H. Hoi, D. Mallik, M. Sayah and M. G. Organ, Angew. Chemie Int. Ed., 2012, **51**, 3314–3332.

[4] T. Mizoroki, K. Mori and A. Ozaki, Bull. Chem. Soc. Jpn., 1971, **44**, 581–581.

[5] K. F. Heck and J. P. Nolley, J. Org. Chem., 1972, **37**, 2320–2322.

[6] E. Negishi and S. Baba, *J. Chem. Soc. Chem. Commun.*, 1976, 596b–597b.

[7] S. Baba and E. Negishi, *J. Am. Chem. Soc.*, 1976, **98**, 6729–6731.

[8] N. Miyaura, K. Yamada and A. Suzuki, Tetrahedron Lett., 1979, **20**, 3437–3440.

[9] N. Miyaura and A. Suzuki, J. Chem. Soc. Chem. Commun., 1979, 866–867.

[10] https://www.nobelprize.org/prizes/chemistry/2010/summary/ accessed March 2022

[11] P. Fristrup, S. Le Quement, D. Tanner and P. O. Norrby, *Organometallics*, 2004, **23**, 6160–6165.

[12] J. Ruan, J. A. Iggo and J. Xiao, *J. Organomet. Chem.*, 2019, **880**, 150–155.

[13] A. S. Gruber, D. Pozebon, A. L. Monteiro and J. Dupont, *Tetrahedron Lett.*, 2001, **42**, 7345–7348.

[14] T. Kawano, T. Shinomaru and I. Ueda, *Org. Lett.*, 2002, **4**, 2545–2547.

[15] M. Buback, T. Perković, S. Redlich and A. De Meijere, *European J. Org. Chem.*, 2003, 2003, **13**, 2375–2382.

[16] A. C. Albéniz, P. Espinet, B. Martín-Ruiz and D. Milstein, J. Am. Chem. Soc., 2001, **123**, 11504–11505.

[17] F. Berthiol, H. Doucet and M. Santelli, *Tetrahedron Lett.*, 2004, **45**, 5633–5636.

[18] A. F. Schmidt and V. V. Smirnov, *Kinet. Catal.*, 2003, **44**, 518–523.

[19] T. Rosner, A. Pfaltz and D. G. Blackmond, *J. Am. Chem. Soc.*, 2001, **123**, 4621–4622.

[20] U. Christmann and R. Vilar, *Angew. Chemie - Int. Ed.*, 2005, **44**, 366–374.

[21] M. Qadir, T. Möchel and K. K. Hii, *Tetrahedron*, 2000, **56**, 10097.

[22] F. Schroeter and T. Strassner, *Inorg. Chem.*, 2018, **57**, 5159–5173.

[23] Y. Ben-David, M. Portnoy, M. Gozin and D. Milstein, *Organometallics*, 1992, **11**, 1995–1996.

[24] M. T. Reetz, G. Lohmer and R. Schwickardi, *Angew. Chemie - Int. Ed.*, 1998, **37**, 481–483.

[25] A. F. Littke and G. C. Fu, *J. Org. Chem.*, 1999, **64**, 10–11.

[26] D. Morales-Morales, R. Redon, C. Yung and C. M. Jensen, *Chem. Commun.*, 2000, 1619–1620.

[27] R. F. Heck, *J. Am. Chem. Soc.*, 1969, **91**, 6707–6714.

[28] T. Jeffery, *J. Chem. Soc. Chem. Commun.*, 1984, 1287–1289.

[29] T. Jeffery, *Tetrahedron*, 1996, **52**, 10113–10130.

[30] K. H. Shaughnessy, P. Kim and J. F. Hartwig, *J. Am. Chem. Soc.*, 1999, **121**, 2123–2132.

[31] K. Selvakumar, A. Zapf and M. Beller, *Org. Lett.*, 2002, **4**, 3031–3033.

[32] W. A. Herrmann, V. P. W. Böhm and C. P. Reisinger, *J. Organomet. Chem.*, 1999, **576**, 23–41.

[33] D. S. Surry and S. L. Buchwald, *Angew. Chemie - Int. Ed.*, 2008, **47**, 6338–6361.

[34] D. W. Old, J. P. Wolfe and S. L. Buchwald, *J. Am. Chem. Soc.*, 1998, **120**, 9722–9723.

[35] D. S. Surry and S. L. Buchwald, *Chem. Sci.*, 2011, **2**, 27–50.

[36] J. P. Wolfe, R. A. Singer, B. H. Yang and S. L. Buchwald, *J. Am. Chem. Soc.*, 1999, **121**, 9550–9561.

[37] J. P. Wolfe and S. L. Buchwald, *Angew. Chem. Int. Ed*, 1999, **38**, 2413–2416.

[38] A. Aranyos, D. W. Old, A. Kiyomori, J. P. Wolfe, J. P. Sadighi and S. L. Buchwald, *J. Am. Chem. Soc.*, 1999, **121**, 4369–4378.

[39] G. C. Fu, *Acc. Chem. Res.*, 2008, **41**, 1555–1564.

[40] S. D. Edmondson, A. Mastracchio and E. R. Parmee, *Org. Lett.*, 2000, **2**, 1109–1112.

[41] W. A. Herrmann, C. Brossmer, K. Öfele, C. -P Reisinger, T. Priermeier, M. Beller and H. Fischer, *Angew. Chemie Int. Ed. English*, 1995, **34**, 1844–1848.

[42] W. A. Herrmann, C. Brossmer, C. P. Reisinger, T. H. Riermeier, K. Öfele and M. Beller, *Chem. - A Eur. J.*, 1997, **3**, 1357–1364.

[43] C. Amatore, A. Jutand and M. Amine M'barki, *Organometallics*, 1992, **11**, 3009–3013.

[44] C. Amatore and A. Jutand, *J. Organomet. Chem.*, 1999, **576**, 254–278.

[45] C. Amatore and A. Jutand, *Acc. Chem. Res.*, 2000, **33**, 314–321.

[46] C. Amatore, A. Jutand and A. Thuilliez, *Organometallics*, 2001, **20**, 3241–3249.

[47] M. Beller and A. Zapf, *Synlett*, 1998, 792–793.

[48] M. Li, J. Y. Tao, L. N. Wang, J. W. Li, Y. J. Liu and M. H. Zeng, *J. Org. Chem.*, 2021, **86**, 11915–11925.

[49] I. P. Beletskaya and A. V. Cheprakov, *Chem. Rev.*, 2000, **100**, 3009–3066.

[50] A. H. M. De Vries, F. J. Parlevliet, L. Schmieder-van De Vondervoort, J. H. M. Mommers, H. J. W. Henderickx, M. A. M. Walet and J. G. De Vries, *Adv. Synth. Catal.*, 2002, **344**, 996–1002.

[51] A. H. M. de Vries, J. M. C. A. Mulders, J. H. M. Mommers, H. J. W. Henderickx and J. G. de Vries, *Org. Lett.*, 2003, **5**, 3285–3288.

[52] M. T. Reetz and J. G. de Vries, *Chem. Commun.*, 2004, **4**, 1559–1563.

[53] A. Alimardanov, L. Schmieder-van de Vondervoort, A. H. M. de Vries and J. G. de Vries, *Adv. Synth. Catal.*, 2004, **346**, 1812–1817.

[54] Q. Yao, E. P. Kinney and Z. Yang, *J. Org. Chem.*, 2003, **68**, 7528–7531.

[55] D. B. Eremin and V. P. Ananikov, *Coord. Chem. Rev.*, 2017, **346**, 2–19.

[56] A. S. Sigeev, A. S. Peregudov, A. V. Cheprakov and I. P. Beletskaya, *Adv. Synth. Catal.*, 2015, **357**, 417–429.

[57] M. T. Reetz and E. Westermann, *Angew. Chemie Int. Ed.*, 2000, **39**, 165–168.

[58] R. K. Das, B. Saha, S. M. W. Rahaman and J. K. Bera, *Chem. – A Eur. J.*, 2010, **16**, 14459–14468.

[59] G. P. F. van Strijdonck, M. D. K. Boele, P. C. J. Kamer, J. G. de Vries and P. W. N. M. van Leeuwen, *Eur. J. Inorg. Chem.*, 1999, 1073–1076.

[60] T. Rosner, J. Le Bars, A. Pfaltz and D. G. Blackmond, *J. Am. Chem. Soc.*, 2001, **123**, 1848–1855.

[61] J. Burés, *Angew. Chemie Int. Ed.*, 2016, **55**, 2028–2031.

[62] G. Rothenberg, S. C. Cruz, G. P. F. Van Strijdonck and H. C. J. Hoefsloot, *Adv. Synth. Catal.*, 2004, **346**, 467–473.

[63] J. R. H. Ross, *Heterogeneous catalysis : fundamentals and applications*, Elsevier, 1st edn., 2012.

[64] European medicines agency Specification limits for residues of metal catalysts or metal reagents accessed November 2021

[65] N. Nikbin, M. Ladlow and S. V. Ley, *Org. Process Res. Dev.*, 2007, **11**, 458–462.

[66] www.silicycle.com/products/metal-scavengers accessed February 2022

[67] C. Mac Namara, J. Torroba and A. Deacon, *Johnson Matthey Technol. Rev.*, 2015, **59**, 334–352.

[68] C. E. Garrett and K. Prasad, *Adv. Synth. Catal.*, 2004, **346**, 889–900.

[69] O. Chahrour, J. Malone, M. Collins, V. Salmon, C. Greenan, A. Bombardier, Z. Ma and N. Dunwoody, *J. Pharm. Biomed. Anal.*, 2017, **145**, 84–90.

[70] J. H. Clark, D. J. Macquarrie and E. B. Mubofu, *Green Chem.*, 2000, **2**, 53–56.

[71] P. Foley, R. DiCosimo and G. M. Whitesides, *J. Am. Chem. Soc.*, 1980, **102**, 6713–6725.

[72] D. R. Anton and R. H. Crabtree, *Organometallics*, 1983, **2**, 855–859.

[73] V. M. Chernyshev, A. V. Astakhov, I. E. Chikunov, R. V. Tyurin, D. B. Eremin, G. S. Ranny, V. N. Khrustalev and V. P. Ananikov, *ACS Catal.*, 2019, **9**, 2984–2995.

[74] J. A. Widegren and R. G. Finke, *J. Mol. Catal. A Chem.*, 2003, **198**, 317–341.

[75] J. P. Collman, K. M. Kosydar, M. Bressan, W. Lamanna and T. Garrett, *J. Am. Chem. Soc.*, 1984, **106**, 2569–2579.

[76] J. Rebek and F. Gaviña, *J. Am. Chem. Soc.*, 1974, **96**, 7112–7114.

[77] J. Rebek, D. Brown and S. Zimmerman, *J. Am. Chem. Soc.*, 1975, **97**, 454–455.

[78] Y. S. Panova, A. S. Kashin, M. G. Vorobev, E. S. Degtyareva and V. P. Ananikov, *ACS Catal.*, 2016, **6**, 3637–3643.

[79] D. Astruc, F. Lu and J. R. Aranzaes, *Angew. Chemie Int. Ed.*, 2005, **44**, 7852–7872.

[80] N. T. S. Phan, M. Van Der Sluys and C. W. Jones, *Adv. Synth. Catal.*, 2006, **348**, 609–679.

[81] S. J. M. Thomas, *ChemCatChem*, 2010, **2**, 127–132.

[82] V. P. Ananikov and I. P. Beletskaya, *Organometallics*, 2012, **31**, 1595–1604.

[83] S. Schauermann, N. Nilius, S. Shaikhutdinov and H. J. Freund, *Acc. Chem. Res.*, 2013, **46**, 1673–1681.

[84] A. S. Kashin and V. P. Ananikov, *J. Org. Chem.*, 2013, **78**, 11117–11125.

[85] A. J. Reay and I. J. S. Fairlamb, *Chem. Commun.*, 2015, **51**, 16289–16307.

[86] E. M. Barreiro, Z. Hao, L. A. Adrio, J. R. van Ommen, K. Hellgardt and K. K. (Mimi) Hii, *Catal. Today*, 2018, **308**, 64–70.

[87] A. Leyva-Perez, J. Oliver-Meseguer, P. Rubio-Marques, A. Corma, *Angew. Chemie Int. Ed.*, 2013, **52**, 11554–11559.

[88] A. V. Astakhov, O. V. Khazipov, A. Y. Chernenko, D. V. Pasyukov, A. S. Kashin, E. G. Gordeev, V. N. Khrustalev, V. M. Chernyshev and V. P. Ananikov, *Organometallics*, 2017, **36**, 1981–1992.

[89] F. Zhao, B. M. Bhanage, M. Shirai and M. Arai, *J. Mol. Catal. A Chem.*, 2002, **182**, 499.

[90] F. Zhao, K. Murakami, M. Shirai and M. Arai, *J. Catal.*, 2000, **194**, 479–483.

[91] F. Zhao, M. Shirai and M. Arai, *J. Mol. Catal. A Chem.*, 2000, **154**, 39–44.

[92] F. Zhao, M. Shirai, Y. Ikushima and M. Arai, *J. Mol. Catal. A Chem.*, 2002, **180**, 211–219.

[93] R. G. Heidenreich, J. G. E. Krauter, J. Pietsch and K. Köhler, *J. Mol. Catal. A Chem.*, 2002, **182**, 499–509.

[94] K. Kohler, R. G. Heidenreich, J. G. E. Krauter and J. Pietsch, *Chem. – A Eur. J.*, 2002, **8**, 622.

[95] J. S. Bradley, *Clust. Colloids From Theory to Appl.*, 2007, 459–544.

[96] A. F. Schmidt and A. A. Kurokhtina, *Kinet. Catal. 2012 536*, 2012, **53**, 714–730.

[97] A. V. Gaikwad, A. Holuigue, M. B. Thathagar, J. E. Ten Elshof and G. Rothenberg, *Chem. – A Eur. J.*, 2007, **13**, 6908–6913.

[98] A. F. Schmidt, A. Al-Halaiqa, V. V. Smirnov and A. A. Kurokhtina, *Kinet. Catal. 2008 495*, 2008, **49**, 638–643.

[99] Z. Ma and F. Zaera, *Encyclopedia of Inorganic Chemistry*, John Wiley & Sons, Ltd, 2006.

[100] M. Gruber, S. Chouzier, K. Koehler and L. Djakovitch, *Appl. Catal. A Gen.*, 2004, **265**, 161–169.

[101] A. Molnar, *Chem. Rev.*, 2011, **111**, 2251–2320.

[102] H. A. Elazab, A. R. Siamaki, S. Moussa, B. F. Gupton and M. S. El-Shall, *Appl. Catal. A Gen.*, 2015, **491**, 58–69.

[103] A. Papp, K. Miklós, P. Forgo and Á. Molnár, *J. Mol. Catal. A Chem.*, 2005, **229**, 107–116.

[104] V. Polshettiwar and Á. Molnár, *Tetrahedron*, 2007, **63**, 6949–6976.

[105] Á. Mastalir, M. Quiroga, T. Szabó, Á. Zsigmond and I. Dékány, *React. Kinet. Mech. Catal.*, 2014, **113**, 61–68.

[106] C. P. Mehnert, D. W. Weaver and J. Y. Ying, *J. Am. Chem. Soc.*, 1998, **120**, 12289–12296.

[107] M. Benaglia and A. Puglisi, *Catalyst immobilization: methods and applications*, Wiley-VCH, 2020.

[108] P. P. Mpungose, Z. P. Vundla, G. E. M. Maguire and H. B. Friedrich, *Molecules*, 2018, **23**, 1–24.

[109] M. J. Climent, A. Corma, S. Iborra and M. Mifsud, *Adv. Synth. Catal.*, 2007, **349**, 1949–1954.

[110] S. MacQuarrie, B. Nohair, J. H. Horton, S. Kaliaguine and C. M. Crudden, *J. Phys. Chem. C*, 2010, **114**, 57–64.

[111] V. Polshettiwar and Á. Molnár, *Tetrahedron*, 2007, **63**, 6949–6976.

[112] I. Bucsi, Á. Mastalir, Á. Molnár, K. L. Juhász and A. Kunfi, *Struct. Chem.*, 2017, **28**, 501–509.

[113] J. D. Webb, S. MacQuarrie, K. McEleney and C. M. Crudden, *J. Catal.*, 2007, **252**, 97–109.

[114] C. M. Crudden, M. Sateesh and R. Lewis, *J. Am. Chem. Soc.*, 2005, **127**, 10045–10050.

[115] Y. Ji, S. Jain and R. J. Davis, *J. Phys. Chem. B*, 2005, **109**, 17232–17238.

[116] J. M. Richardson and C. W. Jones, *J. Catal.*, 2007, **251**, 80–93.

[117] S. S. Pröckl, W. Kleist, M. A. Gruber and K. Köhler, *Angew. Chemie Int. Ed.*, 2004, **43**, 1881–1882.

[118] C. Ramarao, S. V. Ley, S. C. Smith, I. M. Shirley and N. DeAlmeida, *Chem. Commun.*, 2002, **10**, 1132–1133.

[119] H. Gruber-Woelfler, P. F. Radaschitz, P. W. Feenstra, W. Haas and J. G. Khinast, *J. Catal.*, 2012, **286**, 30–40.

[120] S. Hübner, J. G. De Vries and V. Farina, *Adv. Synth. Catal.*, 2016, **358**, 3–25.

[121] M. B. Thathagar, J. E. Ten Elshof and G. Rothenberg, *Angew. Chemie - Int. Ed.*, 2006, **45**, 2886–2890.

[122] T. N. Glasnov, S. Findenig and C. O. Kappe, *Chem. - A Eur. J.*, 2009, **15**, 1001–1010.

[123] R. Greco, W. Goessler, D. Cantillo and C. O. Kappe, *ACS Catal.*, 2015, **5**, 1303–1312.

[124] D. Cantillo and C. O. Kappe, *ChemCatChem*, 2014, **6**, 3286–3305.

[125] X. Fan, M. G. Manchon, K. Wilson, S. Tennison, A. Kozynchenko, A. A. Lapkin and P. K. Plucinski, *J. Catal.*, 2009, **267**, 114–120.

[126] B. Van Vaerenbergh, J. Lauwaert, J. W. Thybaut, P. Vermeir and J. De Clercq, *Chem. Eng. J.*, 2019, **374**, 576–588.

[127] N. Yuan, V. Pascanu, Z. Huang, A. Valiente, N. Heidenreich, S. Leubner, A. K. Inge, J. Gaar, N. Stock, I. Persson, B. Martín-Matute and X. Zou, *J. Am. Chem. Soc.*, 2018, **140**, 8206–8217.

[128] N. Yuan, M. H. Majeed, É. G. Bajnóczi, A. R. Persson, L. R. Wallenberg, A. K. Inge, N. Heidenreich, N. Stock, X. Zou, O. F. Wendt and I. Persson, *Catal. Sci. Technol.*, 2019, **9**, 2025–2031.

[129] M. A. Newton, J. B. Brazier, E. M. Barreiro, S. Parry, H. Emmerich, L. A. Adrio, C. J. Mulligan, K. Hellgardt and K. K. M. Hii, *Green Chem.*, 2016, **18**, 406–411.

[130] M. A. Newton, J. B. Brazier, E. M. Barreiro, H. Emerich, L. A. Adrio, C. J. Mulligan, K. Hellgardt and K. K. Hii, *Catal. Sci. Technol.*, 2016, **6**, 8525–8531.

[131] M. A. Newton, R. Nicholls, J. B. Brazier, B. N. Nguyen, C. J. Mulligan, K. Hellgardt, E. M. Barreiro, H. Emerich, K. K. (Mimi) Hii, I. Snigireva and P. B. J. Thompson, *Catal. Struct. React.*, 2017, **3**, 149–156.

[132] M. A. Newton, D. Ferri, C. J. Mulligan, I. Alxneit, H. Emerich, P. B. J. Thompson and K. K. Hii, *Catal. Sci. Technol.*, 2020, **10**, 466–474.

[133] J. B. Brazier, B. N. Nguyen, L. A. Adrio, E. M. Barreiro, W. P. Leong, M. A. Newton, S. J. A. Figueroa, K. Hellgardt and K. K. M. Hii, *Catal. Today*, 2014, **229**, 95–103.

[134] A. Bourouina, V. Meille and C. de Bellefon, *J. Flow Chem.*, 2018, **8**, 117–121.

[135] J. M. Richardson and C. W. Jones, *Adv. Synth. Catal.*, 2006, **348**, 1207–1216.

[136] H. Veisi and N. Mirzaee, *Appl. Organomet. Chem.*, 2018, **32**, e4067.

[137] P. Forzatti and L. Lietti, *Catal. Today*, 1999, **52**, 165–181.

[138] J. Heveling, *J. Chem. Educ.*, 2012, **89**, 1530–1536.

[139] J. A. Riddick, W. B. Bunger and T. K. Sakano, *Organic solvents: physical properties and methods of purification. Fourth edition*, Wiley, New York N.Y., 1986.

[140] L. A. Adrio, B. N. Nguyen, G. Guilera, A. G. Livingston and K. K. Hii, *Catal. Sci. Technol.*, 2012, **2**, 316–323.

[141] J. Sherwood, J. H. Clark, I. J. S. Fairlamb and J. M. Slattery, *Green Chem.*, 2019, **21**, 2164–2213.

[142] J. A. Molina De La Torre, P. Espinet and A. C. Albéniz, *Organometallics*, 2013, **32**, 5428–5434.

[143] R. Tao, X. Ma, X. Wei, Y. Jin, L. Qiu and W. Zhang, *J. Mater. Chem. A*, 2020, **8**, 17360–17391.

[144] F. G. Zhao, B. M. Bhanage, M. Shirai and M. Arai, *Stud. Surf. Sci. Catal.*, 1999, **122**, 427–430.

[145] M. R. Eberhard, *Org. Lett.*, 2004, **6**, 2125–2128.

[146] C. S. Consorti, F. R. Flores and J. Dupont, *J. Am. Chem. Soc.*, 2005, **127**, 12054–12065.

[147] D. G. Blackmond, *Angew. Chemie - Int. Ed.*, 2005, **44**, 4302–4320.

[148] E. O. Pentsak, D. B. Eremin, E. G. Gordeev and V. P. Ananikov, *ACS Catal.*, 2019, **9**, 3070–3081.

[149] A. Jutand, in *The Mizoroki-Heck Reaction*, John Wiley & Sons, Ltd, 2009, pp. 1–50.

[150] I. J. S. Fairlamb, A. R. Kapdi and A. F. Lee, *Org. Lett.*, 2004, **6**, 4435–4438.

[151] A. C. Skapski and M. L. Smart, *J. Chem. Soc. D Chem. Commun.*, 1970, **11**, 659

[152] A. R. Kapdi, A. C. Whitwood, D. C. Williamson, J. M. Lynam, M. J. Burns, T. J. Williams, A. J. Reay, J. Holmes and I. J. S. Fairlamb, *J. Am. Chem. Soc.*, 2013, **135**, 8388–8399.

[153] A. V. Gaikwad and G. Rothenberg, *Phys. Chem. Chem. Phys.*, 2006, **8**, 3669–3675.

[154] J. Wang, H. F. M. Boelens, M. B. Thathagar and G. Rothenberg, *ChemPhysChem*, 2004, **5**, 93–98.

[155] J. S. Mathew, M. Klussmann, H. Iwamura, F. Valera, A. Futran, E. A. C. Emanuelsson and D. G. Blackmond, *J. Org. Chem.*, 2006, **71**, 4711–4722.

[156] N. W. J. Scott, M. J. Ford, C. Schotes, R. R. Parker, A. C. Whitwood and I. J. S. Fairlamb, *Chem. Sci.*, 2019, **10**, 7898–7906.

[157] F. Fu, J. Xiang, H. Cheng, L. Cheng, H. Chong, S. Wang, P. Li, S. Wei, M. Zhu and Y. Li, *ACS Catal.*, 2017, **7**, 1860–1867.

[158] C. S. Consorti, F. R. Flores and J. Dupont, *J. Am. Chem. Soc.*, 2005, **127**, 12054–12065.

[159] A. Bourouina, V. Meille and C. de Bellefon, *Catalysts*, 2019, **9**, 60.